Theses and Dissertations

Graduate School

2008

Mechanistic Studies on the Electrochemistry of Glutathione and Homocysteine

Olufemi Oyesanya
Virginia Commonwealth University

College of Humanities and Sciences
Virginia Commonwealth University

This is to certify that the dissertation prepared by <u>Olufemi O. Oyesanya</u> entitled <u>Mechanistic Studies on the Electrochemistry of Glutathione and Homocysteine</u> has been approved by his committee as satisfactory completion of the dissertation requirement for the degree of <u>Doctor of Philosophy</u>.

_____

Dr. Julio C. Alvarez, Director of Dissertation, Chemistry Department

_____

Dr. Fred M. Hawkridge, Committee Member, Chemistry Department

_____

Dr. Maryanne M. Collinson, Committee Member, Chemistry Department

_____

Dr. John J. Ryan, Committee Member, Biology Department

_____

Dr. Everett Carpenter, Committee Member, Chemistry Department

_____

Dr. Nicholas Farrell, Chairman, Chemistry Department

_____

Dr. Robert D. Holsworth, Dean, College of Humanities and Sciences

_____

Dr. Douglas F. Boudinot, Dean, School of the Graduate Studies

_____

Date

Mechanistic Studies on the Electrochemistry of Glutathione and Homocysteine

A dissertation submitted in partial fulfillment of the requirements for the degree of
Doctor of Philosophy at Virginia Commonwealth University

by

Olufemi O. Oyesanya

Director: Dr. Julio C. Alvarez

Professor of Chemistry

Virginia Commonwealth University

Richmond, Virginia

April, 2008

ACKNOWLEDGMENTS

In sincerity of heart, I hereby acknowledge God for enabling me to accomplish what He has helped me started. He has granted me protection, good health, provision, sanity, and many more during the course of my Graduate education in the US. I truly acknowledge Dr. Julio Alvarez, my advisor, for allowing me into his research group when I had to join another group. His assistance to me in priceless, I must confess. Dr. Alvarez has inspired and encouraged me in the course of my graduate career. I appreciate his guidance and direction while working on this project.

I would like to acknowledge my committee members: Dr. Fred M. Hawkridge, Dr. Maryanne M. Collinson, Dr. John J. Ryan, and Dr. Everett E. Carpenter. They all have contributed to my success. I appreciate them all. The whole members of Dr. Alvarez's group are acknowledged. My thanks go to Timothy Alligrant, a fellow graduate student, who helped to evaluate my dissertation draft.

My profound gratitude to my parents, who thought it well to send me to the US for my graduate career. My heartfelt appreciation to my lovely wife, Regina A. Oyesanya, for her support, love and encouragement in making my dissertation a reality. I thank her for giving me a wonderful son on my birthday, and we are expecting another child toward my graduation ceremony. I acknowledge my son, Olufemi Oyesanya, for granting me time to write up my dissertation. My siblings are all highly appreciated and thanked for their prayers and encouragement all through my graduate career. I acknowledge my church family as well for their prayers.

In memory of my dear father, Thomas O. Oyesanya, an educationist, who made sure I got good education; and to my sister, Tolu Oyesanya.

TABLE OF CONTENTS

LIST OF TABLES

LIST OF FIGURES

Figure 1. Structures of glutathione, A (GSH) and glutathione disulfide, B (GSSG).......... 5

Figure 2. Glutathione synthesis and utilization in animals 7

Figure 3. Structures of cysteine, A (CSH) and cysteine disulfide, B (CSSC) 10

Figure 4. Structures of Homocysteine (A) and Homocysteine thiolactone (B) 11

Figure 5. Homocysteine Metabolism 12

Figure 6. Reaction scheme proposed for the oxidation of GSH by Fe(III) 16

Figure 7. Reaction scheme proposed for the complexation of GSH by cisplatin 17

Figure 8. Square scheme for the CPET, PT/ET and ET/PT 23

Figure 9. Potential energy profile for electrochemical CPETs 24

Figure 10. General base catalysis of glutathione oxidation by potassium hexachloroiridate (IV) 26

Figure 11. Cyclic voltammogram (CV) of 1.0 mM $Ru(bpy)_3^{2+}$ in 50 mM PBS/0.1 M NaCl, pH 5.0 at 100 mV/s. Glassy carbon working electrode (0.06 cm^2), Pt-wire counter electrode, and an Ag/AgCl reference electrode. CV is background subtracted 27

Figure 12. Typical three electrode cell 28

Figure 13. Cyclic voltammograms in 50 mM sodium phosphate buffer (pH = 5.0) at room temperature in 0.1 M NaCl. (A) Cyclic voltammogram of 1.0 mM glutathione (broken line). (B) Cyclic voltammograms of 1.0 mM $Ru(bpy)_3^{2+}$, experimental (solid) and simulated (open circle). (C) Cyclic voltammograms of 1.0 mM $Ru(bpy)_3^{2+}$ in the presence of 5.0 mM glutathione, experimental (solid) and simulated (open circle). Scan rate used: 100 mV/s. Parameters obtained from simulation: k_h = 0.06 cm/s; k_2= 1.41 ± 0.2 × 10^4 $M^{-1}s^{-1}$; K_{eq} = 1.0 × 10^3 36

LIST OF SCHEMES

LIST OF ABBREVIATIONS AND SYMBOLS

ACES N-(2-Acetamido)-2-aminoethanesulfonic acid

AIDs   Acquired immunodeficiency syndrome

Ag/AgCl   Silver/silver chloride

ATP   Adenosine Triphosphate

α   Brønsted Coefficeint for GAC

α_B Fractional Amount of Brønsted Base

β   Brønsted Coefficeint for GBC

BDD   Boron-Doped Diamond

CA   Citric Acid

ClO_2^- Chlorite

$ClO_2^{\bullet}$ Chlorine Dioxide Radical

$ClPz^{2+/+}$ Chlorpromazine Couples

CNT   Carbon NanoTube

Co(II)   Cobalt (II)

CPET   Concerted Proton Electron Transfer

Cr(IV)   Chromium (IV)

CSH   Cysteine

CSSC   Cystine

Cu(II)   Copper (II)

CV   Cyclic Voltammogram

D   Diffusion Coefficeint

DMSO   Dimethyl Sulfoxide

DNA	Deoxyribonucleic Acid
D_2O/H_2O	Deuterated Water/Water
e^-	Electron
E_a	Activation Energy
ΔE	Potential Change
E_p	Peak Potential
ΔE_p	Peak Potential Change
$E_{1/2}$	Half-wave Potential
$E^{o\prime}$	Formal Potential
ER	Endoplasmic Recticulum
ET	Electron Transfer
Fe(II/III)	Iron Couples
ΔG^o	Standard Free Energy Change
GAC	General Acid Catalysis
GBC	General Base Catalysis
GCE	Glassy Carbon Electrode
GCS	γ-Glutamylcysteine Synthetase
GSH	Glutathione
GS	Glutathione Synthetase
GS^-	Glutathione Anion
$GS^{\bullet}$	Glutathiyl Radical
GSSG	Glutathione Disulfide
HAT	Hydrogen Atom Transfer

HCSH	Homocysteine
HIV	Human Immunodeficiency Virus
^{1}H NMR	Proton Nuclear Magnetic Resonance
i_{cat}	Catalytic Current
i_d	Diffusion Current
IR	Infra Red
$IrCl_6^{3-/2-}$	Hexachloroiridate Couples
K_{ass}	Association Equilibrium Constant
k_{ass}	Association Rate Constant
k_B	Boltzmann's Constant
KCl	Potassium Chloride
K_{dep}	Deprotonation Equilibrium Coonstant
k_{dep}	Deprotonation Rate Coonstant
k_{dim}	Dimerization Rate Constant
K_{eq2}	Electrooxidation Equilbrium Constant for Protonated Thiol
K_{eq3}	Electrooxidation Equilibrium Constant for Deprotonated Thiol
k_2	Electrooxidation Rate Constant for Protonated Thiol
k_3	Electrooxidation Rate Constant for Deorotonated Thiol
k_{ET}	Electron Transfer Rate Constant
k_h	Heterogeneous Rate Constant
KIE	Kinetic Isotope Exchange
MA	Maleic Acid
MHz	Mega Hertz

Mn(II)	Manganese (II)
NaCl	Sodium Chloride
$NADP^+$	Oxidized Nicotinamide Adenine Dinucleotide Phosphate
NADPH	Reduced Nicotinamide Adenine Dinucleotide Phosphate
NaH_2PO_4	Sodium Phosphate Monobasic
Na_2HPO_4	Sodium Phosphate Dibasic
NaOH	Sodium hydroxide
NHE	Normal Hydrogen Electrode
OH^-	Hydroxyl Ion
$^\bullet OH$	Hydroxyl Radical
PA	Propionic Acid
PB	Phosphate Buffer
PET	Proton Electron Transfer
PT	Proton Transfer
Pt/Pt(II)	Platinum/Platinum (II)
RDS	Rate Determining Step
RNA	Ribonucleic Acid
$RS^\bullet$	Thiyl Radical
RSSR	Thiol Disulfide
RS^-	Thiol Anion
RSH	Thiol
$Ru(bpy)_3^{2+/3+}$	Tris(2,2′−bipyridyl)dichlororuthenium (II/III) Hexahydrate
tHCSH	Homocysteine−Thiolactone

tRNA   Transfer Ribonucleic Acid

TRIS   Tris(hydroxymethyl)aminomethane

TS   Transition State

UV-Vis   Ultra Violet - Visible

V   Volt

λ Reorganization Energy

ABSTRACT

MECHANISTIC STUDIES ON THE ELECTROCHEMISTRY OF GLUTATHONE
AND HOMOCYSTEINE

Olufemi O. Oyesanya, Ph.D.

A dissertation submitted in partial fulfillment of the requirements for the degree of
Doctor of Philosophy at Virginia Commonwealth University.

Virginia Commonwealth University, 2008

Major Director: Julio C. Alvarez, Ph.D., Department of Chemistry

This research work has investigated the electrochemistry of glutathione (GSH) and homocysteine (HCSH) in order to develop sensors for these biological thiols. $Ru(bpy)_3^{3+}$ and $IrCl_6^{2-}$ have been used as mediators for the electrooxidation of GSH and HCSH because direct oxidation of these thiols is slow at most conventional electrodes. The electrochemical detection of GSH and HCSH has been pursued because of their biological roles.

Concerted proton electron transfer (CPET) and stepwise proton electron transfer (PT/ET) pathways have been observed in the electrooxidation of GSH and HCSH. Oxidation of GSH by $Ru(bpy)_3^{3+}$ carried out in deuterated and undeuterated buffered (pH = pD = 5.0) and unbuffered solutions (pH = pD 5.0−9.0) indicates a CPET pathway. At pH 7.0 buffered solution, the involvement of the buffer was obvious, with rate increasing as the buffer concentration increases − an indication of a general base catalysis. The oxidation of GSH by $IrCl_6^{2-}$ follows through CPET at pH 7.0 when the optimum

concentration of the buffer is established. The plot of the rate vs. buffer concentration gave a curvature at lower buffer concentration and then a plateau at higher concentration, which implies a change in the rate determining step as the buffer concentration increases. At lower buffer concentration, proton transfer was seen to be the rate determining step as the reduction current increases upon scan rate increase.

In the oxidation of HCSH by $IrCl_6{}^{2-}$, CPET was observed at pH = pD values of 7.0 and 8.0, whereas PT/ET was seen at pH = pD values of 9.0 and 10. Increase in the buffer concentration at pH 7.0 revealed the contribution of the buffer, in that, the oxidation proceeds more efficiently, seeing that the catalytic peak current shifts more negatively and the peak broadness diminishes. Increase in the temperature for the electrooxidation of HCSH resulted in increase in the rate.

1.0 OVERVIEW

The presence of glutathione, an antioxidant, in the cellular system has afforded defense from deleterious substances produced in the biological cell [1]. Amongst the deleterious substances are the reactive oxygen species (free radicals) [1,2]. In addition to antioxidant defense, glutathione plays important roles in DNA and protein syntheses, cell proliferation and apoptosis, and immune response [1]. Reactive oxygen species are generated during oxidative stress – which is a condition in which there is imbalance between the production of reactive oxygen species and a biological system's ability to readily detoxify the reactive intermediates or easily repair the consequent damage [1]. Thus, the function of glutathione is to reduce these species before any damage is done within the cell. The functional group conferring this antioxidative activity on glutathione is its *thiol* (−SH) [2]. During the inactivation of the reactive oxygen species, glutathione acts as an electron donor, as well as a proton donor, while it is oxidized as a result. Deficiency or decrease in the amount of glutathione in the cell has been associated with diseases like cancer, inflammation, seizure, cystic fibrosis, heart attack, diabetes, liver disease, kwashiorkor, infection, stroke, Alzheimer's and Parkinson's diseases [2, 3], AIDs [4], HIV [4-8], hemolytic anemia [9-12], Wilson disease [11, 12]. Due to the importance of glutathione in the cellular fluid, this research has sought to further understand its role in order to develop a sensor for it. On the other hand, homocysteine (HCSH), another biological thiol, poses a threat to the cellular system when its concentration is high, leading to cardiovascular disease and stroke in humans [13-15].

In order to develop sensors for both glutathione and homocysteine, complete understanding of their oxidation mechanism must be obtained. This work is divided into

three specific aims: i) understanding the oxidation mechanism of glutathione by tris(2,2′-bipyridyl)dichlororuthenium (III) hexahydrate ($Ru(bpy)_3^{3+}$), ii) understanding the oxidation mechanism of glutathione by potassium hexachloroiridate (IV) ($IrCl_6^{2-}$), iii) understanding the oxidation mechanism of homocysteine by potassium hexachloroiridate (IV). These specific aims are steps toward the development and design of glutathione and homocysteine sensors.

1.1 Glutathione

Glutathione (GSH) is the most abundant low-molecular weight thiol in the antioxidant cellular defense, being found in the millimolar range (0.5−10 mM) [1, 16]. It is a tripeptide (γ-glutamyl-cysteinyl-glycine), composed of glutamate, cysteine, and glycine [1, 16, 17]. Most of the cellular GSH (85-90%) is present in the cytosol, where it is synthesized, with the remainder in many organelles [18]. It has long been established that the presence of cysteine (CSH) residue in GSH makes it readily oxidized nonenzymatically to (glutathione radical (GS$^{\bullet}$), which then reacts with another GS$^{\bullet}$ to yield) glutathione disulfide (GSSG) by electrophilic substances (e.g., free radicals [19, 20], reactive oxygen/nitrogen species [21, 22] and metal ions [23, 24], Equation 1. The ratio of reduced (GSH) to disulfide (GSSG) glutathione is approximately 100:1 in the cytosol [25]. Disulfide bond formation is disfavored in this highly reducing environment. Nonetheless, in the endoplasmic reticulum (ER) where disulfide bond formation occurs, the ratio of GSH:GSSG is much more oxidizing at approximately 3:1 [25]. The efflux of GSSG from cells contributes to a net loss of intracellular GSH. Cellular GSH

concentrations are greatly reduced in response to protein malnutrition, oxidative stress, and many pathological conditions [18, 26].

$$GSH \xrightarrow[-H^+]{-e^-} GS^{\bullet} \longrightarrow \frac{1}{2}GSSG \qquad (1)$$
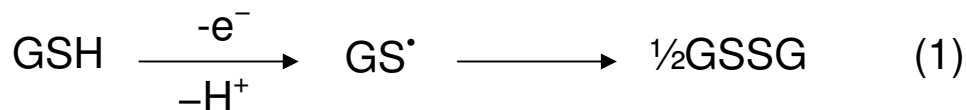
Glutathione content changes in response of a cell to a stress. In the reactions that protect the cell by eliminating the deleterious substance, GSH is first consumed, and is then replenished through either enzymatic reduction of a disulfide by NADPH-dependent glutathione reductase, when that is made possible, or by *de novo* synthesis [16].

1.1.1 Glutathione Redox Couple (GSH/GSSG)

The GSH/GSSG redox couple is a redox regulator ensuring redox buffering in a living cell in the ER and cytosol [25, 27, 28]. Its redox potential has been reported to be -0.263 V (vs. $NADP^+$/NADPH) in 0.1 M phosphate buffer pH 7.07, 25°C [29], which is equivalent to the cytosolic redox potential where it is synthesized [25]. While most glutathione is in its reduced state, it must be oxidized to enable passage through the phospholipids bilayer into the ER [30-33] and probably likewise to the mitochondria [34, 35]. The ratio 3:1 of the reduced and oxidized forms of glutathione is estimated to maintain the ER redox potential at -0.18 V [25]. Four pH-active functional groups are found in reduced GSH (Figure 1A). The glutamyl and glycyl carboxylic groups have pK_a's 2.34 and 3.48, respectively, the sulfhydryl group is 8.62, and the ammonium group is 9.43 [36]. The glutathione disulfide possesses six ionizable groups (Figure 1B): four carboxylic (pK_a's 1.99, 2.68, 3.19, and 4.04) and two ammonium (pK_a's 8.46 and 9.15) groups [37].

A

B
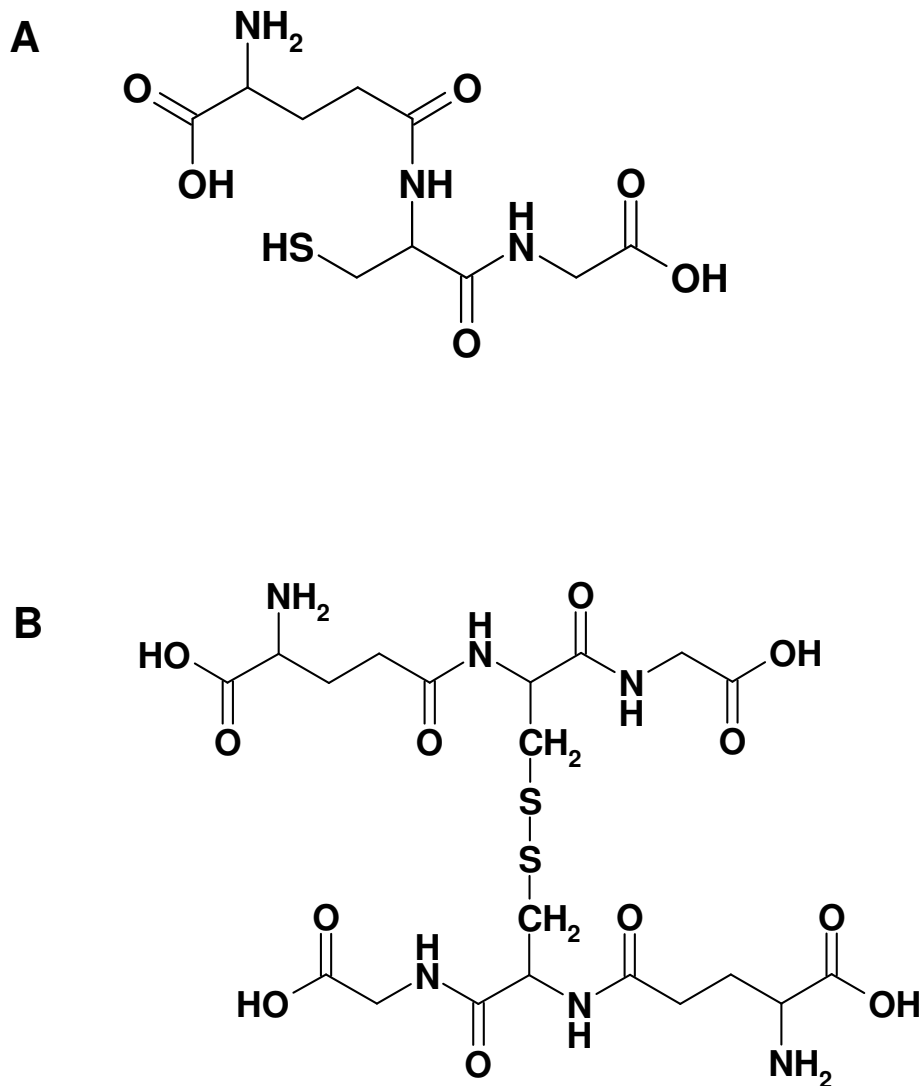
Figure 1. Structures of glutathione, A (GSH) and glutathione disulfide, B (GSSG).

1.1.2 Glutathione Biosynthesis

The synthesis of GSH from its constituent amino acids is both constitutive and regulated, and results from the concerted effort of two cytosolic ATP-dependent enzymes: γ-glutamylcysteine synthetase (GCS) and GSH synthetase (GS) (Figure 2). This pathway occurs in virtually all cell types, with the liver being the major producer

and exporter of GSH [1]. In the reaction of the first enzyme, GCS, the γ-carboxyl group of glutamate reacts with the amino group of cysteine to form a peptide γ-linkage. Because the affinity and activity of GSH synthetase is high, GSH synthesis is favored, although γ-glutamyl-cysteine can be a substrate for γ-glutamylcyclotransferase, which converts it into cysteine and 5-oxoproline [26, 38]. In the *de novo* synthesis of GSH, γ-glutamylcysteine synthetase is the rate-limiting enzyme [16, 18].

However, cysteine has recently been said to be a limiting amino acid in the synthesis of GSH in humans, rats, pigs, and chickens [39-41]. The uptake of cysteine by cells increases the intracellular GSH concentrations [18]. Increase in the supply of cysteine or its precursors (e.g., cystine, *N*-acetyl-cysteine, and L-2-oxothiazolidine-4-carboxylate) via oral or intravenous administration enhances GSH synthesis and prevents GSH deficiency in humans and animals under various nutritional and pathological conditions (including protein malnutrition, adult respiratory distress syndrome, HIV, and AIDS) [2]. In addition, dietary methionine can replace cysteine to support GSH synthesis *in vivo*, because cysteine can be generated from methionine catabolism [1].

Extracellularly and intracellularly generated glutamate can be used for the synthesis of GSH [42]. Plasma glutamate is chiefly derived from its *de novo* synthesis and protein degradation [1]. Glutamate regulates the synthesis of GSH through two mechanisms: *1*) the uptake of cystine, and *2*) the prevention of GSH inhibition of GCS [1]. When the extracellular glutamate concentrations are high, cystine uptake is competitively inhibited by glutamate, resulting in reduced GSH synthesis [43]; whereas, when intracellular glutamate concentrations are unusually high GSH synthesis is enhanced and its concentration is particularly high [26].
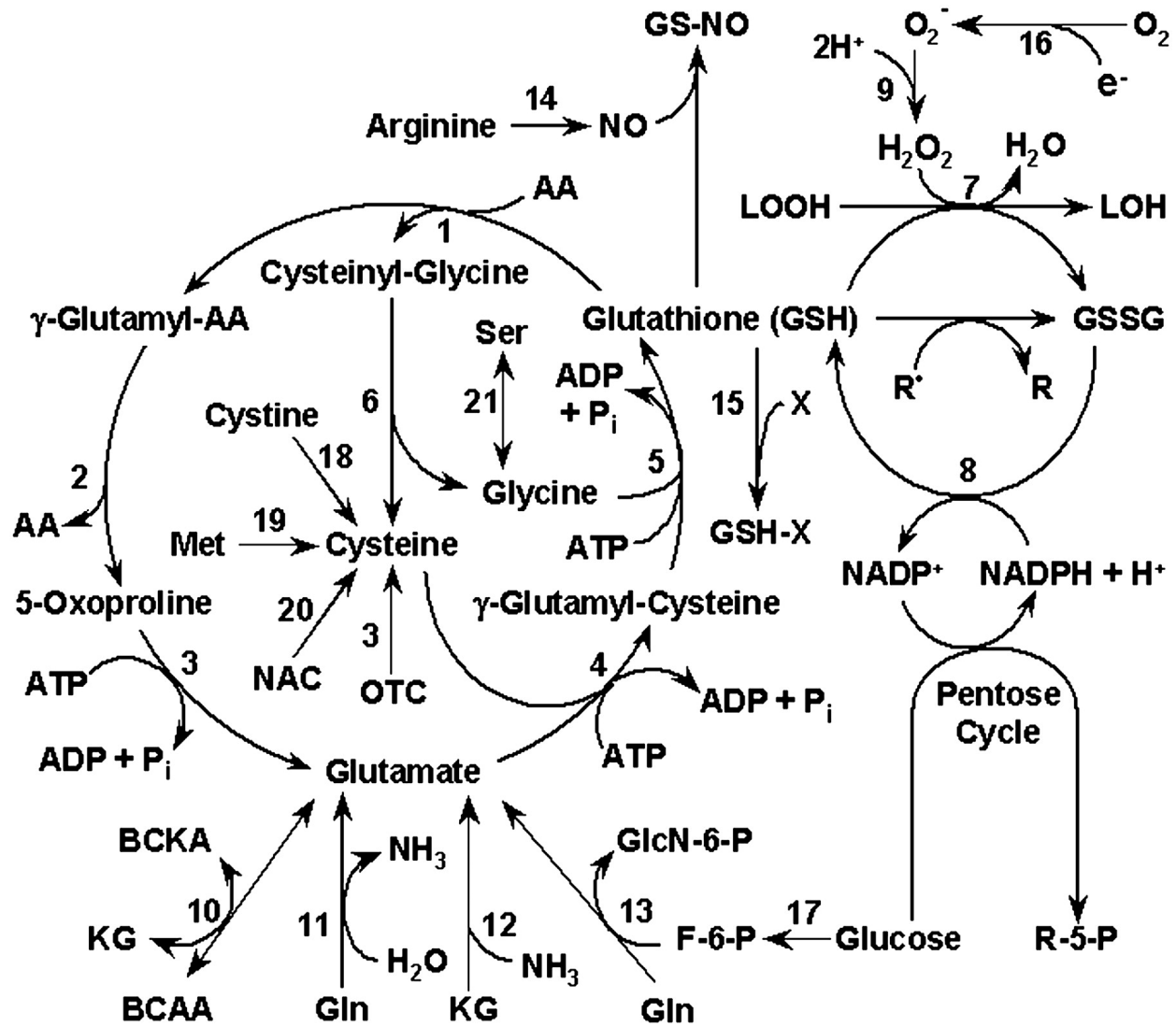
Figure 2. Glutathione synthesis and utilization in animals. Enzymes that catalyze the indicated reactions are: *1*) -glutamyl transpeptidase, *2*) -glutamyl cyclotransferase, *3*) 5-oxoprolinase, *4*) -glutamyl-cysteine synthetase, *5*) glutathione synthetase, *6*) dipeptidase, *7*) glutathione peroxidase, *8*) glutathione reductase, *9*) superoxide dismutase, *10*) BCAA transaminase (cytosolic and mitochondrial), *11*) glutaminase, *12*) glutamate dehydrogenase, *13*) glutamine:fructose-6-phosphate transaminase (cytosolic), *14*) nitric oxide synthase, *15*) glutathione *S*-transferase, *16*) NAD(P)H oxidase and mitochondrial respiratory complexes, *17*) glycolysis, *18*) glutathione-dependent thioldisulfide or thioltransferase or nonenzymatic reaction, *19*) transsulfuration pathway, *20*) deacylase, and *21*) serine hydroxymethyltransferase. Abbreviations: AA, amino acids; BCKA, branched-chain -ketoacids; GlcN-6-P, glucosamine-6-phosphate; GS-NO, glutathione-nitric oxide adduct; KG, -ketoglutarate; LOO·, lipid peroxyl radical; LOOH, lipid hydroperoxide; NAC, *N*-acetylcysteine; OTC, L-2-oxothiazolidine-4-carboxylate; R·, radicals; R, nonradicals; R-5-P, ribulose-5-phosphate; X, electrophilic xenobiotics. (Taken from reference [1]).

The second enzyme, GS, necessary for *de novo* biosynthesis of GSH is responsible for the addition of glycine to γ-glutamyl-cysteine produced by GCS to form GSH, γ-glutamyl-cysteinyl-glycine [16]. The availability of glycine – the last amino acid for the complete synthesis of GSH – may be reduced in response to protein malnutrition, sepsis, and inflammatory stimuli [44, 45].

1.1.3 Role of Glutathione in Heme Biosynthesis

GSH has proven to exhibit a profound role in the cellular oxidative stress, its deficiency or decrease in the cellular concentrations has been associated with various cellular diseases, and its *de novo* biosynthesis from glutamate, cysteine, and glycine occurs in the cytosol. Besides, GSH functions in the production of heme because of its role in iron metabolism [46]. The terminal step in heme biosynthesis is chelation of iron by protoporphyrin [47]. Iron (II) reacts with porphyrin to form hemes, whereas Fe(III) does not under nonreducing conditions; however, GSH activates the formation of heme from Fe(III) and porphyrin by reducing Fe(III) to Fe(II) [48-50]. Heme formation from Fe(II) is inhibited by GSH [51] because it competes with the porphyrin for Fe(II) [52]. If peradventure, iron dechelates from the heme as a consequence of oxidation to Fe(III), then GSH would be able to reduce the "free iron" and solubilize it so that heme could be readily reconstituted [52].

1.2 Cysteine

Cysteine (CSH) is a sulfur-containing amino acid which possesses thiol (−SH) functionality (Figure 3A). It is a component of glutathione; thus, functions as a cellular

antioxidant. It is readily oxidized to its disulfide form, cystine (CSSC) (Figure 3B), in oxygenated cellular solutions [1]. The plasma concentration of cysteine (10-25 µM) is lower than that of cystine (50-150 µM) [1]. Cysteine and cystine are transported by distinct membrane carriers, though cells efficiently transport one more than the other [18]. Certain cells have little or no ability for direct transport of extracellular cystine. However, GSH that moves from the liver can reduce cystine to cysteine on the outer cell membrane, so that cysteine can be absorbed. Whereas, other cells can absorb cystine and reduce it intracellularly to cysteine (Figure 2) [1].

The cysteine/cystine redox pair is a ubiquitous buffering redox couple [28, 53]. The redox potential of cysteine is reported as -0.245 V (vs. NADP$^+$/NADPH) [29]; thus, cellular reducing conditions normally favor the presence of cysteine in animal cells [1]. Cysteine consists of three pH-active functional groups: carboxylic, thiol, and ammonium groups. The pK_a of the thiol is 8.30 [54]. The cysteine disulfide, cystine, has four ionizable groups (two amino and two carboxylic groups). The redox modulation of cysteine containing proteins results in the formation of intra- and intermolecular disulfide bonds. These modifications can activate or inactivate proteins due to the changes in the conformation of the protein binding sites [55].
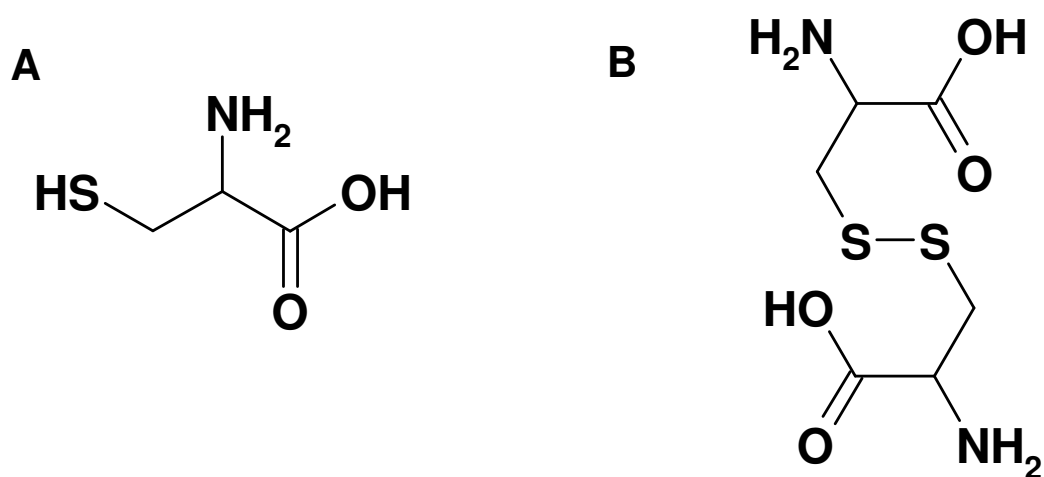
Figure 3. Structures of cysteine, A (CSH) and cystine, B (CSSC).

Studies have recently supported the view that cysteine may be the limiting amino acid for the biosynthesis of GSH in humans [39-41]. However, cysteine may be biosynthesized in various ways in the cell as shown in Figure 2. Besides, increase in the supply of cysteine or its precursors (e.g., cystine, *N*-acetyl-cysteine, and L-2-oxothiazolidine-4-carboxylate) via oral or intravenous administration will lead to increase in the cellular cysteine [2].

1.3 Homocysteine

Homocysteine (HCSH) is a homologue of naturally-occurring amino acid, cysteine, differing in that its side-chain contains an additional methylene ($-CH_2-$) group before the thiol (Figure 4). Also, its similarity to the protein amino acid, methionine, enables it to enter the protein biosynthesis [13]. However, HCSH cannot complete the

protein biosynthetic pathway and is edited by conversion to HCSH-thiolactone, a reaction catalyzed by methionyl-transfer RNA synthetase [13]. HCSH has been known a risk factor for cardiovascular disease and stroke in humans [13-15]. The toxicity of which has been ascribed to the formation of HCSH-thiolactone (tHCSH), which was shown to acylate protein lysine side chains in an irreversible manner [13, 56-59]. Nutrients, such as folic acid, vitamins B6 and B12 have been shown to involve in the pathways of HCSH degradation [14, 15].
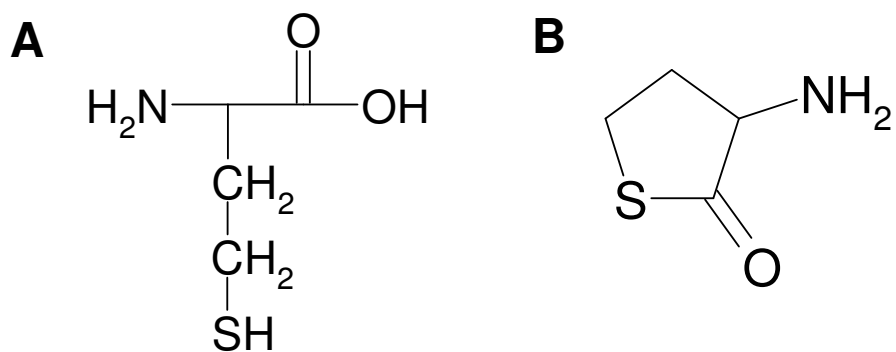
Figure 4. Structures of Homocysteine (A) and Homocysteine thiolactone (B).

Metabolism of Homocysteine: Metabolism of amino acid methionine, a limiting amino acid in the synthesis of many proteins, involves in the production of essential nutrients for the optimal functioning of the cardiovascular, skeletal, and nervous system [15]. Homocysteine is an intermediate product of methionine metabolism and is itself metabolized by two pathways (Figure 5): the re-methylation pathway which regenerates methionine, and the trans-sulfuration pathway which degrades HCSH into CSH and then taurine [15]. The re-methylation pathway is comprised of two intersecting biochemical pathways and results in the transfer of a methyl group ($-CH_3$) to HCSH by either methylcobalamin or betaine (trimethylglycine) [15].
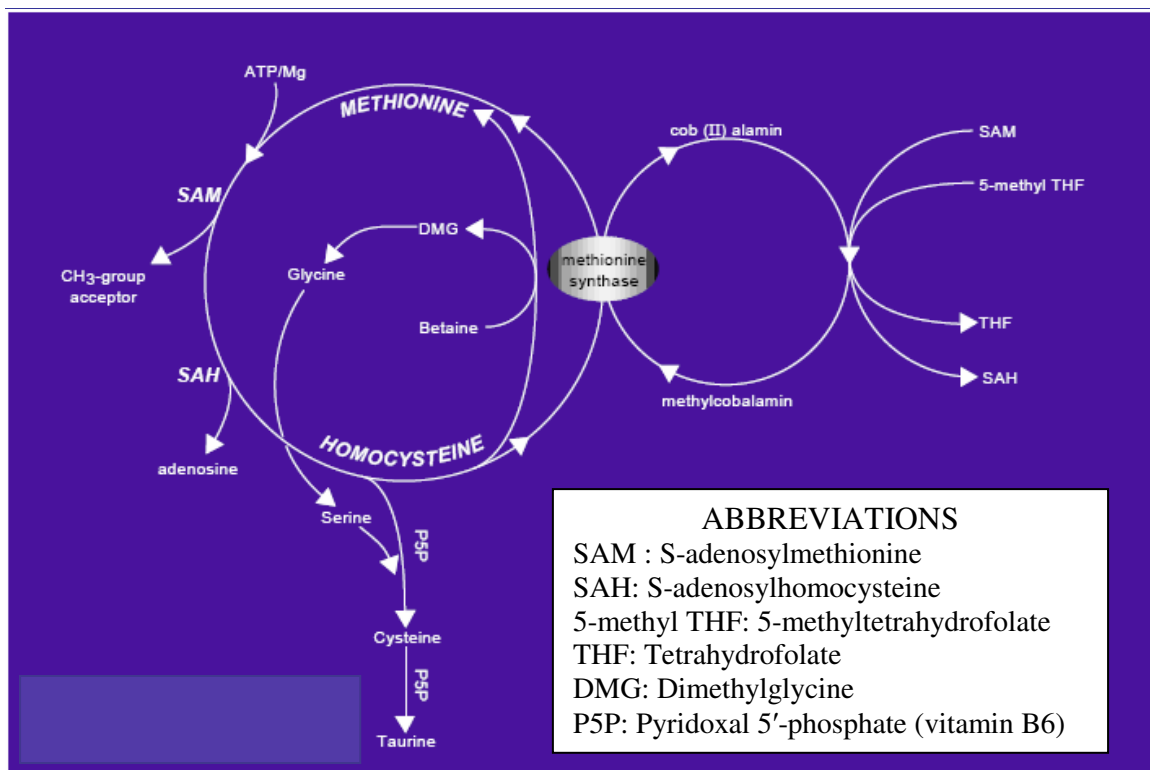
Figure 5. Homocysteine Metabolism. (Taken from reference [15]).

1.4 Oxidation of Glutathione (GSH)

Due to the significant role GSH plays in cellular systems during oxidative stress, and its association with various pathological conditions [1], many researchers have been interested in the study of glutathione chemistry [19-22, 60-80]. In addition, there has been interest in the determination of glutathione analytically in order to develop its analytical sensor [75-79, 81-84]. The works that have been done to understand the chemistry of glutathione have targeted the thiol functionality either through oxidation by an electrophile or reaction with a reactant to form a covalent bond. Both electrochemical and non-electrochemical methods have been used for this process and will be discussed.

1.4.1 Reaction with Metal Ions

GSH is a polydentate ligand, offering its potential binding sites, i.e., two carboxylate oxygens, an amino nitrogen, a sulfhdryl group, and two amide groups (Figure 1A) [46]. The structure of GSH is such that all its potential binding sites cannot be simultaneously coordinated to the same metal ion and consequently its coordination chemistry is characterized by the formation of protonated and polynuclear complexes [23, 24]. The oxidation of GSH by O_2 is catalyzed by traces of metal ions such as Cu(II), Fe(III), Co(II), Mn(II), and Cr(IV). The simultaneous reduction of the metal ion alters its reactivity with cellular components [23, 46]. The coordination chemistry of GSH is of vital importance as it serves as a model system for the binding of metal ions by larger peptide and protein molecules, and that metal-GSH complexes are involved in the toxicology of several metals [85, 86]. Because of the high affinity of sulfur for many metals, GSH may be involved in their uptake and excretion [85, 86]; and almost certainly

will be involved in their intracellular coordination chemistry (for reviews, see [23, 24]). Only three of the metal ions will be discussed below.

Copper: The complexation of Cu(II) by GSH may be involved in the metabolism of both Cu(II) and GSH [86, 87]. The hemolytic anemia [9-12] that typically accompanies copper toxicity is usually accounted for by Cu(II) catalyzed oxidation of GSH and by inhibition of glutathione reductase [86, 88-90]. Both interactions reduce the ability of GSH to protect the cells from damage by reactive oxygen species generated in the cellular processes [23].

It is complicated to characterize the complexation of Cu(II) by GSH because of the ease with which it catalyzes the oxidation of sulfhydryl groups [91, 92]. Spectrophotometric studies have been performed, which indicate that at Cu:GSH ratios less than 0.5, all the copper is associated with the sulfhydryl group, possibly as GSCuSG, while some Cu is associated with the peptide bonds at higher ratios [93]. In solutions of GSH and Cu(II), similar conclusions have been reached with the use of ^{1}H NMR [23]. The equation 2 below gives the reaction stoichiometry of the reduction of Cu(II) to Cu(I) by GSH [36]:

$$2Cu(II) + 2GS^- \rightleftharpoons 2Cu(I) + GSSG \qquad (2)$$

Iron: Oxidation of GSH by Fe(III) and iron-catalyzed oxidation of GSH by molecular oxygen have been studied, and the nature of the Fe-GSH interactions in both reactions has been investigated [49, 50, 52, 94, 95]. Mössbauer spectroscopy and fast-reaction kinetic techniques have been used for the study of GSH oxidation by Fe(III) [95]. Under anaerobic conditions, GSH reduces Fe(III) to Fe(II) (Equation 3).

In this reaction, complex formation and electron transfer are thought to be involved in the overall mechanism (Figure 6) [95]. Stopped-flow kinetic experiments have shown that there are rapid initial binding and electron transfer leading to the blue intermediate (complex I), and that the rate limiting step in the second-order process is the formation of the complex. In the step 2, the blue intermediate complex decays to the final product, in which the iron was determined on frozen solutions to be Fe(II) by Mössbauer spectroscopy. Since GSH is the reducing species, the other product was assumed to be GSSG [49].

$$2Fe(III) + 2GS^- \rightleftharpoons 2Fe(II) + GSSG \qquad\qquad (3)$$
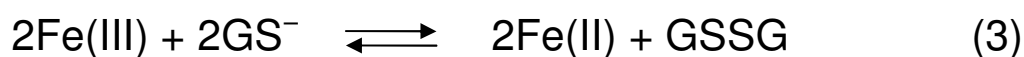
The overall reaction for the iron-catalyzed oxidation of GSH by molecular oxygen is shown in Equation 4. The first step involves the reaction of Fe(III) with GSH to produce Fe(II), which then forms a complex with another molecule of GSH. This Fe(II)−GSH complex reacts with oxygen to form a red complex that undergoes an autocatalytic oxidation of the thiol [50].

$$2GS^- + O_2 + 2H^+ \longrightarrow H_2O_2 + GSSG \qquad\qquad (4)$$
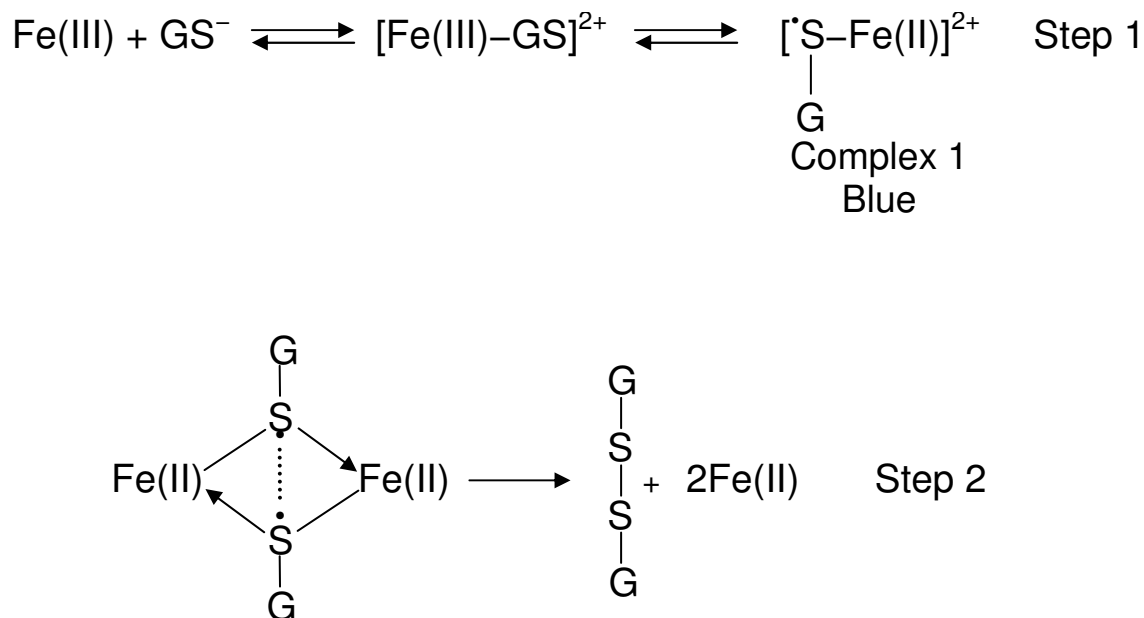
Figure 6. Reaction scheme proposed for the oxidation of GSH by Fe(III). (Taken from reference [50])

Platinum: A good example of a Platinum (Pt) compound that reacts with GSH is *cis*-Dichlorodiammineplatinum (II) (cisplatin), which is a widely used chemotherapeutic agent towards human tissues [96]. Its two chloro ligands are relatively labile and can be replaced by water molecules or hydroxide ions. Platinum (II) is a "soft" Lewis acid and as a result is expected to have a high affinity for sulfur ligands. There have been reports of cisplatin reaction with GSH and other sulfur-containing molecules [97-100]. In a study performed with a solution containing GSH:Pt(II) ratio of 2:1, a complex with a GSH:Pt(II) ratio of 2:1 was obtained [98]. The investigation of the complex with infra red (IR) spectrophotometer showed no SH band, which is indicative of the formation of a Pt−S bond. Elemental analysis showed that all four of the original ligands in cisplatin

have been displaced. GSH in this reaction with cisplatin coordinates as a bidentate ligands, chelating to Pt(II) via its sulfur and the amide nitrogen of the glutamyl residue. It is postulated that coordination of Pt(II) to sulfur at a site vacated by a chloro ligand labilizes the trans ammine ligand, facilitating the binding of the second GSH ligand. The proposed complexation reactions and the binding scheme proposed for the bis complex are shown in Figure 6 [98].

Cisplatin (I)   Glutathione (II)   Complex (III)

Glutathione (II)   +   Complex (III)
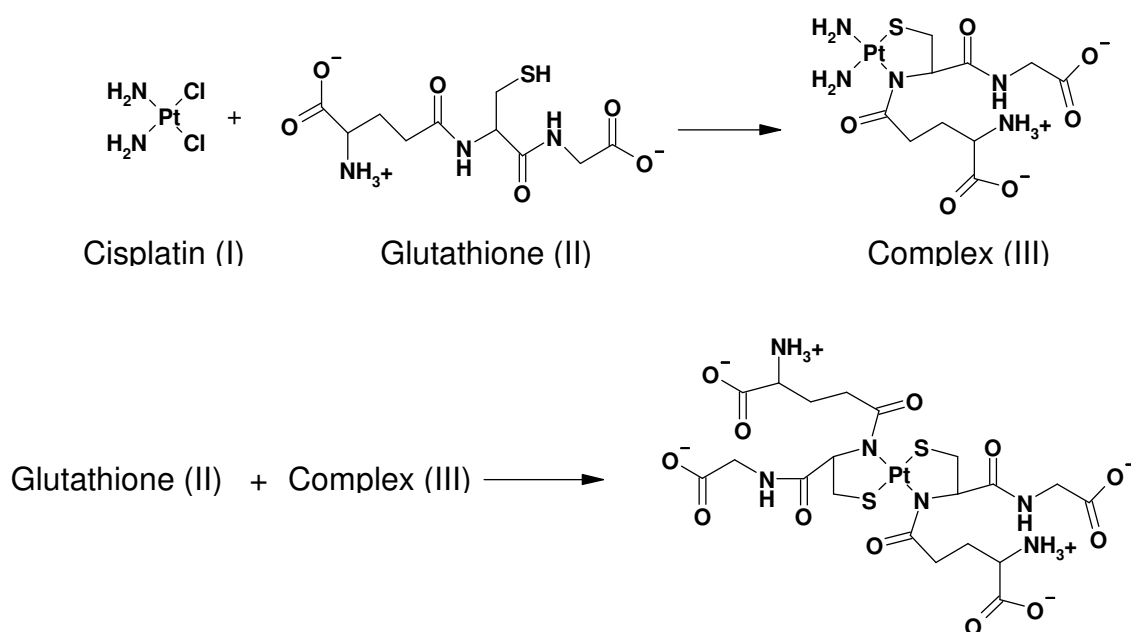
Figure 7. Reaction scheme proposed for the complexation of GSH by cisplatin. (Taken from reference [98])

1.4.2 Reaction with Radicals

Non-electrochemical methods for the study of GSH chemistry have been done by reaction with radicals [20, 22]:

Chlorine Dioxide Radical: The chlorine dioxide radical ($ClO_2^\bullet$) is a powerful one-electron oxidant known for its proclivity to oxidize inorganic [101-104] and organic

species [105]. The oxidation of GSH by $ClO_2^{\bullet}$ has been studied under pseudo-first order conditions with excess GSH from pH 3.0−6.0 and μ = 1.0 M. It is reported that there is decay of $ClO_2^{\bullet}$ in the presence of GSH as observed at 359 nm, which indicates the oxidation of GSH by $ClO_2^{\bullet}$. There is a linearity of the first-order rate constant with increasing substrate concentration at constant pH. It was suggested that a sharp increase in the observed rate constant will ensue with increasing the pH due to the formation of the reactive glutathione anion (GS^-) by deprotonation of the thiol [22]. Equations 5−7 are used to describe the $ClO_2^{\bullet}$ oxidation of GSH. The rate-determining step (Equation 6) is an electron transfer from GS^- to $ClO_2^{\bullet}$ to form $GS^{\bullet}$ and chlorite (ClO_2^-). Equation 7 involves a rapid coupling reaction between the $GS^{\bullet}$ and a second equivalent of $ClO_2^{\bullet}$ [22]. Thiol group of GSH is reported to be the target of $ClO_2^{\bullet}$ based on similarity between the second-order rate constants in the $ClO_2^{\bullet}$ oxidation of GSH and CSH [22].

Oxidation of GSH by chlorite (ClO_2^-) was described to show similar behavior as the ClO_2^- oxidation of CSH [22]. Though ClO_2^- can oxidize GSH, but that is approximately six orders of magnitude slower than the reaction of $ClO_2^{\bullet}$ with GSH as observed. This study [22] that the reactivity of S−H group decreases above pH 7.0, under pseudo-first order conditions with GSH in excess, as the pK_a value of the S−H group is approached.

$$GSH \rightleftharpoons GS^- + H^+ \qquad (5)$$

$$GS^- + ClO_2^{\bullet} \rightleftharpoons GS^{\bullet} + ClO_2^- \qquad (6)$$

$$GS^{\bullet} + ClO_2^{\bullet} \xrightleftharpoons{fast} product \qquad (7)$$
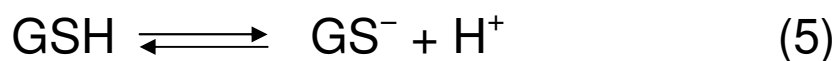
Hydroxyl and thiyl Radicals: The generation and reactivity of some of the free radicals produced have been studied by pulse radiolysis [106-108]. Most of these studies have focused on the formation (e.g., by reaction with $^\bullet$OH radicals) and the reaction of the formed thiyl radicals, RS$^\bullet$. The suggested predominant reaction mechanisms in these studies are due to either (a) hydrogen transfer from the thiol to organic free radicals, R$^{1\bullet}$, and/or (b) competition between thiol and organic molecules for the oxidizing $^\bullet$OH radicals, which means, competition among reactions in the Equations 8, 10, and 13.

$$RSH + {}^\bullet OH \longrightarrow RS^\bullet + H_2O \qquad (8)$$

$$RSH + OH^- \rightleftharpoons RS^- + H_2O \qquad (9)$$

$$RS^- + {}^\bullet OH \rightleftharpoons RS^\bullet + OH^- \qquad (10)$$

$$RS^\bullet + RS^- \rightleftharpoons RSSR^- \qquad (11)$$

$$R^{1\bullet} + RSH \rightleftharpoons R^1H + RS^\bullet \qquad (12)$$

$$R^1H + {}^\bullet OH \rightleftharpoons R^{1\bullet} + H_2O \qquad (13)$$

A weak transient absorption found in the region of 300-400 nm, with a rising absorption below ~300 nm in the reaction of $^\bullet$OH with GSH were said to be produced via reaction 8 and thus, assigned to the thiyl (RS$^\bullet$) radicals [20]. The rate of the thiyl radicals decay (1.5×10^9 M^{-1}s^{-1}) was found to be relatively high to produce presumably RSSR [20]. The studies on the reaction of thiyl radicals with RSH and RS$^-$ have been performed, and thiyl radicals produced via reactions 8 and 10 react with RS$^-$ to produce RSSR$^-$ according to Equations 11 and 14.

$$RS^{\bullet} + RSH \rightleftharpoons RSSR^{-} + H^{+} \qquad (14)$$

The rate constant for the reaction of thiyl radicals with RSH was evaluated by monitoring the formation of the 410 nm band under pH conditions where either RSH or RS^{-} is the predominant species. In alkaline solution where >90% of the RSH is present as RS^{-}, $k(RS^{\bullet} + RS^{-}) > 10^9$ $M^{-1}s^{-1}$, except in the case of GSH, amongst other thiols [20]. The reason for this was explained in part on the basis of the overall charges of the $RS^{\bullet}$ and RS^{-} species. For example, cysteamine, for which the $RS^{\bullet}$ and RS^{-} charges are 0 and −1, respectively, exhibits the highest rate $(8.0 \times 10^9$ $M^{-1}s^{-1})$ while GSH $(6.2 \times 10^8$ $M^{-1}s^{-1})$, for which the corresponding charges are −2 and −3, is more than an order of magnitude slower [20].

1.4.3 Electrochemical Reaction of Glutathione

The use of electrochemical methods for the analysis of GSH is a more attractive option because they are inexpensive, highly sensitive, and have long-term reliability and reproducibility. The electrochemical detection of sulfur-containing compounds has been investigated using carbon, platinum, mercury, and gold as working electrodes [110-113]. Different electrochemical techniques have been employed in the electroanalysis and determination of GSH as discussed below.

Modified Electrodes: Direct electrochemical oxidation of GSH at conventional electrodes is slow [76, 114], and strong adsorption is inherent; therefore, the use of modified electrodes has been employed. Examples of these modified electrodes are

boron-doped diamond (BDD) [82, 115] and well-aligned carbon nanotube (CNT) [76] electrodes. Other types of modified electrodes for the oxidation of GSH and other thiols, can also be obtained from these references [75, 77, 79-81, 84, 116-119].

BDD is a thin film, a new material, which has many physical and electronic properties [82]. The use of BDD as an electrode substrate is due to its four main properties: wide potential in aqueous solutions [120], low background currents [121], long term stability [122], and low sensitivity to dissolved oxygen [123, 124]. BDD was shown to be better than glassy carbon electrode (GCE) for its low and stable background current [82]. BDD has been described to be non-polar, and suffers less adsorption of polar molecules [125]. The electrooxidation of GSH showed that peak potential shifted positively with increasing sweep rate and the current response was linear with the square root of the scan rate. Tafel plot revealed that the reaction involves one electron transfer, and it is the rate determining step (RDS) [82].

Carbon nanotubes (CNTs) are new carbon materials which have been given much attention due to their nanometer size and interesting versatility, such as, nanobioelectronics [126] and biosensors [127]. CNTs have been utilized as electrodes to promote the electron transfer reactions of a wide range of biological species [128-131]. In the electrochemical oxidation of GSH, there is no observed oxidation peak at GCE, but there is at CNTs. Overview, CNTs have provided fast response time (within 5 s), high sensitivity (254.8 nA cm^{-2} μM^{-1}) and low detection limit (0.2 μM) [76].

Bare Electrodes: Oxidation of GSH, including thiols, does not occur readily at some unmodified conventional electrode surfaces without the use of homogeneous mediator. The oxidation of biological thiols by vanadium and ruthenium compounds as

solution mediators has been reported [83]. The vanadium compound (Amavadine) was said to be an effective mediator for thiols in aqueous solution at glassy carbon electrode, while ruthenium compounds in DMSO [83]. In each case, the thiol is oxidized at the potential of the mediator itself.

GSH has been oxidized at GCE in aqueous solution by amavadine, yielding enhancement in the anodic current and a correspondingly decrease in cathodic current of the mediator. This suggests a catalytic cycling of the mediator – the evidence of a true effect of a mediator. The oxidation peak of GSH at the bare GCE was not observed. It can be said that the applied potential at which GSH is oxidized can be adjusted by the choice of mediator. Besides, the oxidation of cysteine (CSH) at unmodified GCE has been reported with octacyanomolybdate (V) and (ferrocenylmethyl)trimethylammonium in aqueous solutions [114, 132].

1.5 Proton-Coupled Electron Transfer

Proton-coupled electron transfer (PCET) where proton and electron transfers involve different molecular centers is of much active attention [133-144], as it is important in a variety of chemical and biological processes [145, 146]. These reaction processes can occur by concerted or stepwise mechanisms. The stepwise mechanism includes initial proton transfer followed by electron transfer (PT/ET), and initial ET followed by PT (ET/PT). It has been suggested that reactions in which proton and electron transfers occur in one single kinetic step be termed "concerted proton electron transfer" (CPET) [140]. Concerted mechanism in this context means that the reactants proceed to products without the formation of a reaction intermediate. This definition is

illustrated by the square schemes in Figure 8 (GSH is given as an example), where horizontal lines refer to proton transfer (PT) and the vertical lines to electron transfer (ET). CPET is a diagonal process, and is to be contrasted with stepwise pathways (PT/ET, Red; ET/PT, Blue) that involve mechanistically distinct ET and PT steps with an intermediate [133, 134]. The definition of PCET has been made to encompass both hydrogen atom transfer (HAT) and other kinds of concerted electron/proton transfers [133, 134].
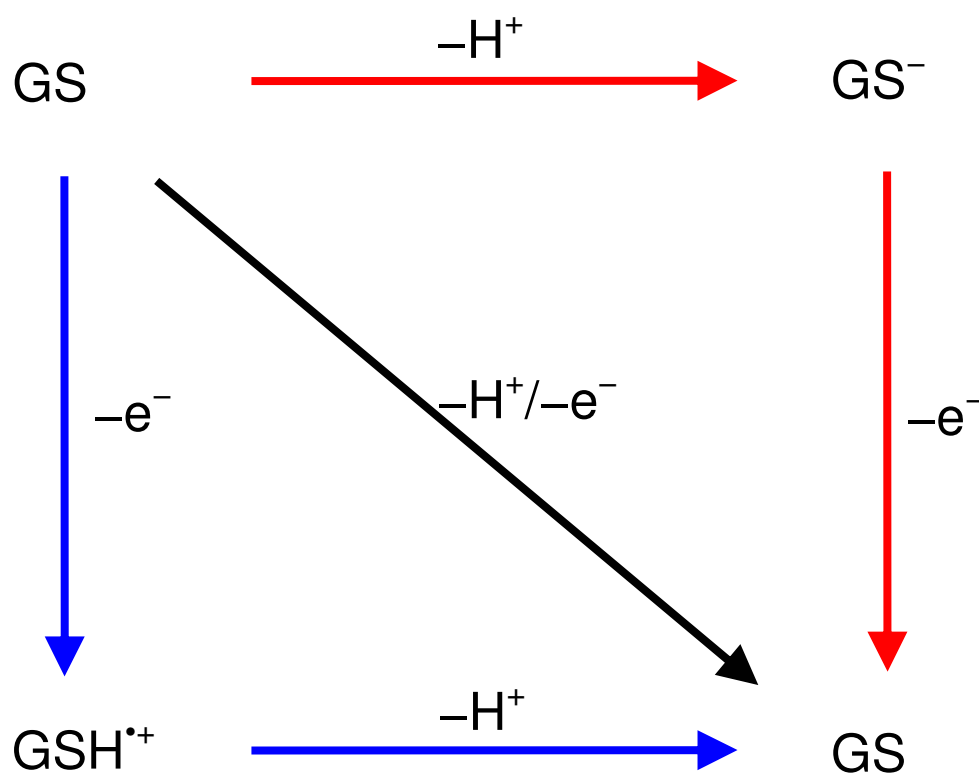
Figure 8. Square scheme for the CPET, PT/ET and ET/PT.

Explanation for CPET has been given that in most practical situations where CPET occurs within an intermolecular hydrogen-bonded complex, the proton activation barrier is significant, i.e., much higher than the proton vibrational ground state. In most cases, the resonance energy is small compared to the proton activation barrier. While a proton is heavier than an electron, the proton is light enough to tunnel through this significant barrier (Figure 9) [141]. Studies on distinguishing CPET from ET/PT or PT/ET have been reported based on reactions in both H_2O and D_2O [133, 134, 140, 141]. Depending on the oxidant and substrate, the kinetic isotope effect is said to be above 1.6 [133, 140].
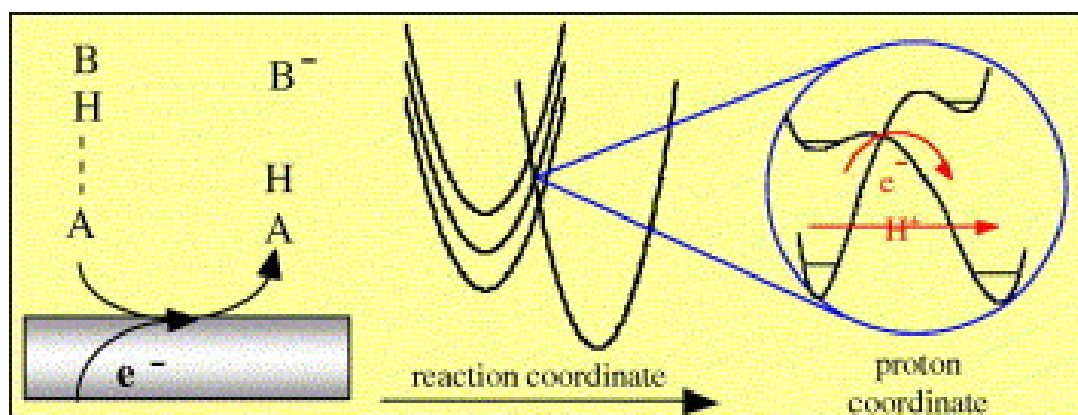
Figure 9. Potential energy profile for electrochemical CPETs. (Taken from reference [141])

1.6 General Acid/Base Catalysis

Proton transfer catalysis by Brønsted acids and bases is a recurring theme in organic reaction mechanisms [147-153]. Considerable interest has been given to this form of catalysis in physical organic chemistry for its mechanistic role. The simplest Brønsted species, H_3O^+ and OH^-, are termed *specific* catalysts and the rest, generally donated HA and A^-, are termed *general* [147]. The relationship between the effectiveness of an acid catalyst and its catalyzed rate constant is described by the Brønsted equation, the original free energy relationship [148]. The acid (HA) form of the Brønsted equation is usually given in its logarithmic form,

$$\log k_{HA} = \alpha \log K_{HA} + b \quad (15)$$

k = rate constant of the catalytic step,

K_{HA} = dissociation constant of the acid, HA,

α = Brønsted coefficient (normally $0 \leq \alpha \leq 1$). α indicates the sensitivity of the

catalytic step for changes in the strength of the acid, HA (pK_a).

A plot of log k_{HA} against log K_{HA} gives a slope of α; α indicates to what extent a proton is transferred from the acid to the substrate in the transition state:

α = 1: Every change in acid strength fully affects catalysis. The proton is (almost) completely transferred to the substrate in the transition state.

α = 0: The reaction is insensitive to changes in acid strength. All acids catalyze the reaction equally strongly (log k_{HA} = constant). The proton is hardly transferred in the transition state of the reaction.

α = 0.5: The proton is transferred halfway between the acid anion A⁻ and the substrate in the transition state (TS): A⁻····H⁺····S, symmetrical TS.

There is also a Brønsted relation for general base catalysis (GBC):

$$\log k_B = -\beta \log K_{HB}{}^+ + b \qquad (16)$$

The Brønsted coefficient, β, has the same meaning as α for general acid catalysis (GAC). Here are a few references for general base catalysis [149-153]. Figure 10 gives an example of the mechanism of general base catalysis in the oxidation of GSH by $IrCl_6{}^{2-}$.
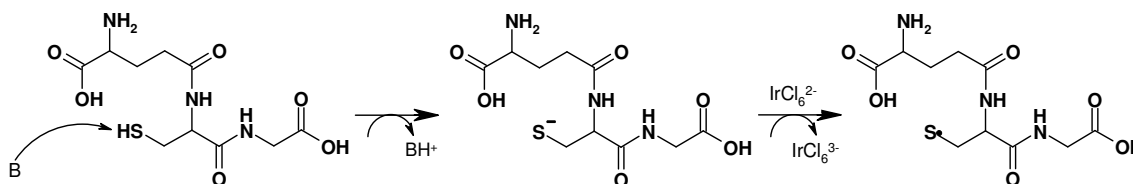
Figure 10. General base catalysis of glutathione oxidation by potassium hexachloroiridate (IV).

1.7 Electrochemical Method: Cyclic Voltammetry

Cyclic voltammetry is a versatile electroanalytical technique used in electrochemistry for the study of nonelectroactive species in a coupled reaction. Its versatility and ease of use have rendered it useful in electrochemistry, inorganic chemistry, organic chemistry, and biochemistry [154]. Furthermore, it can be used to investigate electrode surfaces, adsorption process on electrode surfaces, complicated electrode reactions, and to determine the mechanism and rates of electron transfer [155a-c].

1.7.1 Electrochemical Oxidation of Ru(bpy)$_3$$^{2+}$

Figure 11 shows the voltammetric response obtained for the electrochemical oxidation of

1.0 mM Ru(bpy)$_3$$^{2+}$ to Ru(bpy)$_3$$^{3+}$ and corresponding reduction of Ru(bpy)$_3$$^{3+}$ to

Ru(bpy)$_3$$^{2+}$ at glassy carbon electrode (area = 0.06 cm^2), with Pt-wire acting as counter

electrode and Ag/AgCl as reference electrode. A typical electrochemical cell is shown in

Figure 12. At the start of the scan (0.80 V), only nonfaradaic current flows, that is, no

electron is transferred from the Ru(bpy)$_3$$^{2+}$ to the electrode. As the electrode potential

goes above ~0.95 V, the oxidation of Ru(bpy)$_3$$^{2+}$ to Ru(bpy)$_3$$^{3+}$ begins and current starts

to flow. As the potential continues to grow more positive, the current increases as a result

of decrease in the surface concentration of Ru(bpy)$_3$$^{2+}$, until the Ru(bpy)$_3$$^{2+}$ concentration
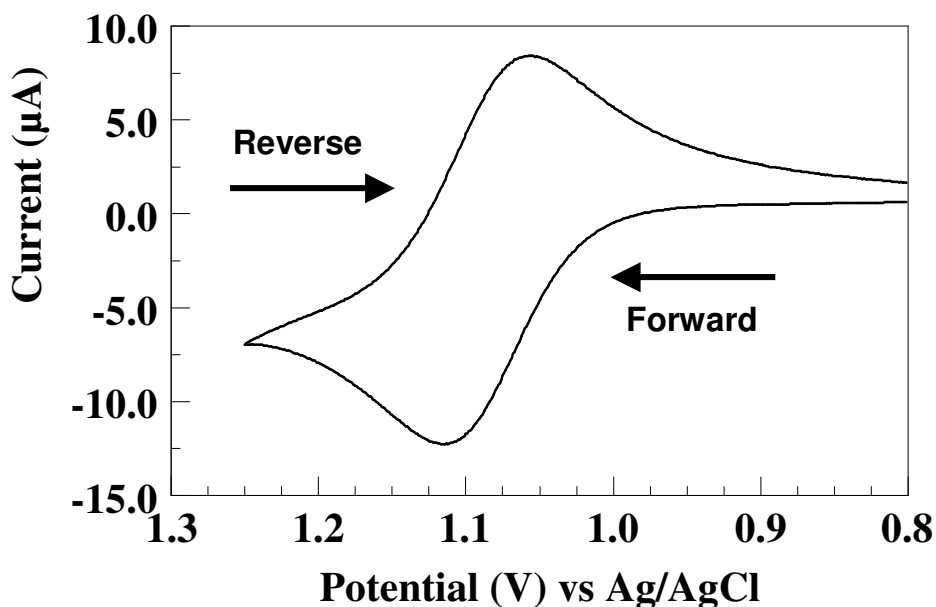
Figure 11. Cyclic voltammogram (CV) of 1.0 mM Ru(bpy)$_3$$^{2+}$ in 50 mM PBS/0.1 M NaCl, pH 5.0 at 100 mV/s. Glassy carbon working electrode (0.06 cm^2), Pt-wire counter electrode, and an Ag/AgCl reference electrode. CV is background subtracted.

at the surface drops nearly to zero. At this point, an anodic current flows and peaks at ~1.12 V. The scan is reversed at 1.25 V, and a large concentration of reducible $Ru(bpy)_3^{3+}$ in the electrode's vicinity begins to be reduced.

$$Ru(bpy)_3^{2+} \rightleftharpoons Ru(bpy)_3^{3+} + e^- \qquad (17)$$

As the potential in the reversed scan grows more negative, the reduction of $Ru(bpy)_3^{3+}$ back to $Ru(bpy)_3^{2+}$ is favored. At this point, a cathodic current flows and peaks at 1.06 V. From the CV, the $E_{1/2}$ is 1.09 V and the voltammetry is reversible with $\Delta E_p = 59$ mV. Equation 17 illustrates the reaction mechanism.

Figure 12. Typical three electrode cell.

2.0 ELECTROCATALYTIC OXIDATION OF GLUTATHIONE BY TRIS(2,2′-BIPYRIDYL)DICHLORORUTHENIUM (III) HEXAHYDRATE

2.1 Introduction

The biological importance of glutathione (GSH) and its mechanism of oxidation during cellular oxidative stress bring about interest in its electroanalysis. This work reports the kinetic modulation of homogenous proton-coupled electron transfer in the mediated oxidation of naturally occurring thiols, glutathione (GSH) and cysteine (CSH) by electrogenerated $Ru(bpy)_3^{3+}$, on glassy carbon electrodes in aqueous solution. Two different kinetic regimes were discovered by varyin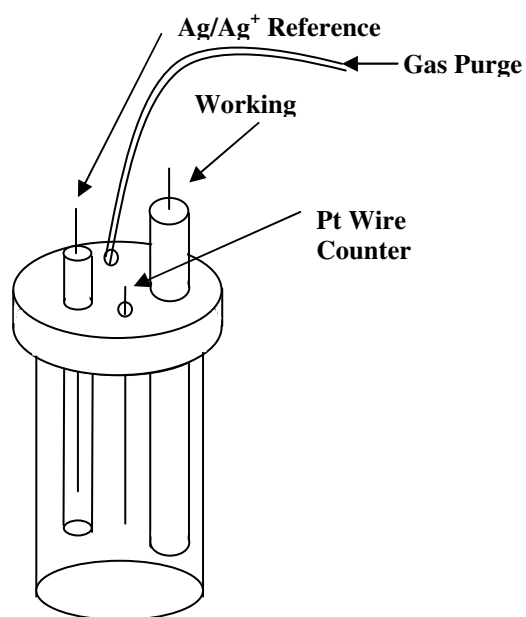g the pH and/or the pKa of the buffer acting as the proton acceptor. The evidence indicates that in the first regime, when no "suitable" proton acceptor is available other than H_2O, the mediated oxidation of GSH and CSH is dominated by a *concerted* (CPET) pathway. In the second regime, the presence of a base with a suitable pK_a, allows the voltammetric response to be controlled by what is suggested as a *stepwise* pathway (PT/ET) mechanism. The most significant and unique aspect of this work in comparison to previous research on PET [133, 135-138, 140, 142, 143] is that the two major mechanisms that appear to control the proton-electron transfer (PET) for these thiols, can be studied individually because their voltammetric features are conspicuously different. The evidence that is presented herein to support the claim of discriminating CPET from PT/ET in the mediated oxidation of GSH and CSH by electrogenerated $Ru(bpy)_3^{3+}$ is: i) By maintaining a constant pH but changing the base/acid components ($HPO_4^{2-}/H_2PO_4^-$ and $[OHCH_2]_3CNH_3OH/[OHCH_2]_3CNH_3Cl$) of the buffering medium, the rate constant for the oxidation of RSH by $Ru(bpy)_3^{3+}$ showed a huge increase due to the mediated
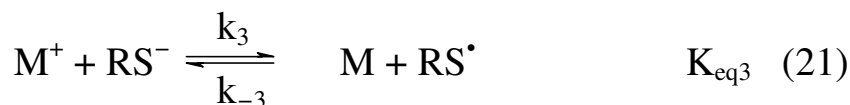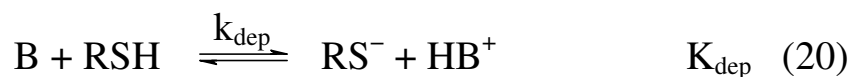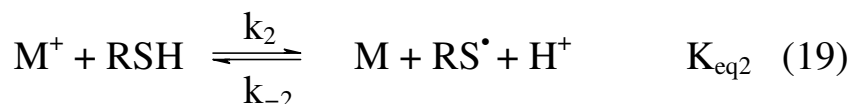
oxidation of these thiols at less positive potentials, when the dominant mechanism switched from CPET to PT/ET. ii) When performing the experiments by adjusting the pH using strong base or acid without a buffer, the CPET dominates.

Overall, the kinetic behavior found in the RSH-Ru(bpy)$_3$$^{3+}$ system, shares common features with the *general base catalysis* documented in many chemical and biochemical reactions that are catalyzed by Brønsted acids and bases [149-153, 156]. In such cases, the reaction rate is dependent on the concentration of a component of the buffer and the catalytic effect can be detected by doing rate measurements at different buffer concentrations and constant pH around the pK_a of the buffer [147, 157]. The deprotonation of thiols by Brønsted bases has also been reported as a case of *general base catalysis* in different chemical and biochemical oxidations of thiols [149, 157, 158]. The results presented here are also related to the electrocatalytic oxidation of tyrosine recently reported by Meyer and Thorp, in which parallel competing pathways of CPET and PT/ET were proposed to occur in the presence of proton acceptors with different pK_a's [135].

The oxidation of certain biomolecules such as nucleic bases, amino acids and other complex organic electron donors has been conveniently studied via redox mediation with metal complexes such as Ru(bpy)$_3$$^{2+}$ at different electrode surfaces [137, 159-161]. Ru(bpy)$_3$$^{2+}$ undergoes a one-electron reversible oxidation with rapid heterogeneous kinetics (0.06 cm/s) at many electrodes and has a relatively high redox potential (~1.0 V vs. NHE) which makes it an effective redox mediator [159, 161]. In this work, electrogenerated Ru(bpy)$_3$$^{3+}$ at glassy carbon electrodes was used (Equation 18, Scheme 1) to drive the homogeneous oxidation of GSH and CSH (Equation 19) that produces

protons and thiyl radicals which eventually dimerize into the corresponding disulfide (Equation 20) [29, 60, 162]. Direct oxidation of the thiols at the electrode has very slow kinetics (see below).

Reaction 19 entails the transfer of a proton and an electron from the RSH group to two different molecular sites. The proton is taken by a base, which can be the solvent or any other proton acceptor present in solution, and the electron goes to the oxidizing agent $Ru(bpy)_3^{3+}$, generated at the electrode. Both concerted and stepwise pathways can be observed in the oxidation of RSH, as they have been found to compete in solution [138, 143, 163]. They seem to possess fairly distinctive kinetic characteristics [138, 143, 163], for instance, CPET has been suggested to be slower than the corresponding stepwise pathway because of the requirement to move the proton and electron in a concerted fashion through one kinetic step without intermediates [133, 138, 143, 163]. As a result,

$$M \underset{k_h}{\overset{E^{o\prime}}{\rightleftharpoons}} M^+ + e^- \tag{18}$$

$$M^+ + RSH \underset{k_{-2}}{\overset{k_2}{\rightleftharpoons}} M + RS^\bullet + H^+ \qquad K_{eq2} \tag{19}$$

$$B + RSH \overset{k_{dep}}{\rightleftharpoons} RS^- + HB^+ \qquad K_{dep} \tag{20}$$

$$M^+ + RS^- \underset{k_{-3}}{\overset{k_3}{\rightleftharpoons}} M + RS^\bullet \qquad K_{eq3} \tag{21}$$

$$RS^\bullet + RS^\bullet \overset{k_4}{\longrightarrow} RSSR \qquad K_{dim} \tag{22}$$

Scheme 1. Mechanisms of oxidation. RSH = GSH, CSH, or HCSH; B = Base; M = Metal complex.

kinetic isotopic effects of 1.6 and above have been attributed to CPET pathways [133, 136, 140, 142], whereas values around 1.0 have been taken as indicative of stepwise mechanisms, that is, the proton transfer is not involved in the RDS [136, 140, 142]. It has been suggested that biological systems might prefer the CPET route over the stepwise counterpart because the latter involves charged intermediates (Figure 8 [143, 164]) that can be reactive and are not favored in the low-dielectric environments of enzyme active sites. Preliminary data describing the modulation of kinetics for the electrochemical oxidation of these thiols using Brønsted bases are presented. The oxidation, which is mediated by electrogenerated $Ru(bpy)_3^{3+}$ at glassy carbon electrodes, is monitored by voltammetry and mechanistically evaluated using digital simulations with the commercial package DigiSim®.

2.2 Experimental Section

2.2.1 Reagents and Materials

$Ru(bpy)_3^{2+}$, L-glutathione reduced (99%), N-acetylmethionine (99%), D_2O (99.9%), and DCl (35%) were purchased from Aldrich (St. Louis, MO). Na_2HPO_4 (99%), NaH_2PO_4 (98%), and NaOH (97%) were purchased from EM Science (Cherry Hill, NJ). HCl (37.3%), L-cysteine, obtained as L-cysteine hydrochloride monohydrate (98.5%), tris(hydroxymethyl)aminomethane were purchased from Fisher Scientific (Fair Lawn, NJ). NaCl, 99+% and NaOD, 30 wt% solution in D_2O were purchased from Acros Organics (NJ, USA). Water was purified with a MilliQ purification system (Billerica, MA). All reagents were used without further purification. Na_2DPO_4 and NaD_2PO_4 were prepared by triply dissolving Na_2HPO_4 and NaH_2PO_4 in D_2O and evaporating solvent

[137], then confirming the isotopic purity by ¹HNMR. The pH of the sodium phosphate solutions was measured with standard pH meter, calibrated with H_2O buffers. pH meter readings for D_2O solutions were converted to pD values employing the equation pD = pH + 0.4 [29]. All solutions and subsequent dilutions were prepared using deionized water with a resistivity of 18.2 MΩ cm. All experiments were carried out in a solution volume of 10 cm^3 at room temperature, and deoxygenated with argon. The pH's of the buffer solutions were adjusted with NaOH and HCl; however, for deuterated buffer solutions, NaOD and DCl were used to adjust the pH.

2.2.2 Cyclic Voltammetry and Chronocoulometry

Cyclic voltammograms were collected using a biopotentiostat (CH Instruments, Austin, TX) with a cell equipped with a glassy carbon (GC) working electrode (area = 0.06 cm^2), a Pt-wire counter electrode, and Ag/AgCl reference electrode (3.0 mM KCl). Glassy carbon electrode was polished with 0.05 µm alumina and rinsed with copious amount of water between experiments. In a typical experiment, 1.0 mM metal complex and 5.0 mM L-glutathione/L-cysteine (reduced) were dissolved in 10 cm^3 aqueous solutions of 50 mM buffer/0.1 M NaCl, and 0.1 M NaCl. The potential was scanned from 0.80 V to 1.25 V. The experimental cyclic voltammograms were background subtracted and performed at room temperature. In the case of double step chronocoulometry, 1.0 mM metal complex was dissolved in 50 mM sodium phosphate buffer solutions, pH 5.0, containing 0.1 M NaCl. The initial potential was 0.9 V and the final 1.3 V. The pulse width was 0.25 sec.

2.2.3 Digital Simulation

Second-order cysteine and glutathione oxidation rate constants were determined by fitting the cyclic voltammograms to a mechanism involving Equations 18 and 19 from Scheme 1 (pH 5.0 sodium phosphate buffer, pH 7.0 tris/HCl buffer, and unbuffered solutions). The software package DigiSim version 3.03 (Bioanalytical Systems, Inc., West Lafayette, IN) was used to verify each mechanism at different scan rates by comparing the experimental and simulated CV's. The values of diffusion coefficients were 6.0×10^{-6} cm^2/s for Ru(bpy)$_3{}^{2+}$ [160], 5.0×10^{-5} cm^2/s for cysteine, and 3.0×10^{-5} cm^2/s for glutathione. All other simulation parameters are given in the figure captions and appendix. The heterogeneous electron transfer rate constant was determined by fitting the voltammogram of Ru(bpy)$_3{}^{2+}$ in the absence of cysteine or glutathione.

2.2.4 NMR and UV-Vis Spectroscopic Measurements

^{1}H NMR spectra were recorded at 300 MHz in deuteriated solutions of 50 mM sodium phosphate buffer, pH 5.0 and 9.0, with Varian Mercury 300 MHz spectrometer. The spectra of Ru(bpy)$_3{}^{2+}$ alone, cysteine alone, and titrations of cysteine into Ru(bpy)$_3{}^{2+}$ solutions at pH's 5.0 and 9.0 were recorded at room temperature. UV-Vis measurements were performed in a 1.0 cm quartz cell on a Hewlett−Packard 8453 spectrophotometer. The spectra of Ru(bpy)$_3{}^{2+}$ alone, cysteine alone, and titrations of cysteine into Ru(bpy)$_3{}^{2+}$ solutions at pH's 5.0 and 7.0 were recorded at room temperature.

2.3 Result and Discussion

Since direct oxidations of GSH and CSH have very slow kinetics at the electrode surface, the homogenous oxidation by $Ru(bpy)_3^{3+}$ as indicated in Equations 18 and 19, is usually referred to as electrocatalysis. The catalyst $Ru(bpy)_3^{3+}$ is produced in an electrochemical step (E) followed by a homogeneous chemical (C′) reaction that recycles the catalyst back to $Ru(bpy)_3^{2+}$, which in turn regenerates the catalyst on the electrode surface. In the context of electrochemical coupled reactions, this sequence is typically denoted as EC′ and the catalyst is also called mediator [165]. Figure 13 shows a series of CV's recorded in phosphate buffer 50 mM at pH 5.0. The CV response for a solution containing only GSH (Figure 13A) shows very low anodic current and the absence of any voltammetric peaks confirming the very slow kinetics for the direct oxidation of GSH at the electrode surface. As expected for a reversible redox couple like $Ru(bpy)_3^{2+}$ (Figure 13B), the separation of anodic and cathodic peak potentials (ΔE_p) is 0.059 V and appears at a formal redox potential ($E°′$) of 1.08 V vs Ag/AgCl. In contrast, when $Ru(bpy)_3^{2+}$ and GSH are present (Figure 13C), the cathodic peak for $Ru(bpy)_3^{2+}$ disappears whereas the anodic peak current undergoes an enhancement. This behavior is consistent with an EC′ mechanism because $Ru(bpy)_3^{2+}$ is regenerated by the homogeneous reaction with GSH which uses up all the electrooxidized
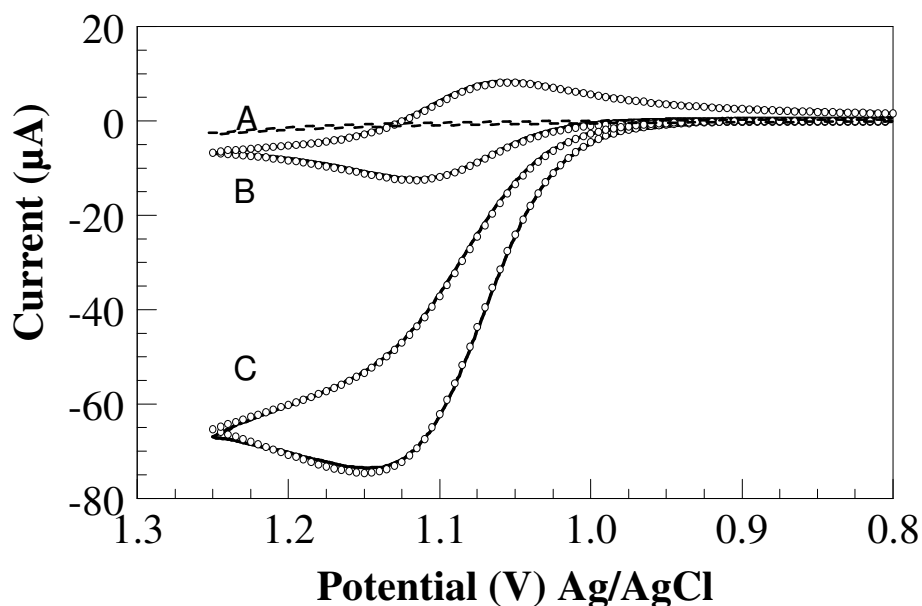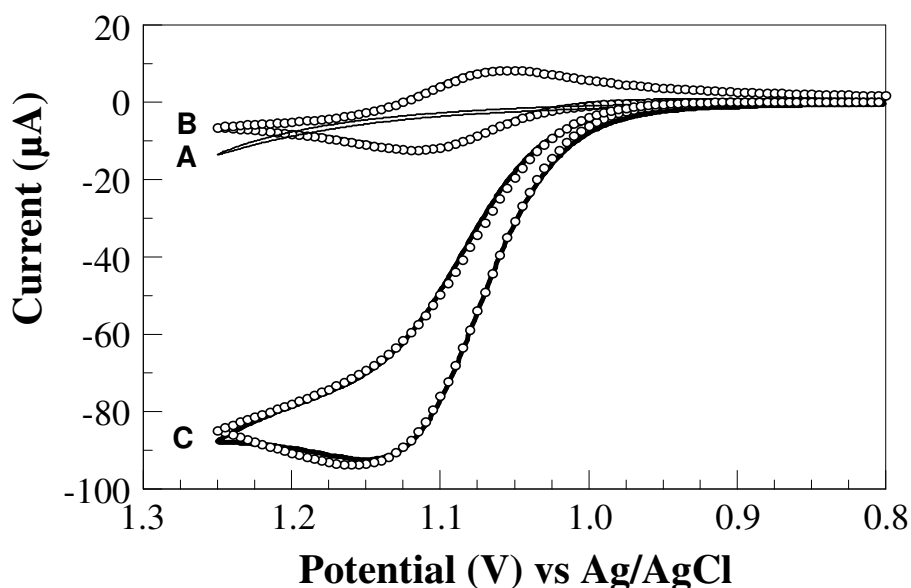
Figure 13. Cyclic voltammograms in 50 mM sodium phosphate buffer (pH = 5.0) at room temperature in 0.1 M NaCl. **(A)** Cyclic voltammogram of 1.0 mM glutathione (broken line). **(B)** Cyclic voltammograms of 1.0 mM $Ru(bpy)_3^{2+}$, experimental (solid) and simulated (open circle). **(C)** Cyclic voltammograms of 1.0 mM $Ru(bpy)_3^{2+}$ in the presence of 5.0 mM glutathione, experimental (solid) and simulated (open circle). Parameters obtained from simulation: $k_h = 0.06$ cm/s; $k_2 = 1.41 \pm 0.2 \times 10^4$ $M^{-1}s^{-1}$; $K_{eq} = 1.0 \times 10^3$.

Table 1. Kinetic and thermodynamic parameters in phosphate buffer 50 mM, 0.1 M NaCl and pH 5.0.

Species	Parameter					
	[a]D (cm^{2}s^{-1})	k_h (cm/s)	[b]α	[c]$E^{\circ\prime}$	K_{eq2}	k_2 (M^{-1}s^{-1})
GSH	3.0×10^{-5}	-	-	-	1×10^3	1.4×10^4
CSH	5.0×10^{-5}	-	-	-	1×10^3	2.3×10^4
Ru(bpy)$_3$$^{2+}$	6.0×10^{-6}	0.06	0.5	1.09	-	-

[a]Diffusion coefficient, [b]Transfer coefficient, [c]V vs. Ag/AgCl and $E^{\circ\prime} \approx E_{1/2}$.

$Ru(bpy)_3^{3+}$ and makes it unavailable for the reverse cathodic scan. The same profile was observed with CSH (Figure 14). All relevant kinetic and equilibrium parameters obtained from digital simulations (denoted by circles on the CV's) with a mechanism involving Equations 18 and 19 are displayed in Table 1. The values for the apparent heterogeneous rate constant k_h (0.06 cm/s) and $E^{\circ\prime}$ obtained for $Ru(bpy)_3^{2+}$ are consistent with previous

Figure 14. Cyclic voltammograms in 50 mM sodium phosphate buffer (pH = 5.0) at room temperature in 0.1 M NaCl. **(A)** Cyclic voltammogram of 1.0 mM cysteine (broken line). **(B)** Cyclic voltammograms of 1.0 mM $Ru(bpy)_3^{2+}$, experimental (solid) and simulated (open circle). **(C)** Cyclic voltammograms of 1.0 mM $Ru(bpy)_3^{2+}$ in the presence of 5.0 mM cysteine, experimental (solid) and simulated (open circle). Parameters obtained from simulation: $k_h = 0.06$ cm/s; $k_2 = 2.32 \pm 0.4 \times 10^4$ $M^{-1}s^{-1}$; $K_{eq} = 1.0 \times 10^3$.

reports [159, 166]. The rate constant k_2 for GSH and CSH in reaction 19 were $1.4 \pm 0.2 \times 10^4$ $M^{-1}s^{-1}$ and $2.3 \pm 0.4 \times 10^4$ $M^{-1}s^{-1}$, respectively. Similar values have been observed for the electrocatalytic oxidation of DNA and guanine by $Ru(bpy)_3^{3+}$ [136, 137, 159]. For the simulations performed here, the dimerization reaction 22 was not considered as an independent step.

Figure 15 shows the CV response for a solution containing 1.0 mM of $Ru(bpy)_3^{2+}$

and 5.0 mM GSH at pH 7.0 in phosphate buffer, 50 mM. The CV has two anodic peak

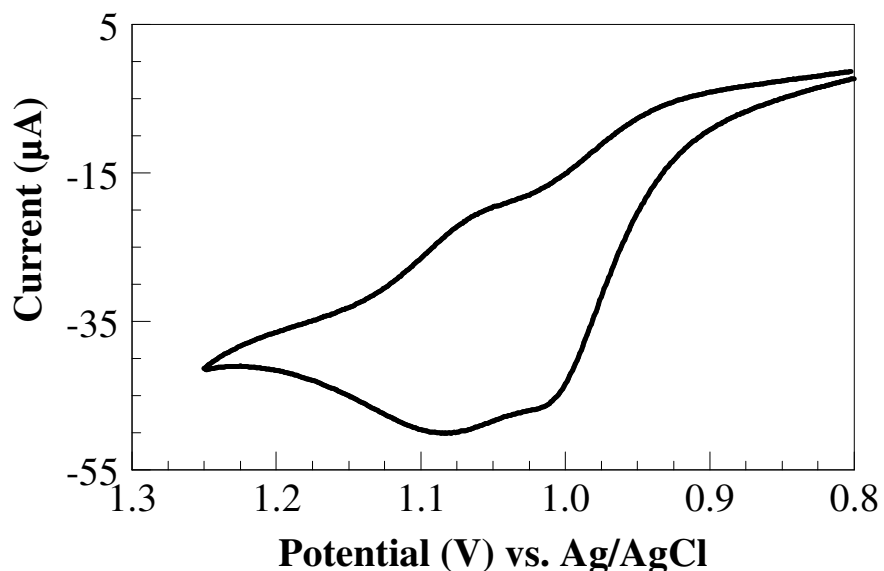currents: the first wave is a pre-wave anodic peak which is evident at 1.01 V vs.

Figure 15. Cyclic voltammogram of 5.0 mM glutathione in the presence of 1.0 mM $Ru(bpy)_3^{2+}$ in 50 mM sodium phosphate buffer, pH 7.0, at room temperature in 0.1 M NaCl. Scan rate used: 100 mV/s.

Ag/AgCl. This pre-wave peak, located at a less positive potential than the corresponding

catalytic peak observed at pH 5.0 in Figure 13 (1.15 V vs. Ag/AgCl), arises from the

rapid oxidation of deprotonated GSH (GS⁻). The oxidation of GSH involves the release

of a proton; therefore, its oxidation rate should depend on the pH of the solution

(Equation 23). There are reports that the oxidation of biological compounds (such as

thiols and tyrosine) proceed more rapidly when they are deprotonated than protonated

[19, 20, 22, 65, 135, 144, 167-169]. The reason for this rapid oxidation may be ascribed

to the change in the formal potential of GSH to a less positive potential as the solution pH

varies. This is supported by a study [170] in which the peak potential (E_p) of a thiol, 4-

amino-3-thio-5-methyl-1,2,4-triazole, showed a linear decrease of 56 mV per pH until about pH 8.0. However, the E_p became independent on pH above 8.0.

$$E_{GSH}^{o\prime} = (E_{GSH}^{o} - 0.059\ pH) \qquad (23)$$

The formal potential ($E^{o\prime}$) for GSH is expected to change if the pH is changed from 5.0 to 7.0. At pH 5.0 phosphate buffer $[HPO_4^{2-}]/[H_2PO_4^{-}]$ is ~0.006, while at pH 7.0 $[HPO_4^{2-}]/[H_2PO_4^{-}]$ is ~0.60. Therefore, the buffer base has the propensity to deprotonate GSH so that there exists a rapid oxidation of GS^- by $Ru(bpy)_3^{3+}$, unlike at pH 5.0 where there is essentially no base, bringing about the appearance of the pre-wave. The second wave arises from $Ru(bpy)_3^{2+}$ because in these conditions, a large part of $Ru(bpy)_3^{3+}$ is not required for the catalytic process to take place so its reversible peak occurs at the potential where it appears when there is no catalysis. Analogous behavior was found for CSH when the pH of the buffer is made 7.0 (Figure 16). The appearance of the two waves has been previously reported in the electrocatalytic oxidation of DNA by different metal complexes [159]. The concern that came up is that: what brings about this rapid oxidation of GSH, the pH change or the fractional amount of the Brønsted base (α_B) present in the buffer at pH 7.0? To further investigate the role of the pH and the Brønsted base of the buffer, CV experiments were performed for GSH and $Ru(bpy)_3^{2+}$ in tris/HCl buffer at pH 7.0 and 9.0. At pH 7.0 (Figure 17A), the CV response shows one catalytic peak at 1.15 V vs. Ag/AgCl, resembling the behavior observed with phosphate buffer at pH 5.0 (Figure 13). When the pH was increased to 9.0 using tris/HCl buffer (Figure 17B), the profile switched to the behavior observed at pH 7.0 phosphate buffer. Despite the pH

being 5.0, 7.0, or 9.0, the proton accepting ability of the Brønsted base is really what determines the rate of GSH oxidation; thus, the profile of the CV.
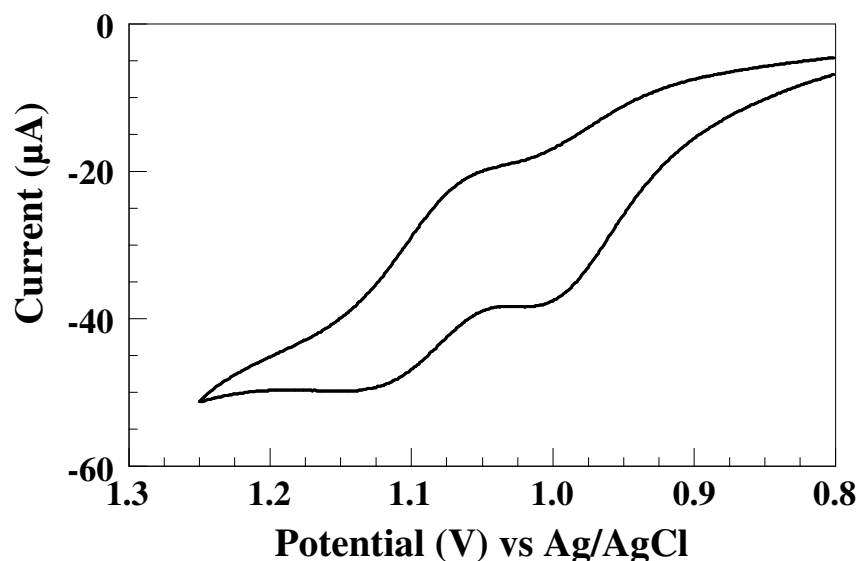

Figure 16. Cyclic voltammogram of 5.0 mM cysteine in the presence of 1.0 mM Ru(bpy)$_3^{2+}$ in 50 mM sodium phosphate buffer, pH 7.0, at room temperature in 0.1 M NaCl. Scan rate used: 100 mV/s.

Table 2. Fractional amounts α$_B$, of Brønsted base for phosphate and tris/HCl buffer at different pH

Base	pK$_a$ Conjugate acid	[a]α$_B$ pH = 5.0	pH = 7.0	pH = 9.0
Na$_2$HPO$_4$	7.20	~0.01	0.39	--
[OHCH$_2$]$_3$CNH$_3$OH	8.06	--	0.08	0.89

Calculated using α$_B$= [B]/F$_{HB}$, where F$_{HB}$ is the formal concentration of HB used, 50 mM.

Table 2 shows the pK$_a$'s for the buffer bases and the corresponding α$_B$'s at the formal concentrations used and the evaluated pH values. For tris/HCl buffer at pH 7.0

there is very low concentration of the tris base and the dominant species is its conjugate

acid, but at pH 9.0 the tris base component is dominant. The results indicate that unless a

base with a suitable pK_a is present, the homogeneous oxidation of RSH will proceed

moderately. For instance, $H_2PO_4^-$ is an amphoteric species that could act as proton
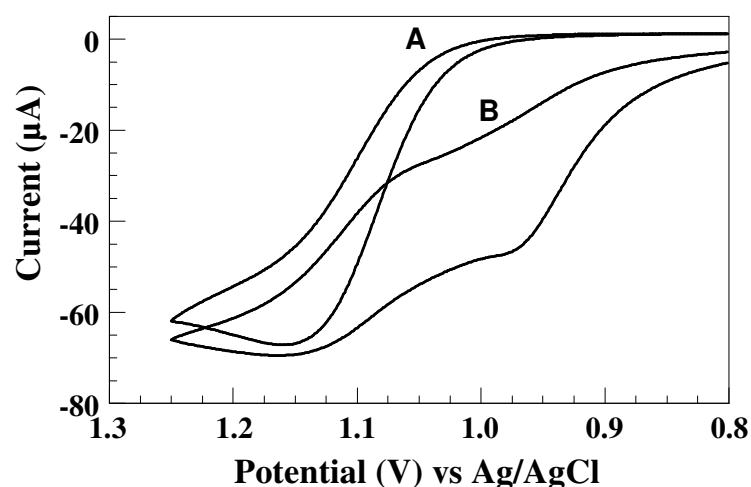
Figure 17. Cyclic voltammograms (CV) of 5.0 mM glutathione in the presence of 1.0 mM Ru(bpy)$_3$$^{2+}$ in 50 mM tris/HCl buffer (pH's = 7.0 and 9.0) at room temperature in 0.1 M NaCl. **(A)** pH 7.0 cyclic voltammogram. **(B)** pH 9.0 cyclic voltammogram. Scan rate used: 100 mV/s.

acceptor as well, but the pK_a of its conjugate acid, H_3PO_4, is 2.12, which as it turns out is

not enough to drive the catalysis rapidly. In solutions where the buffer acid dominates,

there is an increase in i_{cat}, when the phosphate buffer concentration changed gradually

from 0 to 100 mM at pH 5.0, and then decreased with further increase in the buffer

concentration, which may be attributed to increase in viscosity of the solution (Figure 18)

[171]. An increase in i_{cat} when the buffer concentration increases from 0 to 12.5 mM at

pH 7.0 was observed (Figure 19). Rate (k_2) increases as well with increase in buffer concentration, which may be considered a case of general base catalysis (inset in Figure 19).

Figure 18. Catalytic peak current i_{cat} at various concentrations of sodium phosphate buffer (PB). Data points are not corrected for i_d. Data taken from the cyclic voltammograms of 5.0 mM glutathione and 1.0 mM of Ru(bpy)$_3^{2+}$ at pH = 5.0 in 0.1 M NaCl. The decrease in current after 0.1 M of PB was attributed to viscosity effects causing lower diffusion coefficients (D) for all the species contributing to the catalytic current [171]. Control chronocoulometric experiments showed a decrease of 32 % in D for Ru(bpy)$_3^{2+}$ when going from 0.05 to 1.0 M of PB.

Figure 19. Plot of *i* (μA) vs. *E* (V) at different concentrations of sodium phosphate buffer ([PB]). Data taken from the CV's of 5.0 mM glutathione in the presence of 1.0 mM Ru(bpy)$_3^{2+}$ at pH 7.0 in 0.1 M NaCl. Inset: Plot of log k$_2$ vs. [PB].

In addition, water, used as a solvent could also be a proton acceptor; however, the pK$_a$ of its conjugate acid H$_3$O$^+$ is -1.74 [157], which makes it a weaker proton acceptor than H$_2$PO$_4^-$. Figure 20 shows a series of CV's conducted at pH 5.0, 7.0, and 9.0, without buffer and adjusting the initial pH with strong acid or base. As expected, the CV response indicates that despite the pH change from 5.0 to 9.0, the mechanism remains similar to those experiments done in buffered solutions where the conjugate acids dominate because in this case, H$_2$O is too weak base to induce general base catalysis. Nevertheless, the overall trend so far, suggests that the proton transfer and the proton acceptor are the key factors that control the mechanism for the homogeneous oxidation of GSH and CSH by Ru(bpy)$_3^{3+}$.

Figure 20. CV response for 5.0 mM glutathione in the presence of 1.0 mM Ru(bpy)$_3^{2+}$ in unbuffered solutions adjusting the initial pH with strong acid or base in 0.1 M NaCl. (**Red**) pH 5.0; (**Blue**) pH 7.0; and (**Green**) pH 9.0; 100 mV/s. Fitted simulations in open circles; k_h = 0.06 cm/s; K_{eq2} = 1.0 × 10^3. k_2's are given in the text.

Table 3. Kinetic and thermodynamic parameters for the catalytic oxidation of GSH by Ru(bpy)$_3^{3+}$ at different pH and using different bases as proton acceptors.

Base / pH	K_{eq2}	k_2 (M^{-1} s^{-1})	Assigned Mechanism
Na$_2$HPO$_4$ / 5.0	1.0 × 10^3	1.41 ± 0.24 × 10^4	CPET
^{a} Na$_2$HPO$_4$ / 7.0	-	-	-
Tris / 7.0	1.0 × 10^3	1.17 ± 0.31 × 10^4	CPET
H$_2$O / 5.0	1.0 × 10^3	1.12 ± 0.12 × 10^4	CPET
H$_2$O / 7.0	1.0 × 10^3	9.02 ± 2.77 × 10^3	CPET
H$_2$O / 9.0	1.0 × 10^3	9.29 ± 1.06 × 10^3	CPET

^{a} Simulation was not done.

Table 3 shows the kinetic and thermodynamic parameters of simulations fitted to experimental CV's using phosphate and tris/HCl buffers at selected values of pH as well

as the corresponding unbuffered conditions. General base catalysis, which has been reported in many chemical and biochemical systems including thiols [149, 157, 158], occurs when the rate of a reaction that is coupled to a proton transfer step is accelerated by the presence of a Brønsted base other than OH⁻ [147, 157]. Moreover, when the mediated electrooxidation of *N*-Acetylmethionine (a water soluble derivative with a methylated thiol, RS-CH₃), was performed in phosphate buffer pH 7.0, moderate electrocatalysis by $Ru(bpy)_3^{3+}$ was detected without the appearance of the two-wave response observed for GSH or CSH (Figure 21). This indicates a difference between

Figure 21. CV response in 50 mM sodium phosphate buffer pH 7.0 in 0.1 M NaCl. **(A)** 1.0 mM $Ru(bpy)_3^{2+}$. **(B)** 1.0 mM N-Acetylmethionine. **(C)** 1.0 mM $Ru(bpy)_3^{2+}$ and 5.0 mM N-Acetylmethionine; 100 mV/s.

GSH/CSH and *N*-Acetyl-

methionine, in that *N*-Acetyl-methionine lacks a thiol group. In order to confirm that the pre-wave peak observed in the voltammetric oxidation of GSH/CSH at pH's 7.0 and 9.0 phosphate and tris/HCl buffers respectively, was not formed by a new species from

ligand exchange on Ru(bpy)$_3$$^{2+}$ (due to the nucleophilicity of the thiolate anion or other groups in GSH or CSH), ^{1}H NMR and UV-Vis experiments were performed. No evidence of new species by simply mixing GSH/CSH with Ru(bpy)$_3$$^{2+}$ was found in such experiments (Figure 22 and Table 4).

Figure 22A. UV-Vis spectra for various amounts of cysteine and 10 μM Ru(bpy)$_3$$^{2+}$ in 50 mM sodium phosphate buffer pH 5.0 in 0.1 M NaCl.
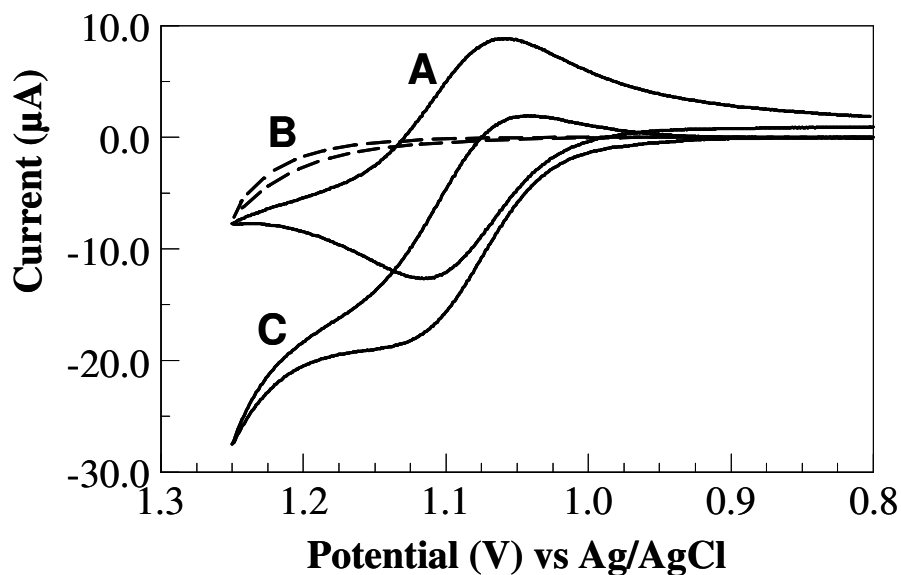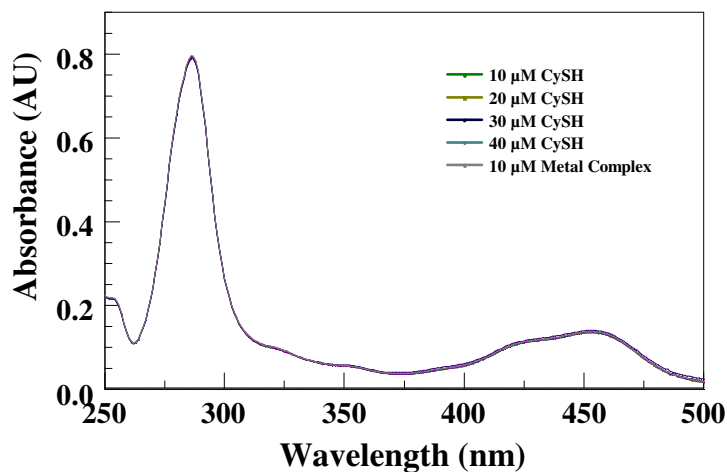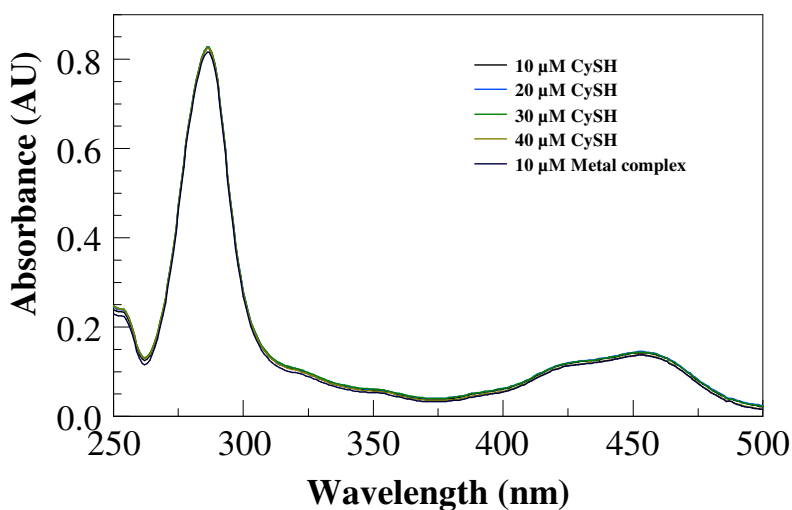
Figure 22B. UV-Vis spectra for various amounts of cysteine and 10 μM Ru(bpy)$_3$$^{2+}$ in 50 mM sodium phosphate buffer pH 7.0 in 0.1 M NaCl.

Chemical Motif on CSH	Chemical Shift (ppm) pD 5.0 PB	Chemical Shift (ppm) pD 9.0 PB
−S−CH$_2$−	2.94	2.91
10(-S-CH$_2$-):1Ru(bpy)$_3{}^{2+}$	2.95	2.92
−N−CH−	3.97	3.83
10(-N-CH-): 1Ru(bpy)$_3{}^{2+}$	4.03	3.84

Table 4. ^{1}HNMR data for 10 equiv. of cysteine (CSH) and 1.0 equiv. of Ru(bpy)$_3{}^{2+}$ in 50 mM deuterated sodium phosphate buffer (PB) pD 5.0 and 9.0 in 0.1 M NaCl.

2.3.1 Isotopic Effects

In order to assign CPET or PT/ET for oxidation of GSH, experiments were performed in deuterated buffer and unbuffered solutions. Figures 23 and 24 show the comparison in the CV responses for the mediated oxidation of GSH and CSH at pH 5.0 (solid) and pD 5.0 (dashed) in H$_2$O and D$_2$O, respectively. For both GSH and CSH, the oxidations in D$_2$O proceed slowly, implying the involvement of proton in the rate-determining step (RDS). The kinetic isotope effect (KIE = k_{2H}/k_{2D}) for k_2 determined from simulations and following the mechanism in Scheme 1 (Equation 18), was 3.58 for GSH and 2.60 for CSH. Table 5 shows a comparative list of isotopic kinetic parameters determined from simulations and recorded under different buffering and pH conditions. Based on these results, CPET has been ascribed to oxidation of GSH and CSH at pH 5.0 phosphate buffer and pH 7.0 tris/HCl (though deuterated experiments were not done for

tris/HCl); and PT/ET has been ascribed to oxidation at pH 7.0 phosphate buffer and pH 9.0 tris/HCl buffer.

Figure 23. CV response in 50 mM sodium phosphate buffer pH 5.0 in 0.1 M NaCl for 5.0 mM glutathione and 1.0 mM Ru(bpy)$_3{}^{2+}$ in H$_2$O (**solid**) and D$_2$O, (**dashed**); 100 mV/s. KIE = 4.09 ± 1.33.

Figure 24. CV response in 50 mM sodium phosphate buffer pH 5.0 in 0.1 M NaCl for 5.0 mM cysteine and 1.0 mM Ru(bpy)$_3{}^{2+}$ in H$_2$O (**solid**) and D$_2$O, (**dashed**); 100 mV/s. KIE = 2.49 ± 0.06.

Table 5. Isotopic effects on the kinetic parameters for the catalytic oxidation of GSH by $Ru(bpy)_3^{3+}$ at different pH and using different bases as proton acceptors.

Base / pD	k_{2D} (M^{-1} s^{-1})	$^aKIE = k_{2H}/k_{2D}$	*Assigned Mechanism*
Na_2DPO_4 / 5.0	$3.94 \pm 2.23 \times 10^3$	4.09 ± 1.33	CPET
$^b Na_2DPO_4$ / 7.0	-	-	-
D_2O / 5.0	$3.92 \pm 0.47 \times 10^3$	2.88 ± 0.29	CPET
D_2O / 7.0	$3.01 \pm 0.36 \times 10^3$	2.96 ± 0.59	CPET
D_2O / 9.0	$3.57 \pm 0.37 \times 10^3$	2.64 ± 0.37	CPET

^{a}The k_{2H} values were taken from Table 3. ^{b} Simulation was not done.

3.0 ELECTROCATALYTIC OXIDATION OF GLUTATHIONE BY POTASSIUM HEXACHLOROIRIDATE (IV)

3.1 Introduction

In order to further understand the mechanism of GSH oxidation in cellular fluids, the previous work (Chapter 2) has been extended with the use of a different metal mediator, potassium hexachloroiridate III (K_3IrCl_6), which possesses a less positive formal potential than $Ru(bpy)_3^{2+}$. The use of $Ru(bpy)_3^{2+}$ resulted in the splitting of the catalytic wave into two, making the mechanism more complex at pH 7.0 phosphate buffer (PB) than at pH 5.0 because of the involvement of the Brønsted base in the catalysis. Thus it is thought that using a metal oxidant of lower formal potential will avert this kinetic regime at pH 7.0 PB so that the oxidation of GSH and the effect of the solution pH on the electrooxidation of GSH can be well studied.

Scheme 2. Mechanism for GSH electroooxidation by $IrCl_6^{2-}$.

This study reports the oxidation of GSH by $IrCl_6^{2-}$ electrogenerated from $IrCl_6^{3-}$ at the surface of glassy carbon electrode in aqueous solution. It is found that

deprotonation of GSH is crucial to its electrooxidation (Scheme 2). When water was used as the solvent, the oxidation of GSH did not proceed efficiently as water is not a strong proton acceptor because the pK_a of its conjugate acid, H_3O^+, is -1.74 [157]. Electrooxidation of GSH was not observed until the solution pH is made 11.5. However, at pH 7.0 PB where [base]/[acid] is ~0.6, the electrooxidation of GSH proceeded efficiently; with HPO_4^{2-} being a stronger proton acceptor than water because the pK_a of its conjugate acid, $H_2PO_4^-$, is 7.2. The electrooxidation rate constant increases as the concentration of PB increases; implying a general base catalysis. At lower PB concentrations, proton transfer to the Brønsted base became the rate-determining step as shown by the scan rate experiments with the reduction current gradually increasing as the scan rate is increased. It is suggested that there exists a change in the rate-determining step in the oxidation of GSH when concentrations of the buffer is gradually increasing. The rate of oxidation of GSH increased with the pK_a of different buffers used. Though the buffer is involved in the catalysis, its concentration must not exceed the optimum concentration required to effectively study the electrooxidation of GSH at certain pH.

3.2 Experimental Section

3.2.1 Reagents and Materials

L-glutathione reduced (99%), K_3IrCl_6, D_2O (99.9%), and DCl (35%) were purchased from Aldrich (St. Louis, MO). Na_2HPO_4 (99%), NaH_2PO_4 (98%), and NaOH (97%) were purchased from EM Science (Cherry Hill, NJ). HCl (37.3%), tris(hydroxymethyl)aminomethane (Tris) were purchased from Fisher Scientific (Fair Lawn, NJ). Maleic acid, MA, (≥99%), citric acid, CA, (≥99.5%), and *N*-(2-Acetamido)-

2-aminoethanesulfonic acid, ACES, ($\geq$99.5%) were purchased from Fluka. NaCl, 99+% and NaOD, 30 wt% solution in D_2O were purchased from Acros Organics (NJ, USA). Water was purified with a MilliQ purification system (Billerica, MA). All reagents were used without further purification. Na_2DPO_4 and NaD_2PO_4 were prepared by triply dissolving Na_2HPO_4 and NaH_2PO_4 in D_2O and evaporating solvent [137], then confirming the isotopic purity by ^{1}HNMR. The pH of the sodium phosphate solutions was measured with standard pH meter, calibrated with H_2O buffers. pH meter readings for D_2O solutions were converted to pD values employing the equation pD = pH + 0.4 [29]. All solutions and subsequent dilutions were prepared using deionized water with a resistivity of 18.2 MΩ cm. All experiments were carried out in a solution volume of 5.0 cm^3 at room temperature, and deoxygenated with argon. The pH's of the buffer solutions were adjusted with NaOH and HCl; however, for deuterated buffer solutions, NaOD and DCl were used to adjust the pH.

3.2.2 Cyclic Voltammetry

Cyclic voltammograms were collected using a potentiostat (CH Instruments, Austin, TX) with a cell equipped with a glassy carbon (GC) working electrode (area = 0.06 cm^2), a Pt-wire counter electrode, and Ag/AgCl reference electrode (3.0 mM KCl). Glassy carbon electrode was polished with 0.05 µm alumina and rinsed with copious amount of water between experiments. In a typical experiment, 1.0 mM metal complex and 3.0 mM L-glutathione (reduced) were dissolved in 5.0 cm^3 aqueous solutions of 35 mM buffer/0.1 M NaCl, and 0.1 M NaCl. The potential was scanned from 0.4 V to 1.0 V.

The experimental cyclic voltammograms were background subtracted and performed at room temperature. The formal potential ($E^{o\prime}$) of $IrCl_6^{3-}$ is 0.72 V vs Ag/AgCl.

3.2.3 Digital Simulation

Second-order glutathione oxidation rate constants were determined by fitting the cyclic voltammograms to a mechanism involving Equations 18, 20 and 21 in Scheme 1 at pH $\geq$ 6.0 phosphate buffer solution, and pH 11.5 − 12.0 water. Equations 18 and 19 were used for conditions in which there is no significant participation of the buffer base in the reaction. The software package DigiSim version 3.03 (Bioanalytical Systems, Inc., West Lafayette, IN) was used to verify each mechanism at different scan rates where simulated and experimental CV's were compared. The values of diffusion coefficients were 8.2×10^{-6} cm^2/s for $IrCl_6^{3-}$ [172] and 3.0×10^{-5} cm^2/s for glutathione. All other simulation parameters are given in the figure captions and appendix. The heterogeneous electron transfer rate constant (0.1 cm/s) was determined by fitting the voltammogram of $IrCl_6^{3-}$ in the absence of glutathione. The electrooxidation equilibrium constant (K_{eq3}), was found to have a profound effect on the CV profile, and a value of 1×10^6 was generally used [135].

3.3 Results and Discussion

Electrooxidation of GSH by $IrCl_6^{2-}$ in water: Electrocatalytic oxidation of GSH was carried out in unbuffered solution in order to study its mechanism without any contribution from buffer components. Solution pH was varied between 5.0 and 12; and as the pH increases up to 11, the tendency of the OH⁻ to deprotonate GSH should increase.

According to Equation 23, it is expected that the formal potential of GSH should vary since its rate of oxidation depends on the pH; GSH was not observed to be deprotonated effectively due to the low pK_a (−1.74) [157] of the conjugate acid of water, H_3O^+. Figure 25 shows the oxidation of GSH by $IrCl_6{}^{2-}$ in unbuffered solution containing 0.1 M NaCl, pH 11. The figure indicates that either the mediator is not an effective one or that water is unable to accept the GSH proton. In order to confirm this, the oxidation was performed at pH 12. Interestingly, electrocatalysis of GSH was observed; and at this pH the $[OH^-]$ is 10 mM. Figure 26 confirms that the mediator is able to electrooxidize GSH when its proton is accepted by an available base in the solution. The onset of GSH oxidation as evident from this figure is at pH 11.5. The rate constants somewhat remain similar until the $[OH^-]$ is further increased above pH 11.

Figure 25. Oxidation of 2.0 mM glutathione (GSH) by $IrCl_6{}^{2-}$ (1.0 mM) in unbuffered solutions containing 0.1 M NaCl at pH 11. $IrCl_6{}^{3-}$ alone (Black) and $IrCl_6{}^{3-}$ in the presence of GSH (Blue). Scan rate = 100 mV/s.

Figure 26. Plot of log k_2 vs. pH. Oxidation of glutathione (GSH), 2.0 mM, by 1.0 mM $IrCl_6^{2-}$ in unbuffered solutions containing 0.1 M NaCl at various pH values. Rate constants were obtained from digital simulations by fitting the experimental CV's. Scan rate = 100 mV/s.

Electrooxidation of GSH by $IrCl_6^{2-}$ in PB solution: The electrooxidation of GSH by $IrCl_6^{2-}$ performed at various pH values of PB revealed the involvement of Brønsted base, HPO_4^{2-}. Figure 27 shows the plot of log k_3 vs. pH of PB. Evidently, electrooxidation of GSH at both pH's 4.0 and 5.0 are similar to those carried out in water containing 0.1 M NaCl at pH $\leq$ 11. Their rate constants are similar, as well as their CV profiles (Figure 28) to those in water. When the pH = 6.0 ($[HPO_4^{2-}]/[H_2PO_4^-]$ = ~0.06), the electrooxidation of GSH was more favored compared to those at pH's 4.0 and 5.0, indicating the onset of the participation of the Brønsted base in the reaction. When the pH = 7.0 ($[HPO_4^{2-}]/[H_2PO_4^-]$ = ~0.6), the rate of electrooxidation of GSH considerably increased over that of pH 6.0 PB. The explanation for this is the increase in the fraction

of the basic (HPO_4^{2-}) component of the buffer. Other studies [19, 22, 167-169] have shown that the oxidation of GSH and other thiols involves the reactive deprotonated species, and that the oxidation rate increases as solution pH increases [19, 22]. Optimum

Figure 27. Plot of log k_3 vs. pH. Oxidation of glutathione, 3.0 mM, by $IrCl_6^{2-}$ (1.0 mM) in 35 mM sodium phosphate buffer solutions containing 0.1 M NaCl at various pH values. Digital simulations were used to obtain rates constant by fitting the experimental CV's. Scan rate = 100 mV/s.

oxidation rate of GSH was achieved at neutral pH. Nonetheless, above pH 7.0 PB, the rate of electrooxidation of GSH diminished. The reason for this decrease in rate of oxidation can be ascribed to the deprotonation of the ammonium group ($-NH_3^+$), as already reported for GSH, CSH, and other thiols [19, 20, 22]. The effect yielded another

Figure 28. Oxidation of glutathione by 1.0 mM $IrCl_6^{2-}$ in buffered and unbuffered solutions containing 0.1 M NaCl. $IrCl_6^{3-}$ alone at pH 7.0, 35 mM PB (Brown); $IrCl_6^{3-}$ and GSH at pH 11, water (Blue); $IrCl_6^{3-}$ and GSH at pH 5.0, 35 mM PB (Green); $IrCl_6^{3-}$ and GSH at pH 7.0, 35 mM PB (Black). Scan rate = 100 mV/s.

species of HCSH having its $-NH_3^+$ and $-SH$ deprotonated. This species is simultaneously oxidized along with HCS^-, with the rate constant lower than that for HCS^-. The profile for experimental plot of i_{cat}/i_d vs. pH given in Figure 43 in the appendix was reproduced with DigiSim (Figure 44, Appendix), and a rate law (Equation 28, Figure 45) derived from Equations 24−27 (derivations shown in appendix). Figures 43-45 have the same profile but different optimum pH. The rationale behind this may be due to the stabilization of the product by the presence of the mediator.

$$AH_2 + B \; \underset{k_{-1}}{\overset{k_1}{\rightleftharpoons}} \; AH^- + BH^+ \qquad\qquad (24)$$

$$AH^- + B \; \underset{k_{-1}'}{\overset{k_1'}{\rightleftharpoons}} \; A^{2-} + BH^+ \qquad\qquad (25)$$

$$AH^- + IrCl_6{}^{2-} \; \overset{k_2}{\longrightarrow} \; AH^{\bullet} + IrCl_6{}^{3-} \qquad\qquad (26)$$

$$A^{2-} + IrCl_6{}^{2-} \; \overset{k_2'}{\longrightarrow} \; A^{-\bullet} + IrCl_6{}^{3-} \qquad\qquad (27)$$

$$-\frac{d[IrCl_6{}^{2-}]}{dt} = [AH_2]_T[IrCl_6{}^{2-}]\left[\frac{k_2 10^{pH - pK_a(AH_2)} + k_2' 10^{2pH - pK_a(AH_2) - pK_a(AH^-)}}{1 + 10^{pH - pK_a(AH_2)} + 10^{2pH - pK_a(AH_2) - pK_a(AH^-)}}\right]$$

$$(28)$$

Buffer-assisted GSH electrooxidation: To further verify the influence of PB in the oxidation rate, experiments were carried out with varied concentrations of PB. Figure 29 details the plot of log k_3 vs. [PB]. The rate of electrooxidation increases with increase in

Figure 29. Plot of log k_3 vs. concentrations of sodium phosphate buffer (mM) in the oxidation of glutathione (3.0 mM) by $IrCl_6{}^{2-}$ (1.0 mM). Rate constants were obtained from digital simulations by fitting the experimental CV's.

the [PB]; an implication of general base catalysis. The plot shows a curvature at lower PB concentrations and a somewhat leveling at higher PB concentrations. This plot thus indicates the existence of two kinetic regimes. This behavior has been observed in other studies involving general base catalysis; and has been considered an indication of a change in the rate-determining step of the reaction [152, 156].

Figure 30. Plots of current (µA) vs. potential (V). The oxidation of glutathione (3.0 mM) by $IrCl_6^{2-}$ (1.0 mM) in 10.0 mM sodium phosphate buffer/0.1 M NaCl at pH 7.0. Scan rate increase is shown by the arrow. Scan rates used are: 50, 100, 200 and 300 mV/s.

Scan rate effect: In order to validate the interpretation of Figure 29 as to what the rate-determining step is, scan rate experiments were performed. Deprotonated GSH has been revealed to be the reactive species. Therefore, experiments were carried out at 10 mM and 35 mM PB, pH 7.0. Figure 30 details the experiments done at pH 7.0, 10 mM

PB − having a low concentration of the Brønsted base, at different scan rates. There is increase in the oxidation (anodic) current as the scan rate increases, but also increase in the reduction (cathodic) current. The increase in the cathodic peak current is due to the slow kinetics of proton transfer from GSH to the base, $HPO_4{}^{2-}$; thus all electrogenerated

Figure 31. Plots of current (µA) vs potential (V). The oxidation of glutathione (3.0 mM) by $IrCl_6{}^{2-}$ (1.0 mM) in 35.0 mM sodium phosphate buffer/0.1 M NaCl at pH 7.0. Scan rate increase is shown by the arrow. Scan rates used are: 50, 100, 200 and 300 mV/s.

$IrCl_6{}^{2-}$ at the electrode surface is not used up by GSH. Consequently, the remaining $IrCl_6{}^{2-}$ on the reverse scan will be reduced at the electrode surface; thus giving rise to the reduction current. Though proton transfer from sulfur to oxygen and *vice versa* should be diffusion-controlled (10^{10} $M^{-1}s^{-1}$ [173]); nonetheless, it is found to be rate-determining step. The reaction mechanism in this case is proposed to be through a stepwise pathway. Figure 29 shows a leveling off of the rate constant when the [PB] > 10 mM, and this is attributed to a change in the rate-determining step. In addition, Figure 31 demonstrates the CV's of GSH electrooxidation by $IrCl_6{}^{2-}$ at pH 7.0, 35 mM PB, with increasing scan

rate. From this figure, the reduction current did not show up as the scan rate increases. This implies a more efficient proton transfer from GSH to the base, HPO_4^{2-}, compared to the experiments done at 10 mM PB, pH 7.0. Therefore proton transfer is not the rate-determining step but may partly be involved in the rate-determining step in this case.

Effect of Buffer concentration: Though the electrooxidation of GSH is catalyzed by the buffer, the buffer concentration must be controlled. There appears to be an optimum concentration at which effective electrooxidation of GSH by $IrCl_6^{2-}$ in PB is achieved. This is crucial if a glutathione sensor is to be developed. From Figure 32, it is observed that the oxidation current at pH 7.0 is higher when reaction was carried out in

Figure 32. Plot of i (µA) vs. E (V) of the oxidation of glutathione (3.0 mM) by $IrCl_6^{2-}$ (1.0 mM) in various concentrations of sodium phosphate buffer containing 0.1 M NaCl at pH's 7.0 and 9.0.

35 mM PB compared to 50 mM PB. Likewise, oxidation current higher at pH 9.0, 10 mM PB compared to 35 mM. As earlier mentioned that decrease in the rate constant of the

electrooxidation of GSH by $IrCl_6^{2-}$ as the pH of PB increases (Figure 27) is due to the deprotonation of the ammonium group ($-NH_3^+$); therefore, it is expected that when the PB concentration is significantly lowered, this effect should decrease because the amino group will remain protonated. Figure 32 confirmed this is true. Having optimized this condition, sensing of GSH can be done efficiently and accurately.

Isotope Effects: In order to assign a reaction pathway for the electrooxidation of GSH by $IrCl_6^{2-}$ in 35 mM PB, pH 7.0, experiments were performed in deuterated buffer solutions. Figure 33 shows the comparison in the CV responses for the mediated oxidation of GSH at pH 7.0 (broken) and pD 7.0 (solid) in H_2O and D_2O, respectively. The oxidation of GSH in D_2O proceeded slowly, implying the involvement of proton in the rate-determining step (RDS). The kinetic isotope effect (KIE = k_{3H}/k_{3D}) for k_3 determined from simulations and following the reactions in Equations 18, 20, and 21, was 1.98 ± 0.10. The electrooxidation of GSH in 35 mM PB, pH 7.0, follows through CPET pathway mechanism based on two reasons: the value of kinetic isotope effect assigned to CPET pathway [133, 140], and the fact that proton transfer from GSH to HPO_4^{2-} is not observed to be rate-determining step (though involved in the RDS) because of the absence of the reduction current as the scan rate increases. The oxidation of GSH by $IrCl_6^{2-}$ in 10 mM PB, pH 7, shows that proton transfer is the rate determining step due to the increase in the reduction current, experiments done in D_2O revealed even slower proton transfer with KIE = 3.17 ± 0.66 (Figure 34).

Deuterated experiments were carried out in 35 mM PB, pH 6.0, in order to further substantiate if proton transfer is the RDS. Table 6 details the ratio of the catalytic current,

i_{cat}, and the diffusion current, i_d, of the mediator in the absence of GSH (i_{cat}/i_d) in both

deuterated and protonated PB at different pH values. In solutions of 35 mM PB at pH's

Figure 33. Plot of i (μA) vs. E (V) of the oxidation of glutathione (3.0 mM) by $IrCl_6^{2-}$ (1.0 mM) in 35.0 mM deuterated (Solid) and undeuterated (Broken) PB/0.1 M NaCl. Rate constants were obtained from digital simulations. KIE = 1.98 ± 0.10. k_h = 0.1 cm/s, $k_3(H_2O)$ = 7.15 ± 0.1 × 10^5 $M^{-1}s^{-1}$, $K_{eq}(H_2O/D_2O)$ = 1.0 × 10^6. $k_3(D_2O)$ = 3.62 ± 0.2 × 10^5 $M^{-1}s^{-1}$.

Figure 34. Plot of i (μA) vs. E (V) of the oxidation of GSH (3.0 mM) by $IrCl_6^{2-}$ (1.0 mM) in 10 mM PB/0.1 M NaCl. Rates were obtained from digital simulations. k_h = 0.1 cm/s, $k_3(H_2O)$ = 2.44 ± 0.2 × 10^5 $M^{-1}s^{-1}$, $K_{eq3}(H_2O/D_2O)$ = 1.0 × 10^6, $k_2(D_2O)$ = 7.71 ± 1.0 × 10^4 $M^{-1}s^{-1}$, KIE = 3.17 ± 0.66.

Table 6. Isotopic effects in the oxidation of GSH by $IrCl_6^{2-}$ in deuterated and protonated 35 mM PB at different pH values. i_{cat} = catalytic current; i_d = diffusion current of $IrCl_6^{2-}$ alone.

pH	i_{cat}/i_d (PB/H$_2$O)	i_{cat}/i_d (PB/D$_2$O)
4.0	1.18	[a] –
5.0	1.17	[a] –
6.0	1.95	1.19
7.0	3.20	2.64

[a] **Deuterated experiments were not done.**

4.0 and 5.0, similar i_{cat}/i_d values were recorded because there was no effective oxidation of GSH. However, the i_{cat}/i_d value at pH 6.0, 35 mM PB, changed from 1.95 to 1.19 at pD 6.0, 35 mM PB. Obviously, isotope exchange caused the inability of $IrCl_6^{2-}$ to oxidize GSH just as in the case with experiments done in protonated PB at pH's 4.0 and 5.0. These results further confirm the proton transfer as the RDS.

Driving-force dependence: Understanding the dependence of electron-transfer rates on the driving force is an area of active interest [133, 135-137, 160, 174]. Figure 35 shows the ratio of the catalytic current to diffusion current (i_{cat}/i_d) for the oxidation of GSH by $IrCl_6^{2-}$ in different buffers at pH = 7.0 and pH = pK$_a$ of the buffers. This figure demonstrates the roles of both the buffer base and pK$_a$ of the buffer. The buffers used are: maleic acid (MA), pK$_a$ 6.2; citric acid (CA), pK$_a$ 6.4; *N*-(2-acetamido)-2-aminoethanesulfonic acid (ACES), pK$_a$ 6.8; sodium phosphate buffer (PB), pK$_a$ 7.2; tris(hydroxylmethyl)aminomethane (Tris), pK$_a$ 8.1 [175]. The value of i_{cat}/i_d increases from MA to PB when the pH was kept at 7.0 for all buffers, except for tris/HCl. The

increase in i_{cat}/i_d is a result of increase in the pK_a from MA to PB (together with some contribution from the buffer base), even though the buffer base composition decreases from MA to PB. However, at pH 7.0 tris/HCl (where the buffer base composition is very low), i_{cat}/i_d is very small even though the pK_a of tris is 8.1. Experiments performed when the pH = pK_a show that i_{cat}/i_d increases as the pK_a increases up to PB. Because buffer base composition decreases at pH = pK_a, there is decrease in i_{cat}/i_d up to ACES from MA compared to values obtained at pH 7.0. On the other hand, there is increase in the value of i_{cat}/i_d for tris/HCl though lower than that of PB. The reason for the increased value of i_{cat}/i_d unlike at pH 7.0 is that there is essential amount of buffer base participating in the reaction. Moreover, the decrease in i_{cat}/i_d compared to that for PB may be due to the deprotonation of $-NH_3^+$ group as explained earlier.

Figure 35. Plot of i_{cat}/i_d vs. various buffers for the oxidation of glutathione (3.0 mM) by $IrCl_6^{2-}$ (1.0 mM). Experiments performed at pH = 7.0 and pH = pK_a of the buffers. i_{cat} is the catalytic current; i_d is diffusion current of metal oxidant in the absence of glutathione. The percent compositions of the buffer bases are indicated on respective bar.

4.0 ELECTROCATALYTIC OXIDATION OF HOMOCYSTEINE BY POTASSIUM HEXACHLOROIRIDATE (IV)

4.1 Introduction

This work has extended the investigation into the mechanism of glutathione oxidation to another biologically important thiol, homocysteine (HCSH). HCSH, having a slightly higher pK_a (8.9) [65] than GSH is known to be a risk factor for cardiovascular disease and stroke in humans [13]. The toxic effect of HCSH has been attributed, amongst other factors, to homocysteine thiolactone (tHCSH), a product of HCSH editing by tRNA synthetases [13]. tHCSH was shown to acylate protein lysine side chains in an irreversible fashion, thereby causing protein damage and autoimmune responses [13, 56-59].

Due to HCSH's role in the cellular systems, and its similarity to GSH based on the thiol functionality, it is interesting to study its mediated electrooxidation mechanism if a sensor is to be developed, as a high concentration of HCSH is associated with hyperhomocysteinemia [15]. It is also important to know if its medicated electrooxidation is similar to that of GSH. The reaction of $IrCl_6^{2-}$ with HCSH undergoes an EC′ reaction mechanism (Figure 36). Buffer-assisted electrooxidation of HCSH was pronounced when the concentration of the buffer was greater than 10 mM. It is obvious that as the buffer concentration increases, the peak potential gradually shifts less positive, implying a more efficient electrooxidation of HCSH, and the peak becomes less broad, indicating the involvement of the buffer. Electrooxidation at pH < 7.0 was not effective as the production of the HCSH anion (the reactive species) is less favored. As already observed with GSH previously, the rate of electrooxidation of HCSH decreases as the solution pH

changes from 7.0 to 10 (Section 3.3, Figure 27). The role of buffer as the driving-force of electrooxidation of HCSH was investigated. It was observed that the rate of electrooxidation increases with increasing pK_a of the buffer. This same effect has been reported in other studies as well [174, 176]. The Brønsted plot gave a slope of ~0.6, which is an indication of *concerted* (CPET) mechanism [152, 174]. The reactivity of HCSH (8.9 [65]), GSH (8.6 [36]), and CSH (8.3 [54]) toward $IrCl_6^{2-}$ correlates to increase in their pK_a. Experiments revealed that the reaction mechanism pathway changed from CPET to PT/ET between pH 7.0 − 10 as observed from kinetic isotope effect (KIE) values. Activation energy (E_a) and reorganization energy (λ) were determined by measuring the rate constant for the electron transfer between 10−30 ^{o}C.

4.2 Experimental Section

4.2.1 Reagents and Materials

L-glutathione reduced (99%), K_3IrCl_6, D_2O (99.9%), and DCl (35%) were purchased from Aldrich (St. Louis, MO). Propionic acid, PA, was purchase from Aldrich (Milwaukee, WI). Na_2HPO_4 (99%), NaH_2PO_4 (98%), and NaOH)97%) were purchased from EM Science (Cherry Hill, NJ). Maleic acid, MA, ($\geq$99%), citric acid, CA, ($\geq$99.5%), and *N*-(2-Acetamido)-2-aminoethanesulfonic acid, ACES, ($\geq$99.5%) were purchased from Fluka. HCl (37.3%), tris(hydroxymethyl)aminomethane (Tris) were purchased from Fisher Scientific (Fair Lawn, NJ). NaCl, 99+% and NaOD, 30 wt% solution in D_2O were purchased from Acros Organics (NJ, USA). Water was purified with a MilliQ purification system (Millipore). All reagents were used without further purification. Na_2DPO_4 and NaD_2PO_4 were prepared by triply dissolving Na_2HPO_4 and NaH_2PO_4 in

D_2O and evaporating solvent [137]. The pH of the sodium phosphate solutions was measured with standard pH meter, calibrated with H_2O buffers. pH meter readings for D_2O solutions were converted to pD values employing the equation pD = pH + 0.4 [29]. All solutions and subsequent dilutions were prepared using deionized water with a resistivity of 18.2 MΩ cm. All experiments were carried out in a solution volume of 5 cm^3 at room temperature, and deoxygenated with argon. The pH's of the buffer solutions were adjusted with NaOH and HCl; however, for deuterated buffer solutions, NaOD and DCl were used to adjust the pH.

4.2.2 Cyclic Voltammetry

Cyclic voltammograms were collected using a potentiostat (CH Instruments, Austin, TX) with a cell equipped with a glassy carbon (GC) working electrode (area = 0.06 cm^2), a Pt-wire counter electrode, and Ag/AgCl reference electrode (3.0 mM KCl). Glassy carbon electrode was polished with 0.05 µm alumina and rinsed with copious amount of water between experiments. In typical experiment performed, 1.0 mM metal complex and 3.0 mM homocysteine were dissolved in 5.0 cm^3 aqueous 35 mM buffer solutions containing 0.1 M NaCl, and unbuffered solutions containing 0.1 M NaCl. The potential was scanned from 0.4 V to 1.0 V. The experimental cyclic voltammograms were background subtracted and performed at 22^oC. The formal potential of $IrCl_6^{3-}$ is 0.72 V vs. Ag/AgCl.

4.2.3 Digital Simulation

      Second-order glutathione oxidation rate constants were determined by fitting the cyclic voltammograms to a mechanism involving Equations 18, 20, and 21 in Scheme 1. But for propionate buffers, Equation 20 was used as an association (K_{ass}) reaction between the buffer and HCSH, followed by the oxidation. The software package DigiSim version 3.03 (Bioanalytical Systems, Inc., West Lafayette, IN) was used to verify each mechanism at different scan rates where simulated and experimental CV's were compared. The values of diffusion coefficients were 8.2×10^{-6} cm^2/s for IrCl$_6$$^{3-}$ [172] and 3.0×10^{-5} cm^2/s for homocysteine. All other simulation parameters are given in the figure captions and appendix. The heterogeneous electron transfer rate constant (0.1 cm/s) was determined by fitting the voltammogram of IrCl$_6$$^{3-}$ in the absence of homocysteine. The electrooxidation equilibrium constant (K_{eq3}), was found to have a profound effect on the CV profile, and a value of 1×10^6 was generally used [135].

4.3 Results and Discussion

      Electrooxidation of HCSH: The electrooxidation of HCSH follows through an EC′ mechanism as shown in Figure 36 investigated in 35 mM phosphate buffer solution. Though HCSH alone in solution gave some anodic (oxidation) current, the current is small relative to the catalytic current and mediator's diffusion current at the mediator peak potential.

Figure 36. Plot of i (μA) vs. E (V) of the oxidation of homocysteine (3.0 mM) by $IrCl_6^{2-}$ (1.0 mM) in 35 mM sodium phosphate buffer containing 0.1 M NaCl at pH 7.0. (A) $IrCl_6^{3-}$ alone; (B) Homocysteine alone; (C) Homocysteine in the presence of $IrCl_6^{3-}$. Simulated CV's (open circle), Experimental CV's (solid line). Scan rate: 100 mV/s.

Figure 37. Plot of i (μA) vs. E (V) of the oxidation of homocysteine (3.0 mM) by $IrCl_6^{2-}$ (1.0 mM) in various concentrations of sodium phosphate buffer containing 0.1 M NaCl at pH 7.0. Pink (15 mM PB), Blue (20 mM PB), Green (25 mM PB), and Black (35 mM PB). Scan rate: 100 mV/s.

When the electrooxidation of HCSH was carried out at pH 7.0, but at various phosphate buffer concentrations, ([PB]), the catalytic current increases with [PB]. However, when [PB] < 15 mM, the CV's were featureless, and efficient oxidation of HCSH was not observed due to the slow deprotonation step attributed to inadequate amount of the buffer base ($[HPO_4^{2-}]/[H_2PO_4^-]$ = 3.9 mM/6.1 mM for 10 mM PB) and a slightly high pK_a of HCSH (8.9) [65]. Figure 37 reveals the participation of buffer as its concentration increases in the oxidation of GSH. It is vivid that as the [PB] increases, the peak broadness decreases, and the peak potential shifts less positively (more negatively). The implication of these observations is: the electrooxidation of HCSH in the presence of PB becomes easier with increase in [PB]. Other studies have shown that buffer assists in the electrooxidation of biological molecules [174, 176, 177].

Driving-force dependence: Understanding the dependence of electron-transfer rates on the driving force is an area of active interest [133, 135-137, 160, 174]. Recently, the dependence of electrooxidation rate of tyrosine on pK_a of buffers has been reported [174]. In this work, four different buffers have been used: propionic acid (pK_a 4.88), maleic acid (pK_a 6.24), *N*-(2-acetamido)-2-aminoethanesulfonic acid (pK_a 6.80), and sodium phosphate monobasic (pK_a 7.20) [175]. Based on Equation 16, a Brønsted relation (log k_3 vs. pK_a, Figure 38) can be plotted. Over a range of pK_a values of ~2.3, the log k_3 increases with the pK_a with a slope of ~0.6. This result is indicative of a *concerted* transfer of proton and electron to different acceptors [152, 173, 174].

Figure 38. Brønsted plot of log k_3 vs. pK_a of the oxidation of homocysteine (3.0 mM) by $IrCl_6^{2-}$ (1.0 mM) in 35 mM buffer solutions containing 0.1 M NaCl by varying the pK_a of the acceptor base. Plot was fitted to log k_3 = $0.64pK_a$ + 1.64 giving a slope of ~0.6. R^2 = 0.989. Rate constants were determined from digital simulations.

Figure 39. Plot of i (µA) vs. E (V) of the oxidation of glutathione, cysteine, and homocysteine (3.0 mM each) by $IrCl_6^{2-}$ (1.0 mM) in 35 mM sodium phosphate buffer containing 0.1 M NaCl at pH 7. (Green) cysteine and $IrCl_6^{3-}$; (Blue) glutathione and $IrCl_6^{3-}$; (Pink) Homocysteine and $IrCl_6^{3-}$. Scan rate: 100 mV/s.

Varying the pK$_a$ of these biological thiols (HCSH (8.9 [65]), GSH (8.6 [36]), and CSH (8.3 [54])) can serve as driving-force for the reduction of $IrCl_6^{2-}$. Many studies have investigated the dependence of rates on thiol pK$_a$ [60-64]. From Figure 39, the catalytic current increases with increase in pK$_a$ of the thiols. The rationale for this is that an electron-donating group will increase the pK$_a$, while an electron-withdrawing group will decrease it [63]. Therefore, a smaller pK$_a$ implies a lower electron density on S atom of the parent thiol. This electron "deficiency" causes slow oxidation of the thiol, leading to lower catalytic current, for example, cysteine. On the contrary, higher catalytic current observed for HCSH is a result of its electron-rich S atom.

Temperature dependence: In order to determine the activation energy (E_a) and the reorganization energy (λ, *energy necessary to transform the nuclear configurations in the reactant and the solvent to those of the product state* [155d]), rate constants for

Figure 40. Plot of log k$_3$ vs. Temp (K) of the oxidation of homocysteine (3.0 mM) by $IrCl_6^{2-}$ (1.0 mM) in 35 mM sodium phosphate buffer containing 0.1 M NaCl at pH 7.0. Rates were determined by fitting experimental CV's with digital simulator.

electron transfer at different temperatures (10−30 $^{\circ}$C) were measured, and then the temperature dependence was fitted to the Marcus Equations 29 and 30 [178]:

$$k_{ET} = Ae^{-E_a/k_B T} \qquad (29)$$

$$E_a = \frac{(\lambda + \Delta G^{\circ})^2}{4\lambda} \qquad (30)$$

k_{ET}, rate of electron transfer (M^{-1}s^{-1}); A, pre-exponential factor (10^{11} M^{-1}s^{-1}); E_a, activation energy (eV); k_B, Boltzmann constant (8.617×10^{-5} eV/K); T, temperature (K); λ, reorganization energy (eV); ΔG°, free energy change (eV). The driving force, ΔG°, for the electron-transfer reaction (Equation 21) was derived from the difference between the

$$HCSH \rightleftharpoons HCS^- + H^+ \qquad pK_a = 8.9 \qquad (31)$$

$$HCS^{\bullet} + H^+ + e^- \rightleftharpoons HCSH \qquad E^{\circ\prime} = 1.34 \text{ V} \qquad (32)$$
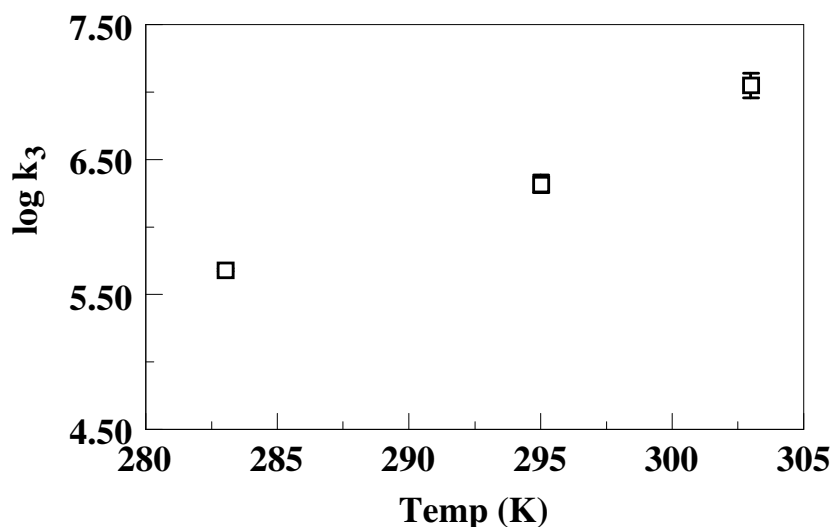
standard potentials of the respective redox couples. The E° value of the HCS$^-$/HCS$^{\bullet}$ couple has been calculated by combining Equations 31 and 32. The $E^{\circ\prime}$ (1.34 V) value was calculated from ΔE° of penicillamine relative to the chlorpromazine (ClPz) half-reaction considering the potential of the ClPz$^{2+/+}$ couple to be 0.83 V [179]. The value of 1.34 V for penicillamine was taken for HCSH because of their similarity in structure, and that various thiols studied in the above reference recorded similar ΔE° relative to ClPz$^{2+/+}$ couple. From the relation $E^{\circ} = E^{\circ\prime} + 0.059(\log K_a)$, E° for HCS$^-$/HCS$^{\bullet}$ couple is 0.815 V.

With the E^o value of the $IrCl_6^{3-/2-}$ couple at $\mu = 0.1$ M (0.892 V) [180], a value of 20 was obtained for the equilibrium constant (K_{eq3}) for the reaction 21. Using the relation $\Delta G^o = -RT\ln K_{eq3}$, $\Delta G^o = -7,422$ J/mol (-0.08 eV). Figure 40 gives the plot of log k_3 vs. Temp (K) showing increase in rate as the temperature increases, which is indicative of decrease in the activation energy (E_a), as well as decrease in the reorganization energy (λ) as depicted in Table 7.

Temp (^{o}C)	E_a (eV)	λ (eV)
10 ^{o}C	0.299	1.35
22 ^{o}C	0.283	1.25
30 ^{o}C	0.247	1.10

Table 7. Activation Energy (E_a) and Reorganization Energy (λ) for the electron transfer from homocysteine to $IrCl_6^{2-}$ at different temperatures.

Isotope Effect: Electrooxidation of HCSH was carried out in both undeuterated and deuterated buffer solutions in order to ascertain its oxidation reaction pathway. From Figure 41, the rate decreases with increase in pH/pD. As already explained from Figure 27, this decrease is due to the deprotonation of the ammonium group ($-NH_3^+$) of HCSH which resulted in the oxidation of HCSH deprotonated at the ($-SH$) and ($-NH_3^+$) groups.
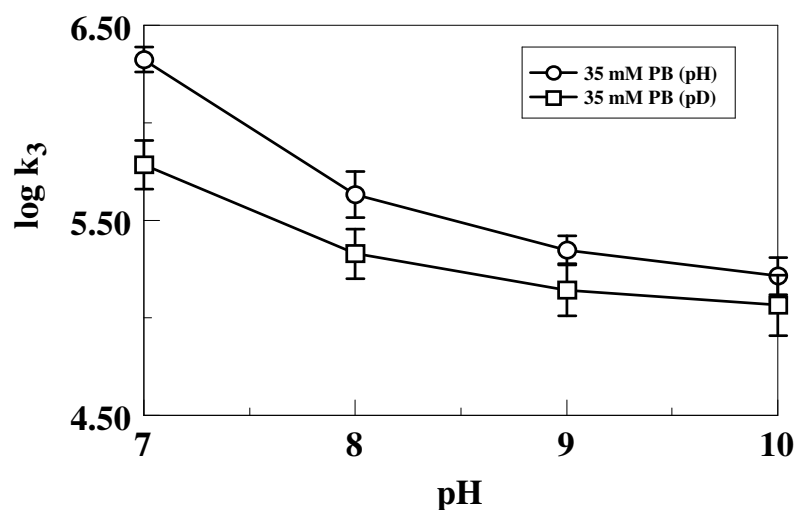
Figure 41. Plot of log k_3 vs. pH for the oxidation of homocysteine (3.0 mM) by $IrCl_6^{2-}$ (1.0 mM) in deuterated and undeuterated 35 mM sodium phosphate buffer containing 0.1 M NaCl at pH = pD 7.0−10. (Circle) homocysteine and $IrCl_6^{3-}$ in undeuterated solutions; (Square) Homocysteine and $IrCl_6^{3-}$ in deuterated solutions. Rates were obtained from digital simulations.
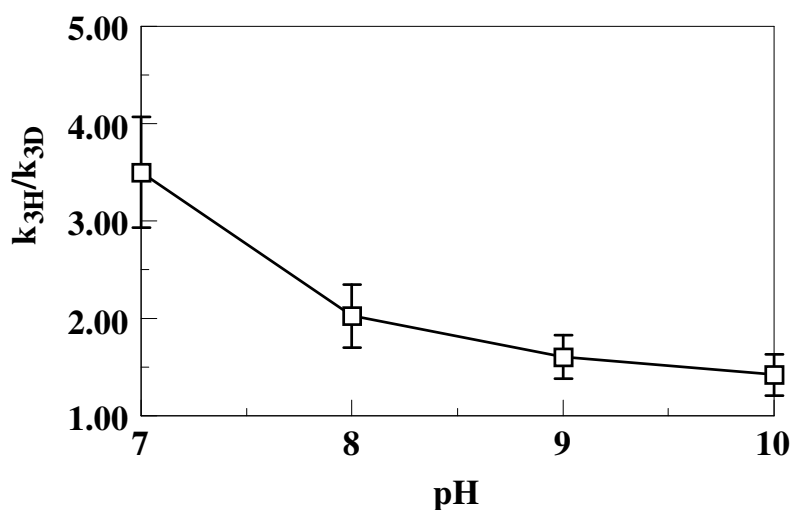
Figure 42. Plot of k_{3H}/k_{3D} vs. pH for the oxidation of homocysteine (3.0 mM) by $IrCl_6^{2-}$ (1.0 mM) in deuterated and undeuterated 35 mM sodium phosphate buffer containing 0.1 M NaCl at pH = pD = 7.0−10. Rates were obtained from digital simulations.

From Figure 42 and Table 8 (data in the Table 8 are used to derive Figure 42), it is clearly seen that the KIE decreases from 3.50 at pH = pD = 7 to 1.42 at pH = pD = 10. KIE value of 1.6 and above has been considered as an experimental marker for CPET mechanism [133, 140]. Therefore, it can simply be said that the electrooxidation of HCSH follows through *concerted* proton and electron transfer (CPET) to both the buffer and $IrCl_6{}^{2-}$, respectively, at pH's 7.0 and 8.0. Electrooxidation at pH 9.0 could be a mixed (both concerted and stepwise) pathway based on KIE value, and at pH 10, a *stepwise* proton and electron transfer (PT/ET) to the different acceptors. In conclusion, where the CPET dominates, both the proton and electron are involved in the rate determining step, and where PT/ET dominates the proton transfer is not the rate determining step (because it is transferred well before the transition state), whereas the electron transfer is the rate determining step.

pH	k_{3H} ($M^{-1}s^{-1}$)	k_{3D} ($M^{-1}s^{-1}$)	k_{3H}/k_{3D}
7.0	$2.13 \pm 0.3 \times 10^6$	$6.29 \pm 1.8 \times 10^5$	3.50 ± 0.57
8.0	$4.41 \pm 1.3 \times 10^5$	$2.20 \pm 0.6 \times 10^5$	2.03 ± 0.32
9.0	$2.24 \pm 0.4 \times 10^5$	$1.44 \pm 0.4 \times 10^5$	1.60 ± 0.22
10.0	$1.66 \pm 0.3 \times 10^5$	$1.22 \pm 0.4 \times 10^5$	1.42 ± 0.21

Table 8. Rates constants for the electrooxidation of homocysteine by $IrCl_6{}^{2-}$ obtained by fitting experimental CV's using digital simulator. Experiments were conducted with deuterated and undeuterated sodium phosphate buffer solution containing 0.1 M NaCl at different pH's. The KIE's were obtained by dividing rates in undeuterated solutions by rates in deuterated solutions.

5.0 CONCLUSION AND FUTURE RESEARCH

The results described in this dissertation show that glutathione, homocysteine, and cysteine are oxidized by EC′ reaction mechanism, a type of EC reaction in which O, for example, electrogenerated from R at the electrode surface reacts with a nonelectroactive species S in solution to regenerate R [155c]. The effects of solution pH and buffer have been identified. While increasing pH of unbuffered solution did not change the reaction mechanism for electrooxidation of GSH by $Ru(bpy)_3^{3+}$, increase in the pH (5.0 to 7.0 for PB; 7.0 to 9.0 for Tris/HCl) of buffered solution drastically altered the reaction mechanism, resulting in splitting of the voltammetric wave into two. At the lower pH values for the respective buffers, there is little or no buffer base, thus the electrocatalysis involved the oxidation of protonated GSH. On the other hand, at higher pH values for the two buffers, the electrocatalysis involved the oxidation of deprotonated GSH. This is true for CSH, likewise.

The assignment of the reaction pathways was done by performing the experiments in both deuterated and undeuterated buffers, as well as unbuffered solutions. The results show that the electrooxidation of GSH proceeds through the *concerted* proton and electron transfer (CPET) at all pH values investigated in unbuffered solutions with the kinetic isotope effect (KIE) in the range of 2.60−4.00, which is consistent with the experimental marker for CPET [133, 140]. In buffered solutions, CPET was also observed for the oxidation of GSH and CSH with values of 4.09 ± 1.33 and 2.49 ± 0.06, respectively.

In the complex case where the voltammetric wave is split into two, investigation as to why the oxidation peak splitting occurs was undertaken. In order to confirm if there

was no new compound formed from coordination of the metal mediator, ($Ru(bpy)_3^{2+}$), with GSH/CSH, UV/Vis experiments were performed in sodium phosphate buffer solutions at pH values of 5.0 and 7.0. The resulting spectra show no indication of any coordination of the metal with the thiol, as no wavelength shift occurs. Similarly, ^{1}HNMR experiments were also conducted at both pD values of 5.0 and 9.0 sodium phosphate buffer. ^{1}HNMR spectra indicate that the titration of CSH into $Ru(bpy)_3^{2+}$ solution did not result in any significant change in the proton chemical shifts of CSH or $Ru(bpy)_3^{2+}$, and no broadening of the proton peaks occurs.

Thus far, the notion of a new complex formation is erased. However, there is a need to consider the thiol (−SH) functionality. The thiol is thought to undergo deprotonation by the buffer allowing rapid oxidation of the thiolate anion, (RS^-). The proof of this is the voltammogram obtained for *N*-Acetylmethionine (*N*-Met), which gave a single oxidation peak at condition in which the pre-wave appears. At this point, the concept of *general base catalysis* surfaces, since the buffer is assisting in the electrooxidation.

In the electrooxidation of GSH by $IrCl_6^{2-}$, GSH was not observed to be effectively oxidized both in fairly acidic buffered (pH ≤ 6) and unbuffered solutions (pH ≤ 11.5) due to lower redox potential of $IrCl_6^{3-}$ compared to $Ru(bpy)_3^{2+}$. While $Ru(bpy)_3^{2+}$ can bring about the oxidation of GSH in acidic solution, $IrCl_6^{3-}$ will require the assistance of a base to carry out the oxidation of GSH. The oxidation of GSH by $Ru(bpy)_3^{3+}$ from pH 5.0 to 7.0 entails a change in the reaction mechanism, just as the oxidation of GSH by $IrCl_6^{2-}$ shows a change in the reaction mechanism. When the solution is unbuffered at 11.5 ≤ pH ≤ 12, oxidation of GSH can be observed. The same can be seen for the oxidation of GSH

when buffered solution is $6.0 \leq pH \leq 10$. It was seen that the oxidation of GSH was effective when the buffer solution pH is 7.0, it is expected that the oxidation rate should increase as the pH increases. Surprisingly, this is not so, due to the role of $-NH_3^+$ group in HCSH. As reported [19, 20, 22], and verified in this work, deprotonation of $-NH_3^+$ resulted in decrease in the rate of reaction between GSH and $IrCl_6^{2-}$.

The concept of general base catalysis was clearly observed between GSH and $IrCl_6^{2-}$. This was further confirmed by measuring the rates of oxidation as [PB] increases. The plot which is curvature in profile implies a change in the rate determining step as the [PB] increases [152, 156]; changing from proton transfer (PT) as rate determining step to both proton transfer (PT) and electron transfer (ET) as subsequent rate determining step. Scan rate experiments done in 10 mM PB, pH 7.0, support the view of PT as the rate determining step with the increase in the cathodic/reduction current as the scan rate increases. Conversely, no increase in the reduction current upon increase in the scan rate was observed at 35 mM PB, pH 7.0.

In order to determine the concentration of GSH by an electroanalytical sensor, it is important that consideration be given to the concentration of the buffer solution used. As ascertained in this work, for example, there is an optimum buffer concentration at which efficient GSH sensing can be achieved, and above this concentration, GSH cannot be detected successfully. This may as well be a result of deprotonation of the $-NH_3^+$ group as elucidated earlier. Deuterated experiments performed at pD = pH = 7.0, indicated that the electrooxidation of GSH follows through a concerted reaction mechanism with KIE value of 1.98 ± 0.10. This work has revealed that there is dependence of catalytic current on the driving-force (buffer pK_a). Experiments carried

out at pH 7.0 shows that as the buffers are varied from maleic acid (pK_a 6.24) to sodium phosphate (pK_a 7.20), i_{cat}/i_d increases but decreases for tris/HCl (pK_a 8.06). The reason for this trend is the contributions from the ratio of the base to acid, $[B]/[BH^+]$, or/and the pK_a. Nonetheless, when experiments were performed at the pK_a's of the buffers, i_{cat}/i_d increases as well, but for tris/HCl. The decrease in i_{cat}/i_d for tris/HCl compared to PB (at pH = pK_a for both) is probably due to the deprotonation of $-NH_3^+$ since its pK_a is close to GSH pK_a of 8.63.

In the last part of this work, the oxidation of HCSH could not be effectively observed in sodium phosphate buffer solution, pH $\leq$ 6.0. The involvement of buffer component as Brønsted base was clear when the peak potential of the catalytic current for the oxidation of HCSH shifts more negatively, and peak broadness decreases with increasing [PB] at constant pH. These results indicate that the electrooxidation of HCSH becomes easier with increasing [PB].

The electrooxidation of HCSH in buffers of different base strength has shown that the rate of oxidation increases with the driving-force (pK_a). Propionic acid with the smallest pK_a drove the oxidation of HCSH the least, while sodium phosphate with the largest pK_a drove the oxidation most. The Brønsted slope obtained is ~0.6, consistent with CPET [152, 173, 174]. Amongst the three biological thiols studied, the catalytic current was seen to increase as the pK_a of these thiols increases.

Temperature experiments revealed an increase in the rate with an increase in the temperature. This is so because there is enough energy provided for the reacting species to interact more effectively. The calculated activation energy (E_a) and reorganization energy (λ) increase with increase temperature. The reaction pathway for the oxidation of

HCSH was assigned by experiments carried out in both deuterated and undeuterated sodium phosphate buffer at pH = pD values of 7.0−10. The results show that between pH = pD values of 7.0 and 8.0, CPET dominates; at pH = pD = 9.0, both CPET and PT/ET could be involved, whereas PT/ET dominates at pH = pD = 10. In concluding, the results presented in the three parts of this work will be very useful if sensors for GSH and HCSH must be developed.

This work contributes to the long term active development of sensors for biological thiols, GSH and HCSH. Because both GSH and HCSH are present in the cellular systems, either can be interference in the detection of the other, and *vice versa*. One of the future works is to qualitatively analyze one without any contribution from the other. Second, experiments will be conducted on various amino acids that have the proclivity of being oxidized. The goal is to selectively oxidize one amino acid in the presence of others, so that only the amino acid will be used for the study of protein oxidation. Similar studies have been conducted in which guanine is the only nucleobase of DNA that metal complexes can electrooxidize [136, 137, 159-161, 181-183]. It is also crucial to investigate the solvent accessibility of amino acids using electron transfer between protein and metal mediator. This will afford the ability to probe the interaction proteins have with other biomolecules.

Third, the reduction of glutathione disulfide (GSSG), the oxidized form of GSH, will be studied. This will be a complementary study of the oxidation of GSH. It is practically significant to understand both the oxidation and reduction of GSH and GSSG, respectively. As the current interesting topics (CPET, PT/ET, and ET/PT) [133-144, 146,

163, 164, 174, 176, 177] in electrocatalysis have been observed in the oxidation of GSH, thus it is crucial to investigate these reaction pathways in the reduction of GSSG.

Fourth, the reaction pathways, concerted or stepwise, will be further investigated in the electrooxidation of these biologically important thiols by attaching a base at the electrode surface. Participation of buffer base has been observed in the homogeneous reaction; consequently it is of interest to investigate what the reaction mechanism will be at the surface of the modified electrode.

6.0 REFERENCES

[1] Wu, G.; Fang, Y.; Yang, S.; Lupton, J. R.; Turner, N. D.; "Glutathione Metabolism and its Implications for Health". *J. Nutr.* **2004,** *134,* 489-492.

[2] Townsend, D. M.; Tew, K. D.; Tapiero, H.; "The Importance of Glutathione in Human Disease". *Biomedicine & Pharmacotherapy* **2003,** *57,* 145-155.

[3] Turrens, J. F.; "Mitochondrial Formation of Reactive Oxygen Species". *J. Physiol.* **2003,** *552,* 335-344.

[4] Roederer, M.; Staal, F. J.; Anderson, M.; Rabin, R.; Raju, P. A.; Herzenberg, L. A.; Herzenberg, L. A.; "Disregulation of Leukocyte Glutathione in AIDS". *Ann. N. Y. Acad. Sci.* **1993,** *677,* 113-125.

[5] Buhl, R.; Jaffe, H. A.; Holroyd, K. J.; Wells, F. B.; Mastrangeli, A.; Saltini, C.; Cantin, A. M.; Crystal, R. G.; "Systemic Glutathione Deficiency in Symptom-Free HIV-Seropositive Individuals". *Lancet* **1989,** *2,* 1294-1298.

[6] de Quay, B.; Malinverni, R.; Lauterburg, B. H.; "Glutathione Depletion in HIV-Infected Patients: Role of Cysteine Deficiency and Effect of Oral N-Acetylcysteine". *AIDS* **1992,** *6,* 815-819.

[7] Kalebic, T.; Kinter, A.; Poli, G.; Anderson, M.; Meister, A.; Fauci, A.; "Suppression of Human Immunodeficiency Virus Expression in Chronically Infected Monocytic

Cells by Glutathione, Glutathione Ester, and N-Acetylcysteine". *Proceedings of the National Academy of Sciences* **1991,** *88,* 986-990.

[8] Staal, F. J. T.; Ela, S. W.; Roederer, M.; Anderson, M. T.; Herzenberg, L. A.; Herzenberg, L. A.; "Glutathione Deficiency and Human-Immunodeficiency-Virus Infection". *Lancet* **1992,** *339,* 909-912.

[9] Fairbank.VF; "Copper Sulfate-Induced Hemolytic Anemia - Inhibition of Glucose-6-Phosphate Dehydrogenase and Other Possible Etiologic Mechanisms". *Arch. Intern. Med.* **1967,** *120,* 428-432.

[10] Manzler, A. D.;Schreine, A. W.; "Copper-Induced Acute Hemolytic Anemia - a New Complication of Hemodialysis". *Ann. Intern. Med.* **1970,** *73,* 409-412.

[11] Deiss, A.; Lee, G. R.; Cartwrig, G. E.; "Hemolytic Anemia in Wilson's Disease". *Ann. Intern. Med.* **1970,** *73,* 413-418.

[12] Attri, S.; Sharma, N.; Jahagirdar, S.; Thapa, B. R. T.; Prasad, R.; "Erythrocyte Metabolism and Antioxidant Status of Patients with Wilson Disease with Hemolytic Anemia". *Pediatr. Res.* **2006,** *59,* 593-597.

[13] Jakubowski, H.; "Molecular Basis of Homocysteine Toxicity in Humans". *Cell. Mol. Life Sci.* **2004,** *61,* 470-487.

[14] Lonn, E.; Yusuf, S.; Arnold, M. J.; Sheridan, P.; Pogue, J.; Micks, M.; McQueen, M. J.; Probstfield, J.; Fodor, G.; Held, C.; Genest, J.; HOPE 2 Investigators;

"Homocysteine Lowering with Folic Acid and B Vitamins in Vascular Disease". *N. Engl. J. Med.* **2006,** *354,* 1567-1577.

[15] Miller, A. L.;Kelly, G. S.; "Methionine and Homocysteine Metabolism and the Nutritional Prevention of Certain Birth Defects and Complications of Pregnancy.". *Alt. Med. Rev.* **1996,** *1,* 220-235.

[16] Dickinson, D. A.;Forman, H. J.; "Cellular Glutathione and Thiols Metabolism". *Biochemical Pharmacology* **2002,** *64,* 1019-1026.

[17] LU, S. C.; "Regulation of Hepatic Glutathione Synthesis: Current Concepts and Controversies". *FASEB J.* **1999,** *13,* 1169-1183.

[18] Lu, S. C.; "Regulation of Glutathione Synthesis.". *Curr. Top. Cell Regul.* **2000,** *36,* 95-116.

[19] Chen, S. -N.; Hoffman, M. Z.; "Effect of pH on the Reactivity of the Carbonate Radical in Aqueous Solution". *Radiat. Res.* **1975,** *62,* 18-27.

[20] Hoffman, M. Z.; Hayon, E.; "Pulse Radiolysis Study of Sulfhydryl Compounds in Aqueous Solution". *J. Phys. Chem.* **1973,** *77,* 990-996.

[21] Scarpa, M.; Momo, F.; Viglino, P.; Vianello, F.; Rigo, A.; "Activated Oxygen Species in the Oxidation of Glutathione A Kinetic Study". *Biophysical Chemistry,* **1996,** *60,* 53-61.

[22] Ison, A.; Odeh, I. N.; Margerum, D. W.; "Kinetics and Mechanisms of Chlorine Dioxide and Chlorite Oxidations of Cysteine and Glutathione". *Inorg. Chem.* **2006,** *45,* 8768-8775.

[23] Rabenstein, D. L.; "Metal Complexes of Glutathione and their Biological Significance". *Coenzymes and Cofactors* **1989,** *3,* 147-186.

[24] Singh, B. K.; "Complexation Behaviour of Glutathione with Metal Ions". *Asian Journal of Chemistry* **2005,** *17,* 1-32.

[25] Hwang, C.; Sinskey, A.; Lodish, H.; "Oxidized Redox State of Glutathione in the Endoplasmic Reticulum". *Science* **1992,** *257,* 1496-1502.

[26] Griffith, O. W.; "Biologic and Pharmacologic Regulation of Mammalian Glutathione Synthesis.". *Free Radical Biology and Medicine* **1999,** *27,* 922-935.

[27] Cuozzo, J. W.;Kaiser, C. A.; "Competition between Glutathione and Protein Thiols for Disulphide-Bond Formation". *Nat. Cell Biol.* **1999,** *1,* 130-135.

[28] Carelli, S.; Ceriotti, A.; Cabibbo, A.; Fassina, G.; Ruvo, M.; Sitia, R.; "Cysteine and Glutathione Secretion in Response to Protein Disulfide Bond Formation in the ER". *Science* **1997,** *277,* 1681-1684.

[29] Millis, K. K.; Weaver, K. H.; Rabenstein, D. L.; "Oxidation/reduction Potential of Glutathione". *J. Org. Chem.* **1993,** *58,* 4144-4146.

[30] Bulleid, N. J.; Freedman, R. B.; "Defective Co-Translational Formation of Disulphide Bonds in Protein Disulphide-Isomerase-Deficient Microsomes". *Nature* **1988,** *335,* 649-651.

[31] Kaderbhai, M. A.; Austen, B. M.; "Studies on the Formation of Intrachain Disulfide Bonds in Newly Biosynthesized Bovine Prolactin - Role of Protein-Disulfide Isomerase". *European Journal of Biochemistry* **1985,** *153,* 167-178.

[32] Scheele, G.; Jacoby, R.; "Proteolytic Processing of Presecretory Proteins is Required for Development of Biological Activities in Pancreatic Exocrine Proteins". *J. Biol. Chem.* **1983,** *258,* 2005-2009.

[33] Scheele, G.; Jacoby, R.; "Conformational Changes Associated with Proteolytic Processing of Presecretory Proteins Allow Glutathione-Catalyzed Formation of Native Disulfide Bonds". *J. Biol. Chem.* **1982,** *257,* 12277-12282.

[34] Martensson, J.; Lai, J.; Meister, A.; "High-Affinity Transport of Glutathione is Part of a Multicomponent System Essential for Mitochondrial Function". *Proceedings of the National Academy of Sciences* **1990,** *87,* 7185-7189.

[35] Kurosawa, K.; Hayashi, N.; Sato, N.; Kamada, T.; Tagawa, K.; "Transport of Glutathione Across the Mitochondrial Membranes". *Biochemical and Biophysical Research Communications,* **1990,** *167,* 367-372.

[36] Osterberg, R.; Ligaarden, R.; Persson, A.; "Copper(I) Complexes of Penicillamine and Glutathione". *J. Inorg. Biochem.* **1979,** *10,* 341-355.

[37] Blais, M. -J.; Berthon, G.; "A New Contribution to the Determination of the Complex Equilibria of Oxidised Glutathione with Proton and Copper(II) in Aqueous Solution.". *J. Chem. Soc., Dalton Trans.* **1982,** 1803-1808.

[38] Meister, A.; Larsson, A.; "*in* the Metabolic Basis of Inherited Diseases.". **1995,** 1461-1477.

[39] Lyons, J.; Rauh-Pfeiffer, A.; Yu, Y. M.; Lu, X. -M.; Zurakowski, D.; Tompkins, R. G.; Ajami, A. M.; Young, V. R.; Castillo, L.; "Blood Glutathione Synthesis Rates in Healthy Adults Receiving a Sulfur Amino Acid-Free Diet". *Proceedings of the National Academy of Sciences* **2000,** *97,* 5071-5076.

[40] Jahoor, F.; Jackson, A.; Gazzard, B.; Philips, G.; Sharpstone, D.; Frazer, M. E.; Heird, W.; "Erythrocyte Glutathione Deficiency in Symptom-Free HIV Infection is Associated with Decreased Synthesis Rate". *Am. J. Physiol. Endocrinol. Metab.* **1999,** *276,* E205-211.

[41] Chung, T. K.; Funk, M. A.; Baker, D. H.; "L-2-Oxothiazolidine-4-Carboxylate as a Cysteine Precursor: Efficacy for Growth and Hepatic Glutathione Synthesis in Chicks and Rats". *J. Nutr.* **1990,** *120,* 158-165.

[42] Reeds, P. J.; Burrin, D. G.; Stoll, B.; Jahoor, F.; Wykes, L.; Henry, J.; Frazer, M. E.; "Enteral Glutamate is the Preferential Source for Mucosal Glutathione Synthesis in Fed Piglets". *Am. J. Physiol. Endocrinol. Metab.* **1997,** *273,* E408-415.

[43] Tapiero, H.; Mathe, G.; Couvreur, P.; Tew, K. D.; "Glutamine and Glutamate". *Biomedecine & Pharmacotherapy* **2002,** *56,* 446-457.

[44] Persaud, C.; Forrester, T.; Jackson, A. A.; "Urinary Excretion of 5-L-Oxoproline (Pyroglutamic Acid) is Increased during Recovery from Severe Childhood Malnutrition and Responds to Supplemental Glycine". *J. Nutr.* **1996,** *126,* 2823-2830.

[45] Grimble, R. F.; Jackson, A. A.; Persaud, C.; Wride, M. J.; Delers, F.; Engler, R.; "Cysteine and Glycine Supplementation Modulate the Metabolic Response to Tumor Necrosis Factor {Alpha} in Rats Fed a Low Protein Diet". *J. Nutr.* **1992,** *122,* 2066-2073.

[46] Rabenstein, D. L., Guevrement, R.; Evans, C. A.; "Metal Ions in Biological Systems". **1979,** Decker, *9,* Ch. 4.

[47] Granick, S.; Gilder, H.; "The Porphyrin Requirements of Haemophilus Influenzae and some Functions of the Vinyl and Propionic Acid Side Chains of Heme". *J. Gen. Physiol.* **1946,** *30,* 1-13.

[48] Goldberg, A.; Ashenbrucker, H.; Cartwright, G. E.; Wintrobe, M. M.; "Studies on the Biosynthesis of Heme in Vitro by Avian Erythrocytes". *Blood* **1956,** *11,* 821-833.

[49] Hamed, M. Y.; Silver, J.; "Studies on the Reactions of Ferric Iron with Glutathione and some Related Thiols. Part II. Complex Formation in the pH Range Three to Seven". *Inorg. Chim. Acta* **1983,** *80,* 115-122.

[50] Hamed, M. Y.; Silver, J.; Wilson, M. T.; "Studies on the Reactions of Ferric Iron with Glutathione and some Related Thiols. Part III. A Study of the Iron Catalyzed

Oxidation of Glutathione by Molecular Oxygen". *Inorg. Chim. Acta* **1983,** *80,* 237-244.

[51] Kassner, R. J.; Walchak, H.; "Heme Formation from Fe(II) and Porphyrin in Absence of Ferrochelatase Activity". *Biochim. Biophys. Acta* **1973,** *304,* 294-303.

[52] Silver, J.;Lukas, B.; "Studies on the Reactions of Ferric Iron with Glutathione and some Related Thiols. Part IV. A Study of the Reaction of Glutathione with Protoporphyrin IX Iron(III)". *Inorg. Chim. Acta* **1985,** *106,* 7-12.

[53] Moran L.K; Gutteridge J.M C; Quinlan G.J; "Thiols in Cellular Redox Signalling and Control". *Curr. Med. Chem.* **2001,** *8,* 763-772.

[54] DeCollo, T. V.; Lees, W. J.; "Effects of Aromatic Thiols on Thiol-Disulfide Interchange Reactions that Occur during Protein Folding". *J. Org. Chem.* **2001,** *66,* 4244-4249.

[55] Kruusma, J.; Benham, A. M.; Williams, J. A. G.; Kataky, R.; "An Introduction to Thiol Redox Proteins in the Endoplasmic Reticulum and a Review of Current Electrochemical Methods of Detection of Thiols". *Analyst* **2006,** *131,* 459-473.

[56] Glowacki, R.; Jakubowski, H.; "Cross-Talk between Cys(34) and Lysine Residues in Human Serum Albumin Revealed by N-Homocysteinylation". *J. Biol. Chem.* **2004,** *279,* 10864-10871.

[57] Jakubowski, H.; "Calcium-Dependent Human Serum Homocysteine Thiolactone Hydrolase - A Protective Mechanism Against Protein N-Homocysteinylation". *J. Biol. Chem.* **2000,** *275,* 3957-3962.

[58] Jakubowski, H.; Zhang, L.; Bardeguez, A.; Aviv, A.; "Homocysteine Thiolactone and Protein Homocysteinylation in Human Endothelial Cells - Implications for Atherosclerosis". *Circ. Res.* **2000,** *87,* 45-51.

[59] Jakubowski, H.; "Protein Homocysteinylation: Possible Mechanism Underlying Pathological Consequences of Elevated Homocysteine Levels". *FASEB J.* **1999,** *13,* 2277-2283.

[60] Shi, T.; Berglund, J.; Elding, L. I.; "Kinetics and Mechanism for Reduction of Trans-Dichlorotetracyanoplatinate(IV) by Thioglycolic Acid, L-Cysteine, DL-Penicillamine, and Glutathione in Aqueous Solution". *Inorg. Chem.* **1996,** *35,* 3498-3503.

[61] Hu, T. M.; Chou, T. C.; "The Kinetics of Thiol-Mediated Decomposition of S-Nitrosothiols". *AAPS J.* **2006,** *8,* E485-92.

[62] Podhradsky, D.; Drobnica, L.; Kristian, P.; "Reactions of Cysteine, its Derivatives, Glutathione, Coenzyme A, and Dihydrolipoic Acid with Isothiocyanates". *Cellular and Molecular Life Sciences* **1979,** *35,* 154-155.

[63] Kun Wang; Yongchun Hou; Wei Zhang; Ksebati, M. B.; Ming Xian; Cheng, J.; Wang, P. G.; " ^{15}N NMR and Electronic Properties of S-Nitrosothiols". *Bioorganic & Medicinal Chemistry Letters,* **1999,** *9,* 2897-2902.

[64] Szajewski, R. P.;Whitesides, G. M.; "Rate Constants and Equilibrium Constants for Thiol-Disulfide Interchange Reactions Involving Oxidized Glutathione". *J. Am. Chem. Soc.* **1980,** *102,* 2011-2026.

[65] Burner, U.; Jantschko, W.; Obinger, C.; "Kinetics of Oxidation of Aliphatic and Aromatic Thiols by Myeloperoxidase Compounds I and II". *FEBS Letters,* **1999,** *443,* 290-296.

[66] Chen, S.; "The Electrocatalytic Reactions of Cysteine and Cystine by Water-Soluble Iron Porphyrin, Manganese Porphyrin and Iron(II) Phenanthrolines". *Electrochimica Acta,* **1997,** *42,* 1663-1673.

[67] Willner, I.; Lapidot, N.; Riklin, A.; Kasher, R.; Zahavy, E.; Katz, E.; "Electron-Transfer Communication in Glutathione Reductase Assemblies: Electrocatalytic, Photocatalytic, and Catalytic Systems for the Reduction of Oxidized Glutathione". *J. Am. Chem. Soc.* **1994,** *116,* 1428-1441.

[68] Rieber, E. E.; Kosower, N. S.; Jaffe, E. R.; "Reduced Nicotinamide Adenine Dinucleotide and the Reduction of Oxidized Glutathione in Human Erythrocytes". *J. Clin. Invest.* **1968,** *47,* 66-71.

[69] Jablonski, P. P.; Anderson, J. W.; "Light-Dependent Reduction of Oxidized Glutathione by Ruptured Chloroplasts". *Plant Physiol.* **1978,** *61,* 221-225.

[70] Jocelyn, P. C.; "The Reduction of Oxidized Glutathione in Erythrocyte Haemolysates in Pernicious Anaemia". *Biochem. J.* **1960,** *77,* 363-368.

[71] Roth, E. J.; Schulman, S.; Vanderberg, J.; Olson, J.; "Pathways for the Reduction of Oxidized Glutathione in the Plasmodium Falciparum-Infected Erythrocyte: Can Parasite Enzymes Replace Host Red Cell Glucose-6-Phosphate Dehydrogenase?". *Blood* **1986,** *67,* 827-830.

[72] Rieber, E. E.; Jaffe, E. R.; "Reduction of Oxidized Glutathione in Normal and Glucose-6-Phosphate Dehydrogenase Deficient Erythrocytes and their Hemolysates". *Blood* **1970,** *35,* 166-172.

[73] Singh, R.; Kats, L.; "Catalysis of Reduction of Disulfide by Selenol". *Anal. Biochem.* **1995,** *232,* 86-91.

[74] Munk, V. P.; Sadler, P. J.; "Palladium(II) Diamine Complex Induces Reduction of Glutathione Disulfide". *Chem. Commun.* **2004,** 1788-1789.

[75] Chen, J.; He, Z.; Liu, H.; Cha, C.; "Electrochemical Determination of Reduced Glutathione (GSH) by Applying the Powder Microelectrode Technique". *J Electroanal Chem* **2006,** *588,* 324-330.

[76] Tang, H.; Chen, J.; Nie, L.; Yao, S.; Kuang, Y.; "Electrochemical Oxidation of Glutathione at Well-Aligned Carbon Nanotube Array Electrode". *Electrochimica Acta* **2006,** *51,* 3046-3051.

[77] Rover, L.; Kubota, L. T.; Hoehr, N. F.; "Development of an Amperometric Biosensor Based on Glutathione Peroxidase Immobilized in a Carbodiimide Matrix for the Analysis of Reduced Glutathione from Serum". *Clinica Chimica Acta* **2001,** *308,* 55-67.

[78] Sakhi, A. K.; Russnes, K. M.; Smeland, S.; Blomhoff, R.; Gundersen, T. E.; "Simultaneous Quantification of Reduced and Oxidized Glutathione in Plasma using a Two-Dimensional Chromatographic System with Parallel Porous Graphitized Carbon Columns Coupled with Fluorescence and Coulometric Electrochemical Detection". *Journal of Chromatography A* **2006,** *1104,* 179-189.

[79] Ruiz-Diaz, J. J. J.; Torriero, A. A. J.; Salinas, E.; Marchevsky, E. J.; Sanz, M. I.; Raba, J.; "Enzymatic Rotating Biosensor for Cysteine and Glutathione Determination in a FIA System". *Talanta* **2006,** *68,* 1343-1352.

[80] Nana, C. G.; Jian, W.; Pinga, D. J.; Qing, C. H.; Xi, C.; Feng, Z. Z.; "The Enhanced Electrogenerated Chemiluminescence of $Ru(Bpy)_3^{2+}$ by Glutathione on a Glassy Carbon Electrode Modified with some Porphine Compounds". *Analyst* **2000,** *125,* 2294-2298.

[81] Halbert, M. K.; Baldwin, R. P.; "Electrocatalytic and Analytical Response of Cobalt Phthalocyanine Containing Carbon Paste Electrodes Toward Sulfhydryl Compounds". *Anal. Chem.* **1985,** *57,* 591-595.

[82] Chailapakul, O.; Aksharanandana, P.; Frelink, T.; Einaga, Y.; Fujishima, A.; "The Electrooxidation of Sulfur-Containing Compounds at Boron-Doped Diamond Electrode". *Sensors and Actuators B: Chemical* **2001,** *80,* 193-201.

[83] Thackrey, R. D.;Riechel, T. L.; "Mediators for the Oxidation of Glutathione and Other Biological Thiols". *J Electroanal Chem* **1988,** *245,* 143.

[84] Nalini, B.; Narayanan, S. S.; "Electrocatalytic Oxidation of Sulfhydryl Compounds at Ruthenium(III) Diphenyldithiocarbamate Modified Carbon Paste Electrode". *Electroanalysis* **1998,** *10,* 779-783.

[85] Ballatori, N.; Clarkson, T. W.; "Biliary-Secretion of Glutathione and of Glutathione Metal-Complexes". *Fund. Appl. Toxicol.* **1985,** *5,* 816-831.

[86] Christie, N. T.; Costa, M.; "Invitro Assessment of the Toxicity of Metal-Compounds .4. Disposition of Metals in Cells - Interactions with Membranes, Glutathione, Metallothionein, and DNA". *Biol. Trace Elem. Res.* **1984,** *6,* 139-158.

[87] Rafter, G. W.; "The Effect of Copper on Glutathione Metabolism in Human-Leukocytes". *Biol. Trace Elem. Res.* **1982,** *4,* 191-197.

[88] Sivertsen, T.; "Copper-Induced GSH Depletion and Methemoglobin Formation Invitro in Erythrocytes of some Domestic-Animals and Man - Comparative-Study". *Acta Pharmacol. Toxicol.* **1980,** *46,* 121-126.

[89] Agar, N. S.; Smith, J. E.; "Effect of Copper on Red-Cell Glutathione and Enzyme Levels in High and Low Glutathione Sheep". *Proc. Soc. Exp. Biol. and Med.* **1973,** *142,* 502-505.

[90] Rafter, G. W.; "Copper Inhibition of Glutathione-Reductase and its Reversal with Gold Thiolates, Thiol, and Disulfide Compounds". *Biochem. Med.* **1982,** *27,* 381-391.

[91] Sakurai, H.; Yokoyama, A.; Tanaka, H.; "Studies on the Sulfur-Containing Chelating Agents. XXXI. Catalytic Effect of Copper (II) Ion to Formation of Mixed Disulfide". *Chem. Pharm. Bull.* **1971,** *19,* 1416-1423.

[92] Martin, R. B.; "*in* Metal Ions in Biological Systems". **1974,** *1,* 129.

[93] Albro, P. W.; Corbett, J. T.; Schroeder, J. L.; "Generation of Hydrogen Peroxide by Incidental Metal Ion-Catalyzed Autooxidation of Glutathione". *J. Inorg. Biochem.* **1986,** *27,* 191-203.

[94] Silver, J.; Hamed, M. Y.; Morrison, I. E. G.; "Studies of the Reactions of Ferric Iron with Glutathione and some Related Thiols. Part V. Solid Complexes Containing Fe(II) and Glutathione Or Fe(III) with Oxidized Glutathione". *Inorg. Chim. Acta* **1985,** *107,* 169-178.

[95] Hamed, M. Y.; Silver, J.; Wilson, M. T.; "Studies of the Reactions of Ferric Iron with Glutathione and some Related Thiols". *Inorg. Chim. Acta* **1983,** *78,* 1-11.

[96] Prestayko, A. W.; Crooke, S. T.; Carter, S. K.; "Cisplatin, Current Status and New Developments". **1980,**.

[97] Litterst, C. L.; Tong, S.; Hirokata, Y.; Siddik, Z. H.; "Alterations in Hepatic and Renal Levels of Glutathione and Activities of Glutathione S-Transferases from Rats Treated with Cis-Dichlorodiamminelatinum-II". *Cancer Chemother. Pharmacol.* **1982,** *8,* 67-71.

[98] Odenheimer, B.;Wolf, W.; "Reactions of Cisplatin with Sulfur-Containing Amino Acids and Peptides I. Cysteine and Glutathione". *Inorg. Chim. Acta* **1982,** *66,* L41-L43.

[99] Leyland-Jones, B.; Morrow, C.; Tate, S.; Urmacher, C.; Gordon, C.; Young, C. W.; "Cis-Diamminedichloroplatinum(II) Nephrotoxicity and its Relationship to Renal {Gamma}-Glutamyl Transpeptidase and Glutathione". *Cancer Res.* **1983,** *43,* 6072-6076.

[100] Chang, J. W.;Martin, R. B.; "Visible Circular Dichroism of Planar Nickel Ion Complexes of Peptides and Cysteine and Derivatives". *J. Phys. Chem.* **1969,** *73,* 4277-4283.

[101] Becker, R. H.; Nicoson, J. S.; Margerum, D. W.; "Nucleophile Assistance of Electron-Transfer Reactions between Nitrogen Dioxide and Chlorine Dioxide Concurrent with the Nitrogen Dioxide Disproportionation". *Inorg. Chem.* **2003,** *42,* 7938-7944.

[102] Odeh, I. N.; Francisco, J. S.; Margerum, D. W.; "New Pathways for Chlorine Dioxide Decomposition in Basic Solution". *Inorg. Chem.* **2002,** *41,* 6500-6506.

[103] Wang, L.; Odeh, I. N.; Margerum, D. W.; "Chlorine Dioxide Reduction by Aqueous Iron(II) through Outer-Sphere and Inner-Sphere Electron-Transfer Pathways". *Inorg. Chem.* **2004,** *43,* 7545-7551.

[104] Wang, L.; Nicoson, J. S.; Huff Hartz, K. E.; Francisco, J. S.; Margerum, D. W.; "Bromite Ion Catalysis of the Disproportionation of Chlorine Dioxide with

Nucleophile Assistance of Electron-Transfer Reactions between ClO_2 and BrO_2 in Basic Solution". *Inorg. Chem.* **2002,** *41,* 108-113.

[105] Alfassi, Z. B.; Huie, R. E.; Neta, P.; "Substituent Effects on Rates of One-Electron Oxidation of Phenols by the Radicals Chlorine Dioxide, Nitrogen Dioxide, and Trioxosulfate(1-)". *J. Phys. Chem.* **1986,** *90,* 4156-4158.

[106] Adams, G. E.; Boag, J. W.; Michael, B. D.; "Reactions of Hydroxyl Radical .1. Transient Spectra of some Inorganic Radical-Anions". *Transactions of the Faraday Society* **1965,** *61,* 1674-1680.

[107] Adams, G. E.; Mcnaught.G.E; Michael, B. D.; "Pulse Radiolysis of Sulphur Compounds .2. Free Radical Repair by Hydrogen Transfer from Sulphydryl Compounds". *Trans. Faraday Soc.* **1968,** *64,* 902.

[108] Purdie, J. W.; Gillis, H. A.; Klassen, N. V.; "Pulse Radiolysis of Penicillamine in Aqueous Solution: The Thiyl Radical and the Disulphide Radical Anion". *J. Chem. Soc. , Chem. Commun.* **1971,** 1163-1165.

[109] Callear, A. B.;Dickson, D. R.; "Transient Spectra and Primary Processes in Flash Photolysis of CH_3SSCH_3, CH_3SCH_3, CH_3SH and C_2H_5SH". *Trans. Faraday Soc.* **1970,** *66,* 1987.

[110] Banica, F. G.; Fogg, A. G.; Moreira, J. C.; "Catalytic Cathodic Stripping Voltammetry of Oxidized Glutathione at a Hanging Mercury Drop Electrode in the Presence of Nickel Ion". *Talanta* **1995,** *42,* 227-234.

[111] Banica, F. G.; Fogg, A. G.; Moreira, J. C.; "Catalytic Cathodic Stripping Voltammetry at a Hanging Mercury Drop Electrode of Glutathione in the Presence of Nickel Ion". *Analyst* **1994,** *119,* 2343-2349.

[112] Heyrovsky, M.;Vavricka, S.; "Electrochemical Reactivity of Homocysteine at Mercury Electrodes as Compared with Cysteine". *Bioelectrochem. Bioenerget.* **1999,** *48,* 43-51.

[113] O'Shea, T. J.;Lunte, S. M.; "Selective Detection of Free Thiols by Capillary Electrophoresis-Electrochemistry using a gold/mercury Amalgam Microelectrode". *Anal. Chem.* **1993,** *65,* 247-250.

[114] Gao, Z.; Yao, H.; Liu, W.; "Study on Electrocatalytic Oxidation of L-Cysteine at Glassy Carbon Electrode by (FcM)TMA and its Electrochemical Kinetics". *Electroanalysis* **2005,** *17,* 619-624.

[115] Nekrassova, O.; Allen, G. D.; Lawrence, N. S.; Jiang, L.; Jones, T. G. J.; Compton, R. G.; "The Oxidation of Cysteine by Aqueous Ferricyanide: A Kinetic Study using Boron Doped Diamond Electrode Voltammetry". *Electroanalysis* **2002,** *14,* 1464-1469.

[116] Raoof, J. -B.; Ojani, R.; Kolbadinezhad, M.; "Electrocatalytic Characteristics of Ferrocenecarboxylic Acid Modified Carbon Paste Electrode in the Oxidation and Determination of L-Cysteine". *Electroanalysis* **2005,** *17,* 2043-2051.

[117] Raoof, J. -B.; Ojani, R.; Beitollahi, H.; Hosseinzadeh, R.; "Electrocatalytic Oxidation and Highly Selective Voltammetric Determination of L-Cysteine at the

Surface of a 1-[4-(Ferrocenyl Ethynyl)Phenyl]-1-Ethanone Modified Carbon Paste Electrode". *Analytical Sciences* **2006,** *22,* 1213-1220.

[118] Toito Suarez, W.; Marcolino, J.,L. H.; Fatibello-Filho, O.; "Voltammetric Determination of N-Acetylcysteine using a Carbon Paste Electrode Modified with Copper(II) Hexacyanoferrate(III)". *Microchemical Journal* **2006,** *82,* 163-167.

[119] Salimi, A.; Hallaj, R.; Amini, M., K.; "Electrocatalytic Properties of [Ru(Bpy)(Tpy)Cl]PF$_6$ at Carbon Ceramic Electrode Modified with Nafion Sol-Gel Composite: Application to Amperometric Detection of l-Cysteine". *Analytica Chimica Acta* **2005,** *534,* 335-342.

[120] Strojek, J. W.; Granger, M. C.; Swain, G. M.; Dallas, T.; Holtz, M. W.; "Enhanced Signal-to-Background Ratios in Voltammetric Measurements made at Diamond Thin-Film Electrochemical Interfaces". *Anal. Chem.* **1996,** *68,* 2031-2037.

[121] Yano, T.; Tryk, D. A.; Hashimoto, K.; Fujishima, A.; "Electrochemical Behavior of Highly Conductive Boron-Doped Diamond Electrodes for Oxygen Reduction in Alkaline Solution". *J. Electrochem. Soc.* **1998,** *145,* 1870-1876.

[122] Popa, E.; Notsu, H.; Miwa, T.; Tryk, D. A.; Fujishima, A.; "Selective Electrochemical Detection of Dopamine in the Presence of Ascorbic Acid at Anodized Diamond Thin Film Electrodes". *Electrochem. Solid-State Lett.* **1999,** *2,* 49-51.

[123] Yano, T.; Popa, E.; Tryk, D. A.; Hashimoto, K.; Fujishima, A.; "Electrochemical Behavior of Highly Conductive Boron-Doped Diamond Electrodes for Oxygen Reduction in Acid Solution". *J. Electrochem. Soc.* **1999,** *146,* 1081-1087.

[124] Rao, T. N.; Yagi, I.; Miwa, T.; Tryk, D. A.; Fujishima, A.; "Electrochemical Oxidation of NADH at Highly Boron-Doped Diamond Electrodes". *Anal. Chem.* **1999,** *71,* 2506-2511.

[125] Xu, J.; Chen, Q.; Swain, G. M.; "Anthraquinonedisulfonate Electrochemistry: A Comparison of Glassy Carbon, Hydrogenated Glassy Carbon, Highly Oriented Pyrolytic Graphite, and Diamond Electrodes". *Anal. Chem.* **1998,** *70,* 3146-3154.

[126] Katz, E.;Willner, I.; "Biomolecule-Functionalized Carbon Nanotubes: Applications in Nanobioelectronics". *Chemphyschem* **2004,** *5,* 1085-1104.

[127] Wang, J.; "Carbon-Nanotube Based Electrochemical Biosensors: A Review". *Electroanalysis* **2005,** *17,* 7-14.

[128] Gao, H.; Kong, Y.; Cui, D.; Ozkan, C. S.; "Spontaneous Insertion of DNA Oligonucleotides into Carbon Nanotubes". *Nano Lett.* **2003,** *3,* 471-473.

[129] GuiseppiElie, A.; Lei, C.; Baughman, R. H.; "Direct Electron Transfer of Glucose Oxidase on Carbon Nanotubes". *Nanotechnology* **2002,** *13,* 559-564.

[130] Wang, J.; Li, M.; Shi, Z.; Li, N.; Gu, Z.; "Direct Electrochemistry of Cytochrome *c* at a Glassy Carbon Electrode Modified with Single-Wall Carbon Nanotubes". *Anal. Chem.* **2002,** *74,* 1993-1997.

[131] Wang, J.; Li, M.; Shi, Z.; Li, N.; Gu, Z.; "Electrocatalytic Oxidation of Norepinephrine at a Glassy Carbon Electrode Modified with Single Wall Carbon Nanotubes". *Electroanalysis* **2002,** *14,* 225-230.

[132] Nekrassova, O.; Kershaw, J.; Wadhawan, J. D.; Lawrence, N. S.; Compton, R. G.; "The Oxidation of Cysteine by Electrogenerated Octacyanomolybdate (v)". *Phys. Chem. Chem. Phys.* **2004,** *6,* 1316-1320.

[133] Rhile, I. J.; Markle, T. F.; Nagao, H.; DiPasquale, A. G.; Lam, O. P.; Lockwood, M. A.; Rotter, K.; Mayer, J. M.; "Concerted Proton-Electron Transfer in the Oxidation of Hydrogen-Bonded Phenols". *J. Am. Chem. Soc.* **2006,** *128,* 6075-6088.

[134] Mayer, J. M.;Rhile, I. J.; "Thermodynamics and Kinetics of Proton-Coupled Electron Transfer: Stepwise vs. Concerted Pathways". *Biochim. Biophys. Acta* **2004,** *1655,* 51-58.

[135] Fecenko, C. J.; Meyer, T. J.; Thorp, H. H.; "Electrocatalytic Oxidation of Tyrosine by Parallel Rate-Limiting Proton Transfer and Multisite Electron-Proton Transfer". *J. Am. Chem. Soc.* **2006,** *128,* 11020-11021.

[136] Weatherly, S. C.; Yang, I. V.; Armistead, P. A.; Thorp, H. H.; "Proton-Coupled Electron Transfer in Guanine Oxidation: Effects of Isotope, Solvent, and Chemical Modification". *J. Phys. Chem. B* **2003,** *107,* 372-378.

[137] Weatherly, S. C.; Yang, I. V.; Thorp, H. H.; "Proton-Coupled Electron Transfer in Duplex DNA: Driving Force Dependence and Isotope Effects on Electrocatalytic Oxidation of Guanine". *J. Am. Chem. Soc.* **2001,** *123,* 1236-1237.

[138] Costentin, C.; Robert, M.; Saveant, J. -M.; "Concerted Proton-Electron Transfer Reactions in Water. are the Driving Force and Rate Constant Depending on pH when Water Acts as Proton Donor Or Acceptor?". *J. Am. Chem. Soc.* **2007,** *129,* 5870-5879.

[139] Costentin, C.; Robert, M.; Saveant, J. -M.; "Electrochemical and Homogeneous Proton-Coupled Electron Transfers: Concerted Pathways in the One-Electron Oxidation of a Phenol Coupled with an Intramolecular Amine-Driven Proton Transfer". *J. Am. Chem. Soc.* **2006,** *128,* 4552-4553.

[140] Costentin, C.; Evans, D. H.; Robert, M.; Saveant, J. -.; Singh, P. S.; "Electrochemical Approach to Concerted Proton and Electron Transfers. Reduction of the Water-Superoxide Ion Complex". *J. Am. Chem. Soc.* **2005,** *127,* 12490-12491.

[141] Costentin, C.; Robert, M.; Saveant, J. -.; "Electrochemical Concerted Proton and Electron Transfers. Potential-Dependent Rate Constant, Reorganization Factors, Proton Tunneling and Isotope Effects". *J. Electroanal. Chem.* **2006,** *588,* 197-206.

[142] Costentin, C.; Robert, M.; Saveant, J. -.; "Carboxylates as Proton-Accepting Groups in Concerted Proton-Electron Transfers. Electrochemistry of the 2,5-Dicarboxylate 1,4-Hydrobenzoquinone/2,5-Dicarboxy 1,4-Benzoquinone Couple". *J. Am. Chem. Soc.* **2006,** *128,* 8726-8727.

[143] Sjodin, M.; Styring, S.; Wolpher, H.; Xu, Y.; Sun, L.; Hammarstrom, L.; "Switching the Redox Mechanism: Models for Proton-Coupled Electron Transfer from Tyrosine and Tryptophan". *J. Am. Chem. Soc.* **2005,** *127,* 3855-3863.

[144] Sjodin, M.; Styring, S.; Akermark, B.; Sun, L.; Hammarstrom, L.; "Proton-Coupled Electron Transfer from Tyrosine in a Tyrosine-Ruthenium-Tris-Bipyridine Complex: Comparison with TyrosineZ Oxidation in Photosystem II". *J. Am. Chem. Soc.* **2000,** *122,* 3932-3936.

[145] Cukier, R. I.;Nocera, D. G.; "Proton-Coupled Electron Transfer". *Annu. Rev. Phys. Chem.* **1998,** *49,* 337-369.

[146] Mayer, J. M.; "Proton-Coupled Electron Transfer: A Reaction Chemist's View". *Annu. Rev. Phys. Chem.* **2004,** *55,* 363-390.

[147] Carey, F. A.;Sundberg, R. J.; " *Advanced Organic Chemistry, Part A: Structure and Mechanisms. 4*[th] *Edition;*". **2000,** 228-233, 823.

[148] Bronsted, J. N.;Pedersen, K. J. Z.; *Physikal. Chem.* **1924,** *108,* 185.

[149] Loechler, E. L.;Hollocher, T. C.; "Reduction of Flavins by Thiols. 2. Spectrophotometric Evidence for a Thiol-C(4a) Flavin Adduct and the Kinetics of Deprotonation of the -SH Group of the Dithiothreitol Adduct". *J. Am. Chem. Soc.* **1980,** *102,* 7322-7327.

[150] Stefanidis, D.;Jencks, W. P.; "General Base Catalysis of Ester Hydrolysis". *J. Am. Chem. Soc.* **1993,** *115,* 6045-6050.

[151] Thompson, J. E.;Raines, R. T.; "Value of General Acid-Base Catalysis to Ribonuclease A". *J. Am. Chem. Soc.* **1994,** *116,* 5467-5468.

[152] Fife, T. H.;Natarajan, R.; "General Acid Catalyzed Acetal Hydrolysis. the Hydrolysis of Acetals and Ketals of Cis- and Trans-1,2-Cyclohexanediol. Changes in Rate-Determining Step and Mechanism as a Function of pH". *J. Am. Chem. Soc.* **1986,** *108,* 8050-8056.

[153] Kwan, E. E.; "Factors Affecting the Relative Efficiency of General Acid Catalysis". *J. Chem. Educ.* **2005,** *82,* 1026-1030.

[154] Kissinger, P. T.; Heineman, W. R.; "Cyclic Voltammetry". *J. Chem. Educ.* **1983,** *60,* 702-706.

[155] Bard, A. J.; Faulkner L. R.; "Electrochemical Methods: Fundamentals and Applications". **2000.** Wiley & Sons, NJ. (a) pp. 580-602; (b) pp. 226-246; (c) p. 474; (d) p. 120.

[156] Jencks, W. P.;Salvesen, K.; "Reaction of Thiols with Acetylimidazole. Evidence for Independent Reaction Pathways". *J. Am. Chem. Soc.* **1971,** *93,* 1419-1427.

[157] Jencks, W. P.; "*Catalysis in Chemistry and Enzymology.*". **1969,** 644.

[158] Okuyama, T.; Komoguchi, S.; Fueno, T.; "Reaction of Thiols with Phenylglyoxal to Give Thiol Esters of Mandelic Acid. II. Intramolecular General-Base Catalysis and Change in Rate-Determining Step". *J. Am. Chem. Soc.* **1982,** *104,* 2582-2587.

[159] Johnston, D. H.;Thorp, H. H.; "Cyclic Voltammetry Studies of Polynucleotide Binding and Oxidation by Metal Complexes: Homogeneous Electron-Transfer Kinetics". *J. Phys. Chem.* **1996,** *100,* 13837-13843.

[160] Johnston, D. H.; Glasgow, K. C.; Thorp, H. H.; "Electrochemical Measurement of the Solvent Accessibility of Nucleobases using Electron Transfer between DNA and Metal Complexes". *J. Am. Chem. Soc.* **1995,** *117,* 8933-8938.

[161] Armistead, P. M.;Thorp, H. H.; "Oxidation Kinetics of Guanine in DNA Molecules Adsorbed Onto Indium Tin Oxide Electrodes". *Anal. Chem.* **2001,** *73,* 558-564.

[162] Neshvad, G.; Hoffman, M. Z.; Mulazzani, Q. G.; Venturi, M.; Ciano, M.; D'Angelantonio, M.; "One-Electron Reduction of Tris(2,2'-Bipyrimidine)Ruthenium(2+) Ion in Aqueous Solution: A Photochemical, Radiation Chemical, and Electrochemical Study". *J. Phys. Chem.* **1989,** *93,* 6080-6088.

[163] Sjodin, M.; Ghanem, R.; Polivka, T.; Pan, J.; Styring, S.; Sun, L. C.; Sundstrom, V.; Hammarstrom, L.; "Tuning Proton Coupled Electron Transfer from Tyrosine: A Competition between Concerted and Step-Wise Mechanisms". *Physical Chemistry Chemical Physics* **2004,** *6,* 4851-4858.

[164] Meyer, T. J.; Huynh, M. H. V.; Thorp, H. H.; "The Possible Role of Proton-Coupled Electron Transfer (PCET) in Water Oxidation by Photosystem II". *Angewandte Chemie-International Edition* **2007,** *46,* 5284-5304.

[165] Saveant, J. -.M,; "*Elements of Molecular and Biomolecular Electrochemistry.*". **2006,** p 485.

[166] Martin, C. R.; Rubinstein, I.; Bard, A. J.; "The Heterogeneous Rate Constant for the Ru(Bpy)$_3{}^{3+/2+}$ Couple at a Glassy Carbon Electrode in Aqueous Solution". *J. Electroanal. Chem.* **1983,** *151,* 267-271.

[167] Hung, M.;Stanbury, D. M.; "Oxidation of Thioglycolate by [Os(Phen)$_3$]$^{3+}$: An Unusual Example of Redox-Mediated Aromatic Substitution". *Inorg. Chem.* **2005,** *44,* 9952-9960.

[168] Saha, B.; Hung, M.; Stanbury, D. M.; "Reduction of Octacyanomolybdate(V) by Thioglycolic Acid in Aqueous Media". *Inorg. Chem.* **2002,** *41,* 5538-5543.

[169] Sun, J.;Stanbury, D. M.; "Kinetics and Mechanism of Oxidation of Thioglycolic Acid by Hexachloroiridate(IV)". *J. Chem. Soc. , Dalton Trans.* **2002,** 785-791.

[170] Fotouhi, L.; Hajilari, F.; Heravi, M. M.; "Electrochemical Behavior of some Thiotriazoles in Aqueous-Alcoholic Media at GCE". *Electroanalysis* **2002,** *14,* 1728-1732.

[171] "The CRC Handbook of Chemistry and Physics, 87Th Edition, Reports an Increase in Relative Viscosity (to Water) from 1.016 to 1.549, when Increasing the Concentration of NaH$_2$PO$_4$ from 0.042 to 1.091 M.". **2006-2007,**.

[172] Llopis, J. F.;Colom, F.; "*in Encyclopedia of Electrochemistry of the Elements;*". **1976,** *6,* 224-226.

[173] Barnett, R. E.;Jencks, W. P.; "Diffusion-Controlled Proton Transfer in Intramolecular Thiol Ester Aminolysis and Thiazoline Hydrolysis". *J. Am. Chem. Soc.* **1969,** *91,* 2358-2369.

[174] Fecenko, C. J.; Thorp, H. H.; Meyer, T. J.; "The Role of Free Energy Change in Coupled Electron-Proton Transfer". *J. Am. Chem. Soc.* **2007,** *129,* 15098-15099.

[175]

http://www.sigmaaldrich.com/Area_of_Interest/Biochemicals/BioUltra/Biological_B
uffers.html;

[176] Irebo, T.; Reece, S. Y.; Sjodin, M.; Nocera, D. G.; Hammarstrom, L.; "Proton-Coupled Electron Transfer of Tyrosine Oxidation: Buffer Dependence and Parallel Mechanisms". *J. Am. Chem. Soc.* **2007,** *129,* 15462-15464.

[177] Ishikita, H.; Soudackov, A. V.; Hammes-Schiffer, S.; "Buffer-Assisted Proton-Coupled Electron Transfer in a Model Rhenium-Tyrosine Complex". *J. Am. Chem. Soc.* **2007,** *129,* 11146-11152.

[178] Marcus, R. A.;Sutin, N.; "Electron Transfers in Chemistry and Biology". *Biochim. Biophys. Acta* **1985,** *811,* 265-322.

[179] Surdhar, P. S.;Armstrong, D. A.; "Reduction Potentials and Exchange Reactions of Thiyl Radicals and Disulfide Anion Radicals". *J. Phys. Chem.* **1987,** *91,* 6532-6537.

[180] Margerum, D. W.; Chellappa, K. L.; Bossu, F. P.; Burce, G. L.; "Characterization of a Readily Accessible Copper(III)-Peptide Complex". *J. Am. Chem. Soc.* **1975,** *97,* 6894-6896.

[181] Neyhart, G. A.; Cheng, C. -.; Thorp, H. H.; "Kinetics and Mechanism of the Oxidation of Sugars and Nucleotides by Oxoruthenium(IV): Model Studies for Predicting Cleavage Patterns in Polymeric DNA and RNA". *J. Am. Chem. Soc.* **1995,** *117,* 1463-1471.

[182] Sistare, M. F.; Holmberg, R. C.; Thorp, H. H.; "Electrochemical Studies of Polynucleotide Binding and Oxidation by Metal Complexes: Effects of Scan Rate, Concentration, and Sequence". *J. Phys. Chem. B* **1999,** *103,* 10718-10728.

[183] Yang, I. V.;Thorp, H. H.; "Kinetics of Metal-Mediated One-Electron Oxidation of Guanine in Polymeric DNA and in Oligonucleotides Containing Trinucleotide Repeat Sequences". *Inorg. Chem.* **2000,** *39,* 4969-4976.

7.0 APPENDIX

$$AH_2 + B \;\underset{k_{-1}}{\overset{k_1}{\rightleftharpoons}}\; AH^- + BH^+ \tag{1}$$

$$AH^- + B \;\underset{k_{-1}'}{\overset{k_1'}{\rightleftharpoons}}\; A^{2-} + BH^+ \tag{2}$$

$$AH^- + IrCl_6{}^{2-} \;\overset{k_2}{\longrightarrow}\; AH^{\bullet} + IrCl_6{}^{3-} \tag{3}$$

$$A^{2-} + IrCl_6{}^{2-} \;\overset{k_2'}{\longrightarrow}\; A^{-\bullet} + IrCl_6{}^{3-} \tag{4}$$
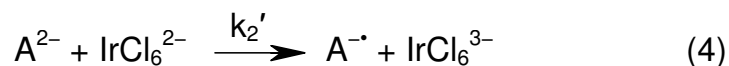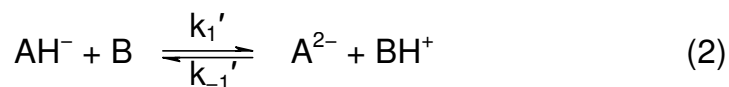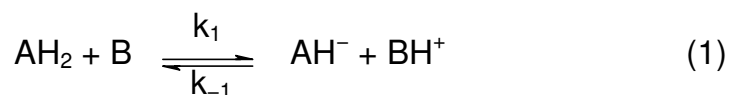
Using equations 1-4.

$$K_{dep}1 = \frac{[AH^-][BH^+]}{[AH_2][B]} = 10^{\,pK_a(B) - pK_a(AH_2)} \tag{5}$$

$$K_{dep}2 = \frac{[A^{2-}][BH^+]}{[AH^-][B]} = 10^{\,pK_a(B) - pK_a(AH^-)} \tag{6}$$

where deprotonation constants, $K_{dep}1$ is for Eq 1 and $K_{dep}2$ is for Eq 2.

$$-\frac{d[IrCl_6{}^{3-}]}{dt} = k_2[AH^-][IrCl_6{}^{2-}] + k_2'[A^{2-}][IrCl_6{}^{2-}] \tag{7}$$

Mass balance: $[AH_2]_T = [AH_2] + [AH^-] + [A^{2-}]$ \tag{8}

From eqs 5,

$$[AH_2] = \frac{[AH^-][BH^+]}{[B]10^{\,pK_a(B) - pK_a(AH_2)}}$$

From eqs 6,

$$[A^{2-}] = \frac{[AH^-][B]10^{\,pK_a(B) - pK_a(AH^-)}}{[BH^+]}$$

Substitute for $[AH_2]$ and $[A^{2-}]$ in Eq 8.

$$[AH_2]_T = \frac{[AH^-][BH^+]}{[B]10^{pK_a(B) - pK_a(AH_2)}} + [AH^-] + \frac{[AH^-][B]10^{pK_a(B) - pK_a(AH^-)}}{[BH^+]}$$

$$\frac{[B]}{[BH^+]} = 10^{pH - pK_a(B)} \tag{9}$$

$$[AH_2]_T = \frac{[AH^-]}{1^{\;pK_a(B) - pK_a(AH_2)}10^{pH - pK_a(B)}} + [AH^-]$$

$$+ [AH^-]10^{pK_a(B) - pK_a(AH^-)}10^{pH - pK_a(B)}$$

$$[AH_2]_T = \frac{[AH^-]}{10^{pH - pK_a(AH_2)}} + [AH^-] + [AH^-]10^{pH - pK_a(AH^-)} \tag{10}$$

$$[AH^-] = \frac{[AH_2]_T 10^{pH - pK_a(AH_2)}}{1 + 10^{pH - pK_a(AH_2)} + 10^{2pH - pK_a(AH_2) - pK_a(AH^-)}} \tag{11}$$

$$-\frac{d[AH^{\cdot}]}{dt} = k_2[AH^-][IrCl_6^{2-}] \tag{12}$$

Substitute for $[AH^-]$ in Eq 12.

$$-\frac{d[AH^{\cdot}]}{dt} = k_2[IrCl_6^{2-}]\left(\frac{[AH_2]_T\, 10^{pH - pK_a(AH_2)}}{1 + 10^{pH - pK_a(AH_2)} + 10^{2pH - pK_a(AH_2) - pK_a(AH^-)}}\right)$$

$$-\frac{d[A^{-\cdot}]}{dt} = k_2'[A^{2-}][IrCl_6^{2-}] \tag{13}$$

$$\frac{[A^{2-}]}{[AH^-]} = 10^{pH - pK_a(AH^-)} \tag{14}$$

Using the value of $[AH^-]$ in Eq 11, substitute for $[A^{2-}]$ in Eq 13.

$$-\frac{d[A^{-\cdot}]}{dt} = k_2'[IrCl_6^{2-}]\left(\frac{[AH_2]_T\, 10^{2pH - pK_a(AH_2) + pK_a(AH^-)}}{1 + 10^{pH - pK_a(AH_2)} + 10^{2pH - pK_a(AH_2) - pK_a(AH^-)}}\right)$$
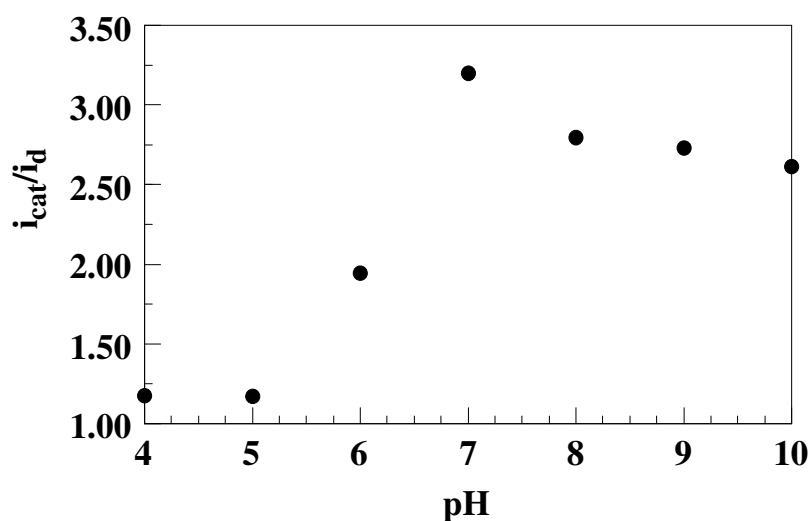
Figure 43. Plot of i_{cat}/i_d vs. pH of sodium phosphate buffer (mM) for the oxidation of glutathione (3.0 mM) by $IrCl_6^{2-}$ (1.0 mM). i_{cat} is the catalytic current; i_d is diffusion current of metal oxidant in the absence of glutathione.

Formation of $[IrCl_6^{2-}]$ from Eqs 3 and 4.

$$-\frac{d[IrCl_6^{3-}]}{dt} = k_2[IrCl_6^{2-}]\left(\frac{[AH_2]_T 10^{pH - pK_a(AH_2)}}{1 + 10^{pH - pK_a(AH_2)} + 10^{2pH - pK_a(AH_2) - pK_a(AH^-)}}\right)$$

$$+ k_2'[IrCl_6^{2-}]\left(\frac{[AH_2]_T 1^{2pH - pK_a(AH_2) + pK_a(AH^-)}}{1 + 10^{pH - pK_a(AH_2)} + 10^{2pH - pK_a(AH_2) - pK_a(AH^-)}}\right)$$

$$-\frac{d[IrCl_6^{3-}]}{dt} = [AH_2]_T[IrCl_6^{2-}]\left(\frac{k_2 10^{pH - pK_a(AH_2)} + k_2' 10^{2pH - pK_a(AH_2) - pK_a(AH^-)}}{1 + 10^{pH - pK_a(AH_2)} + 10^{2pH - pK_a(AH_2) - pK_a(AH^-)}}\right)$$

$$(15)$$
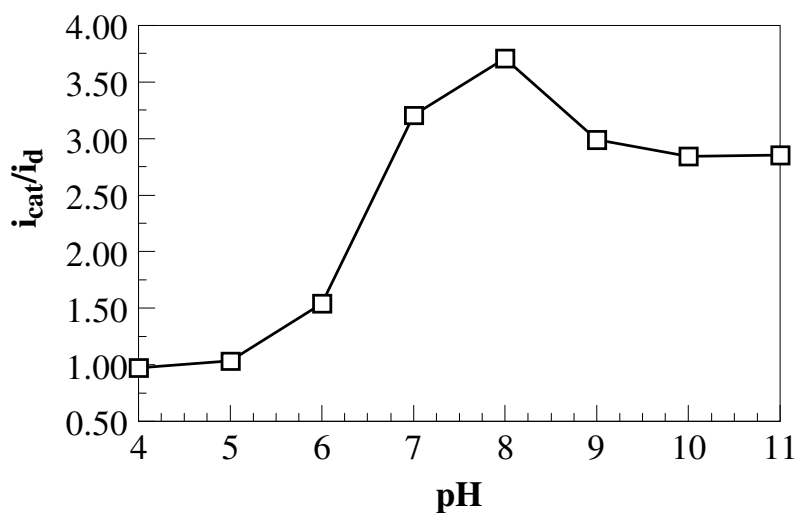
Figure 44. Simulated i_{cat}/i_d vs. pH of PB for the oxidation of GSH by $IrCl_6^{2-}$. Using the two deprotonation reactions of GSH at the thiol and amino groups in the digital simulator. $K_{eq2} = K_{eq2}' = 1.0 \times 10^6$; $k_2 = 4.0 \times 10^5 \ M^{-1}s^{-1}$; $k_2' = 2.0 \times 10^5 \ M^{-1}s^{-1}$. $i_d = 1.5 \times 10^{-5}$ A.
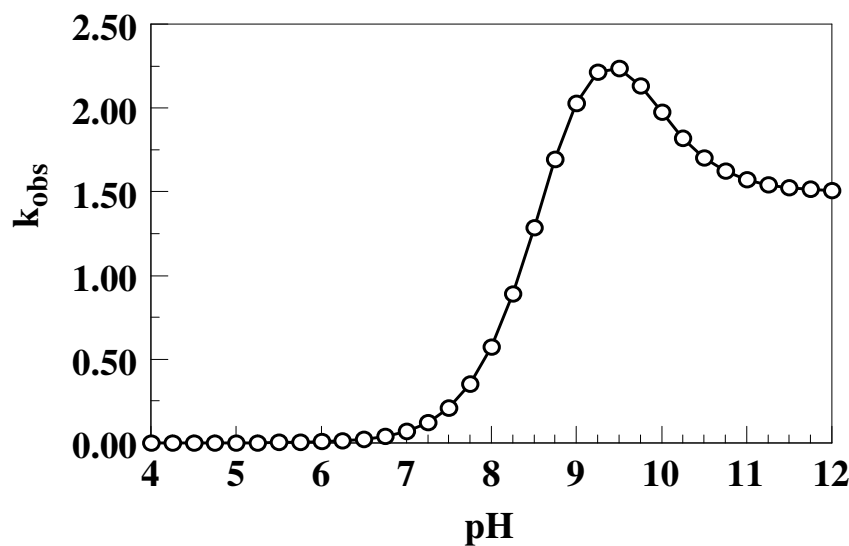
Figure 45. Plot of k_{obs} vs. pH of PB for the oxidation of GSH by $IrCl_6^{2-}$. Using the two deprotonation reactions of GSH at the thiol and amino groups in the kinetic data. $k_2 = 1.0 \times 10^6 \ M^{-1}s^{-1}$; $k_2' = 5.0 \times 10^5 \ M^{-1}s^{-1}$. $pK_a \ (-SH) = 8.63$, $pK_a \ (-NH_3^+) = 9.70$.

1. OXIDATION OF GSH BY Ru(bpy)$_3^{3+}$
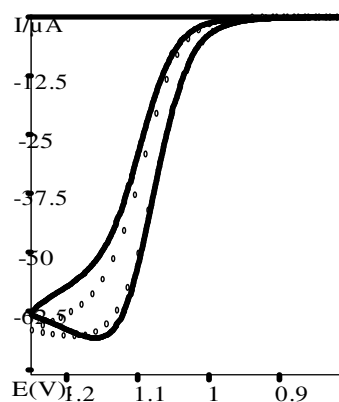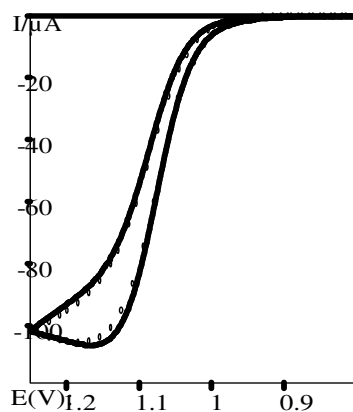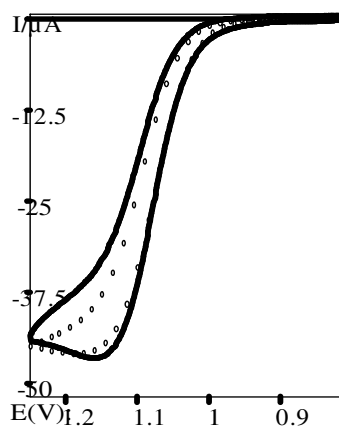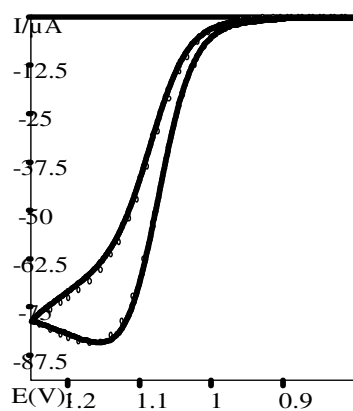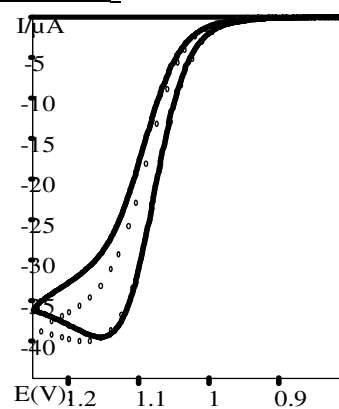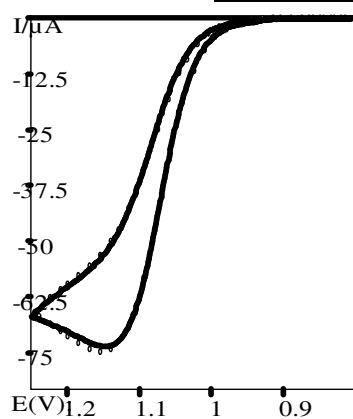
Simulated CV's for oxidation of GSH in 50 mM PB, pH 5.0. Scan rates: 100, 200, 500 mV/s. $k_f = 1.41 \pm 0.2 \times 10^4$ M^{-1}s^{-1}; $K_{eq2} = 1 \times 10^3$; $E^o = 1.08$ V; $k_h = 0.06$ cm/s; $\alpha = 0.5$.
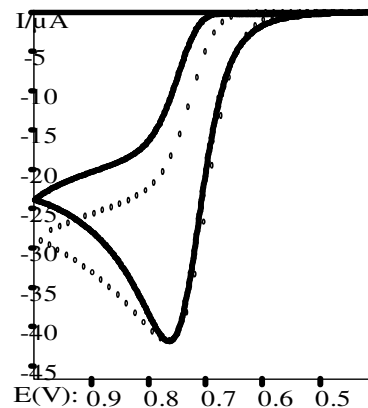
Simulated CV's for oxidation of GSH in 50 mM PB, pD 5.0. Scan rates: 100, 200, 500 mV/s. $k_f = 3.94 \pm 0.2 \times 10^3$ M^{-1}s^{-1}; $K_{eq2} = 1 \times 10^3$; $E^o = 1.08$ V; $k_h = 0.06$ cm/s; $\alpha = 0.5$.
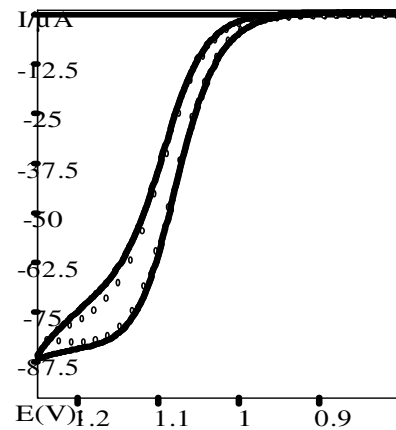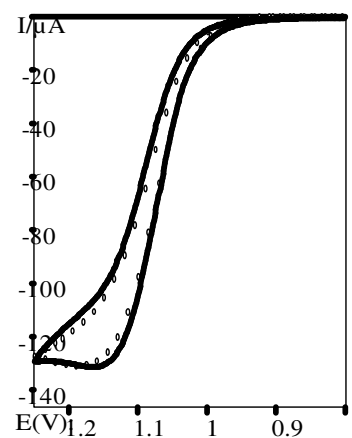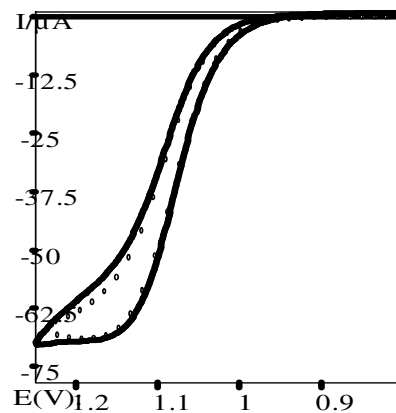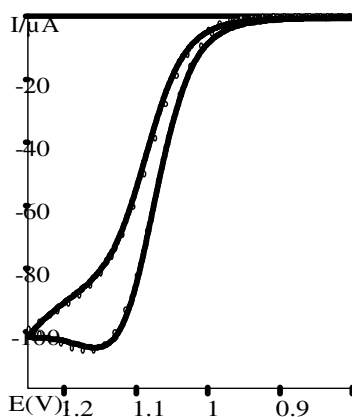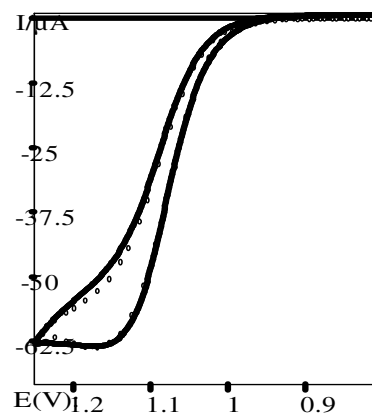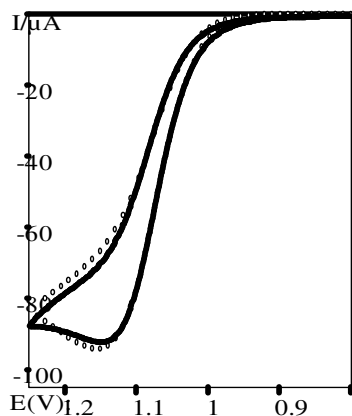
Simulated CV's for oxidation of CSH in 50 mM PB, pH 5.0. Scan rates: 100, 200, 500 mV/s. $k_f = 2.32 \pm 0.4 \times 10^4$ $M^{-1}s^{-1}$; $K_{eq2} = 1 \times 10^3$; $E^o = 1.08$ V; $k_h = 0.06$ cm/s; $\alpha = 0.5$.

Simulated CV's for oxidation of CSH in 50 mM PB, pD 5.0. Scan rates: 100, 200, 500 mV/s. $k_f = 8.86 \pm 0.2 \times 10^3$ $M^{-1}s^{-1}$; $K_{eq2} = 1 \times 10^3$; $E^o = 1.08$ V; $k_h = 0.06$ cm/s; $\alpha = 0.5$.
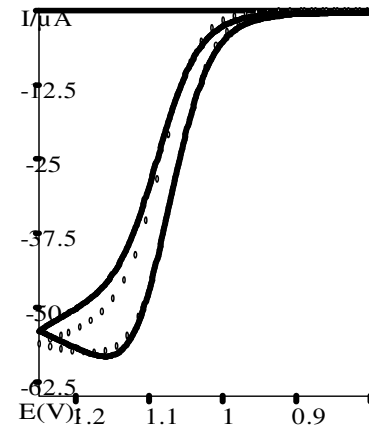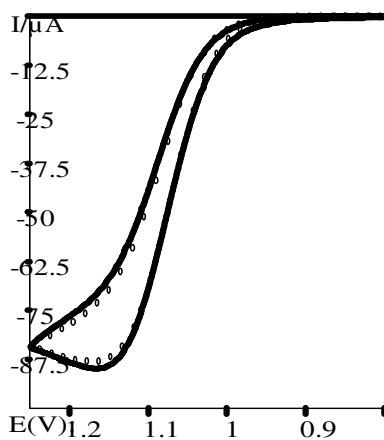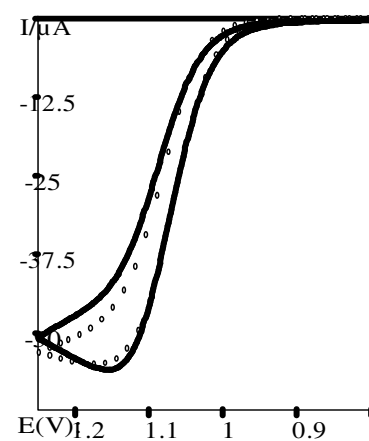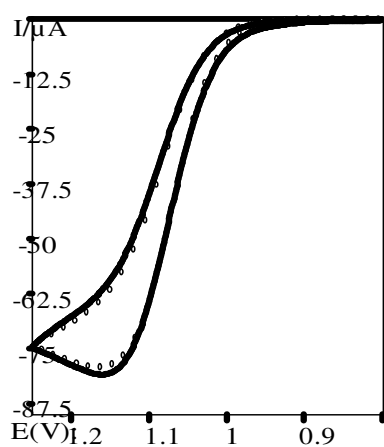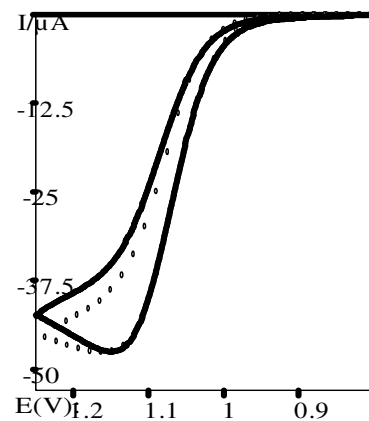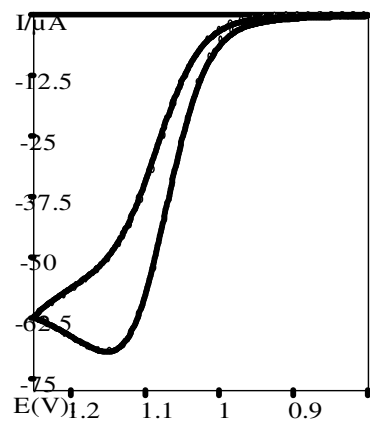
Simulated CV's for oxidation of GSH in 0.1 M NaCl, pH 5.0. Scan rates: 100, 200, 300 mV/s. $k_f = 1.12 \pm 0.1 \times 10^4$ $M^{-1}s^{-1}$; $K_{eq2} = 1 \times 10^3$; $E^o = 1.08$ V; $k_h = 0.06$ cm/s; $\alpha = 0.5$.

Simulated CV's for oxidation of GSH in 0.1 M NaCl, pD 5.0. Scan rates: 100, 200, 300 mV/s. $k_f = 3.92 \pm 0.5 \times 10^3$ $M^{-1}s^{-1}$; $K_{eq2} = 1 \times 10^3$; $E^o = 1.08$ V; $k_h = 0.06$ cm/s; $\alpha = 0.5$.
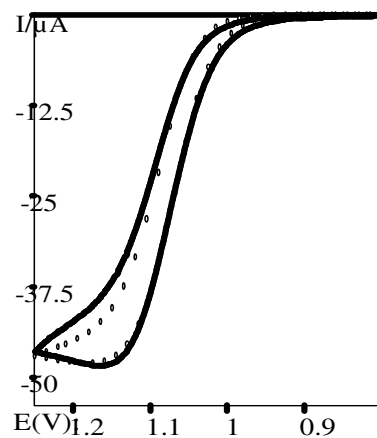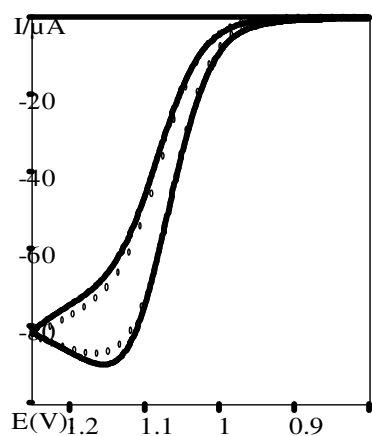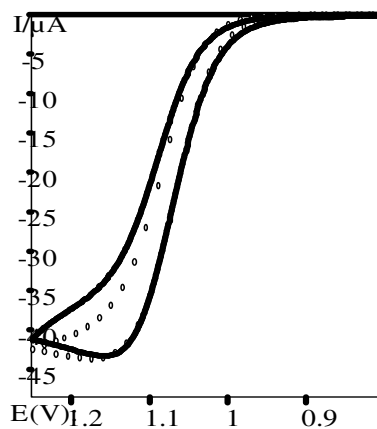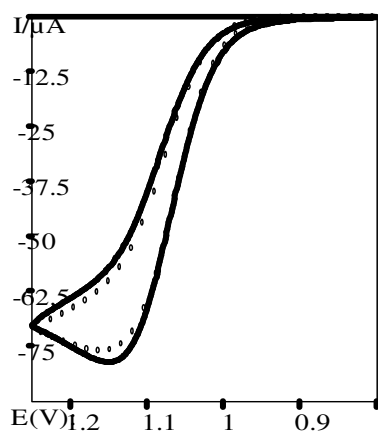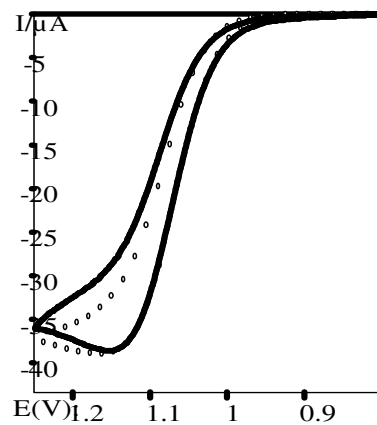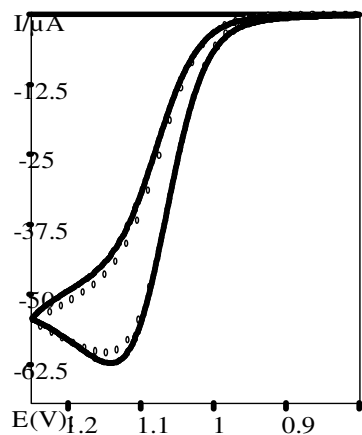
Simulated CV's for oxidation of GSH in 0.1 M NaCl, pH 7.0. Scan rates: 100, 200, 300 mV/s. $k_f = 9.02 \pm 2.3 \times 10^3$ $M^{-1}s^{-1}$; $K_{eq2} = 1 \times 10^3$; $E^o = 1.08$ V; $k_h = 0.06$ cm/s; $\alpha = 0.5$.
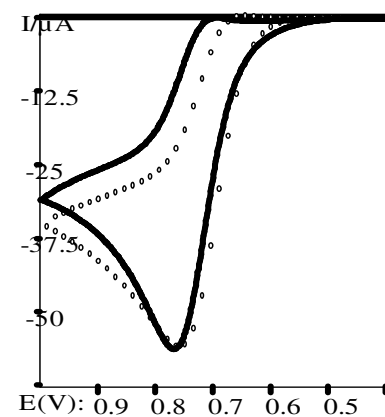
Simulated CV's for oxidation of GSH in 0.1 M NaCl, pD 7.0. Scan rates: 100, 200, 300 mV/s. $k_f = 3.01 \pm 0.4 \times 10^3$ $M^{-1}s^{-1}$; $K_{eq2} = 1 \times 10^3$; $E^o = 1.08$ V; $k_h = 0.06$ cm/s; $\alpha = 0.5$.
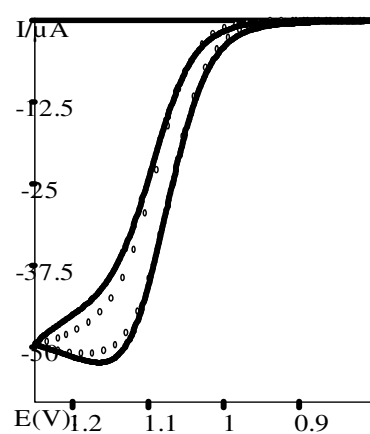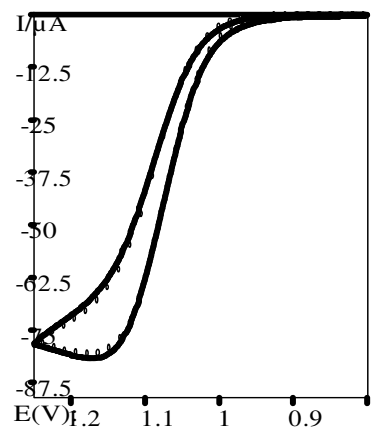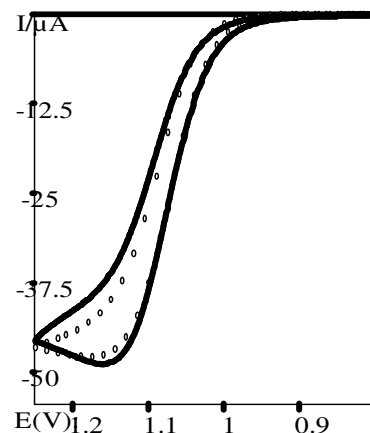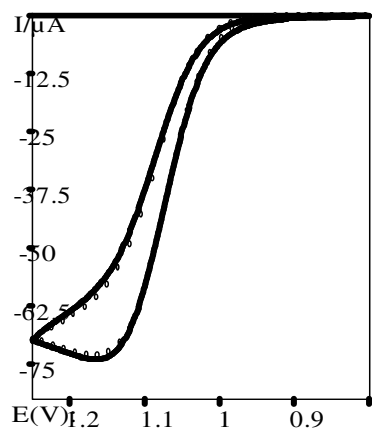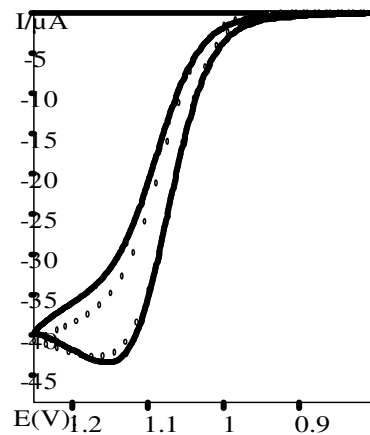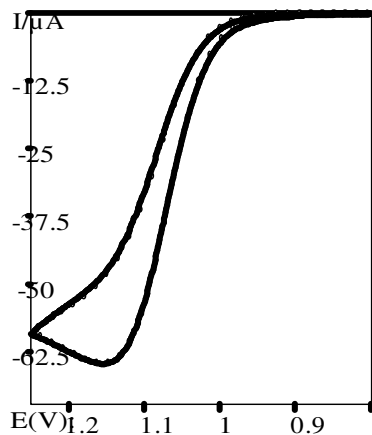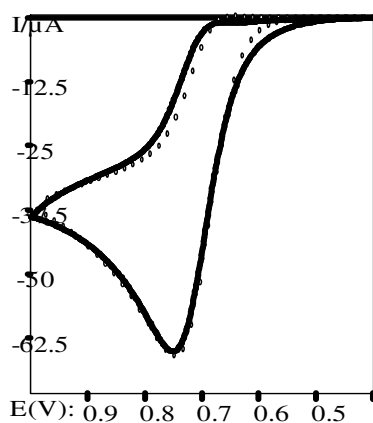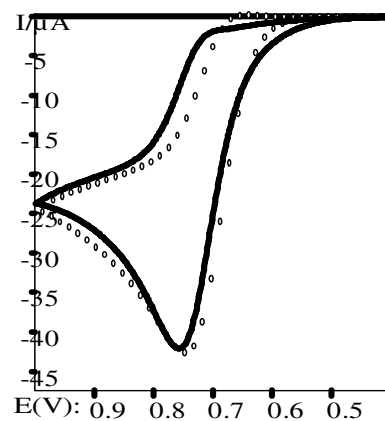
Simulated CV's for oxidation of GSH in 0.1 M NaCl, pH 9.0. Scan rates: 100, 200, 300 mV/s. $k_f = 9.29 \pm 1.1 \times 10^3$ $M^{-1}s^{-1}$; $K_{eq2} = 1 \times 10^3$; $E^o = 1.08$ V; $k_h = 0.06$ cm/s; $\alpha = 0.5$.
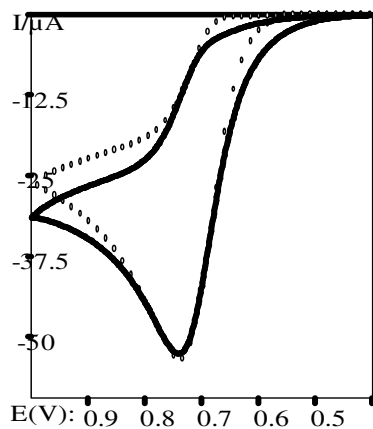
Simulated CV's for oxidation of GSH in 0.1 M NaCl, pD 9.0. Scan rates: 100, 200, 300 mV/s. $k_f = 3.57 \pm 0.4 \times 10^3$ $M^{-1}s^{-1}$; $K_{eq2} = 1 \times 10^3$; $E^o = 1.08$ V; $k_h = 0.06$ cm/s; $\alpha = 0.5$.
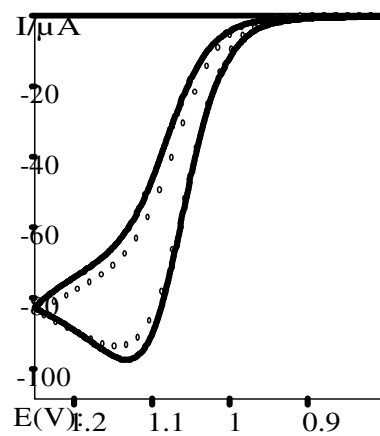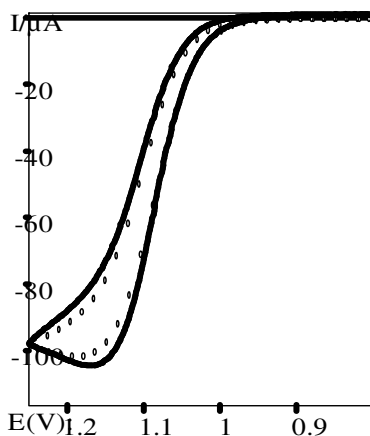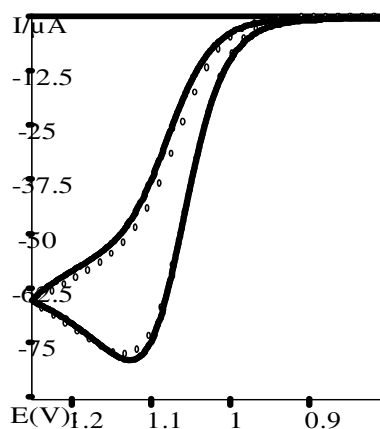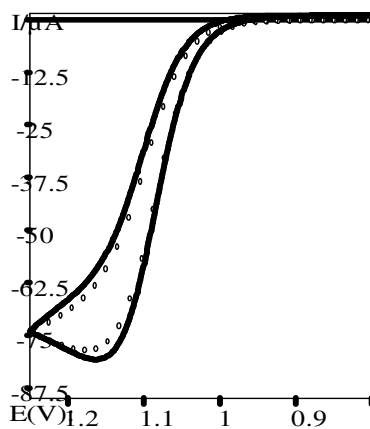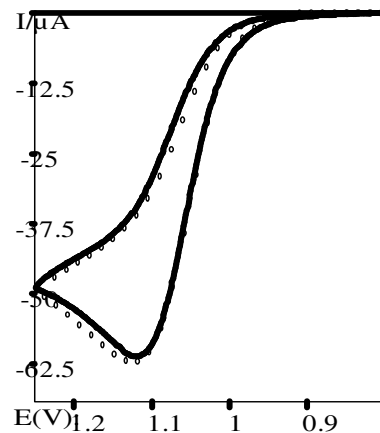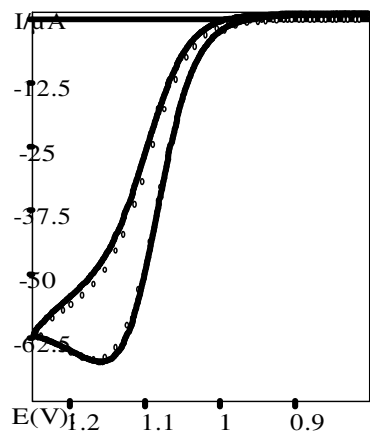
Simulated CV's for oxidation of GSH in 35 mM tris/HCl, pH 7.0. Scan rates: 100, 200, 500 mV/s. $k_f = 1.17 \pm 0.4 \times 10^4$ $M^{-1}s^{-1}$; $K_{eq2} = 1 \times 10^3$; $E^o = 1.09$ V; $k_h = 0.06$ cm/s; $\alpha = 0.5$.

Simulated CV's for oxidation of GSH in 6.25 mM PB, pH 7.0. Scan rates: 50, 100, 200 mV/s. $k_f = 1.00 \pm 0.8 \times 10^4$ $M^{-1}s^{-1}$; $K_{eq2} = 1 \times 10^3$; $E^o = 1.06$ V; $k_h = 0.06$ cm/s; $\alpha = 0.5$.
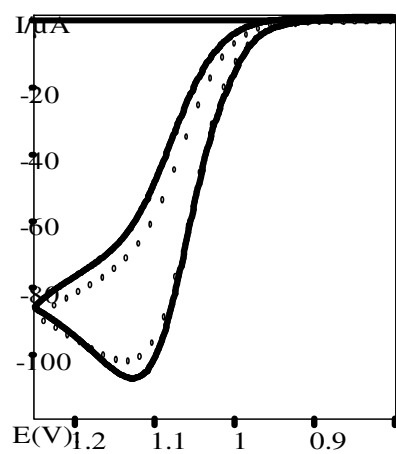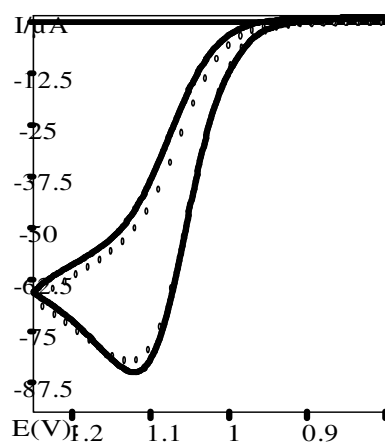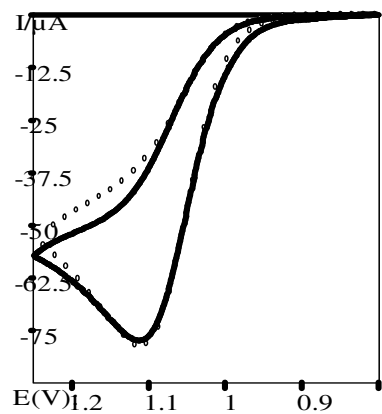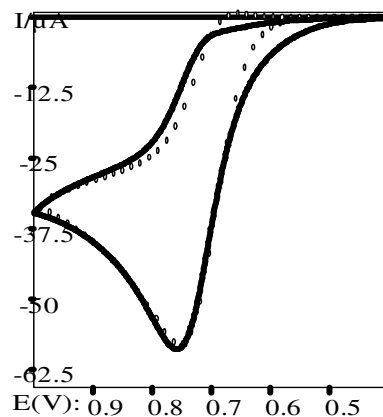
Simulated CV's for oxidation of GSH in 12.5 mM PB, pH 7.0. Scan rates: 50, 100, 200 mV/s. k_f = 2.03 ± 0.5 × 10^4 $M^{-1}s^{-1}$; K_{eq2} = 1 × 10^3; E^o = 1.06 V; k_h = 0.06 cm/s; α = 0.5.

2. OXIDATION OF GSH BY IrCl$_6^{2-}$
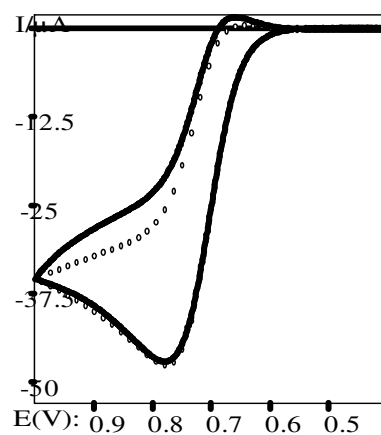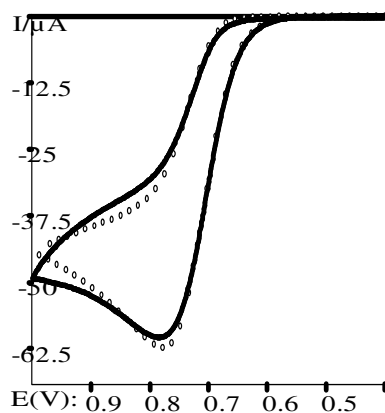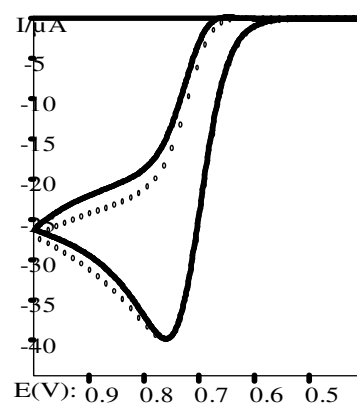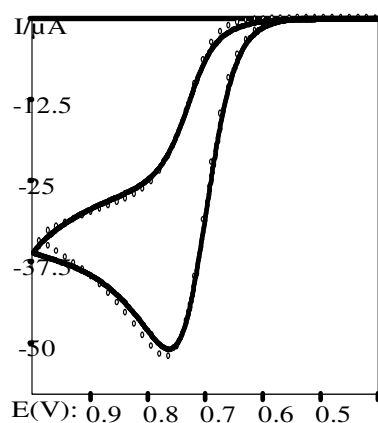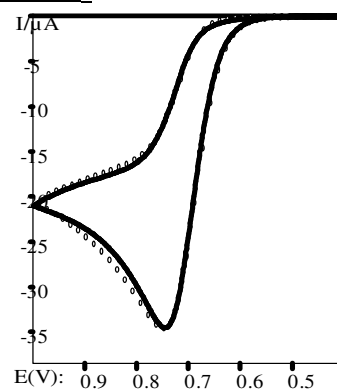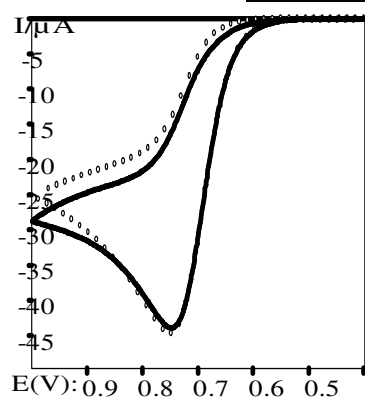
Simulated CV's for oxidation of GSH in 35 mM PB, pH 7.0. Scan rates: 50, 100, 200 mV/s. $k_3 = 7.15 \pm 0.1 \times 10^5$ M^{-1}s^{-1}; $k_{dep} = 1 \times 10^7$ M^{-1}s^{-1}; $K_{dep} = 0.035$; $K_{eq3} = 1 \times 10^6$; $E^o = 0.72$ V; $k_h = 0.1$ cm/s; $\alpha = 0.5$.
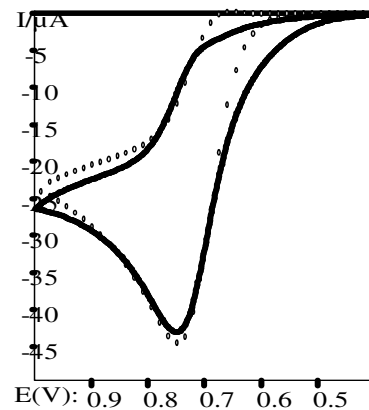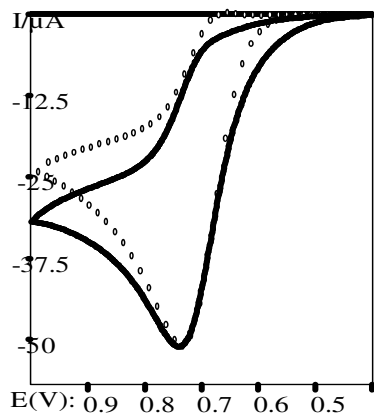
Simulated CV's for oxidation of GSH in 35 mM PB, pD 7.0. Scan rates: 50, 100, 200 mV/s. $k_3 = 3.62 \pm 0.2 \times 10^5$ M^{-1}s^{-1}; $k_{dep} = 1 \times 10^7$ M^{-1}s^{-1}; $K_{dep} = 0.035$; $K_{eq3} = 1 \times 10^6$; $E^o = 0.71$ V; $k_h = 0.1$ cm/s; $\alpha = 0.5$.
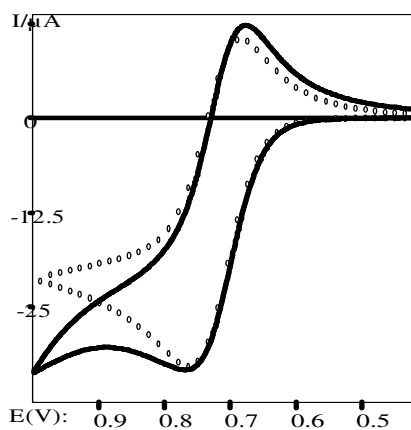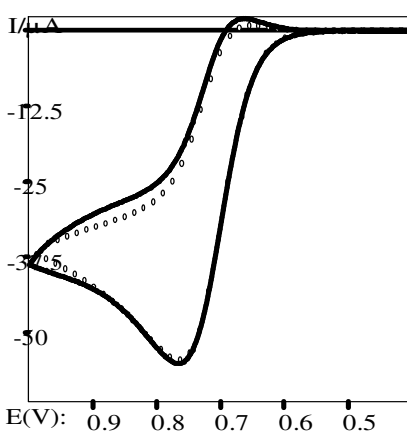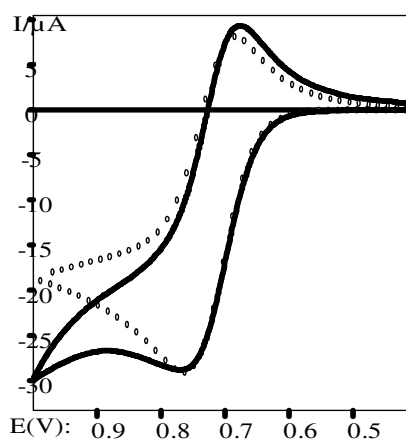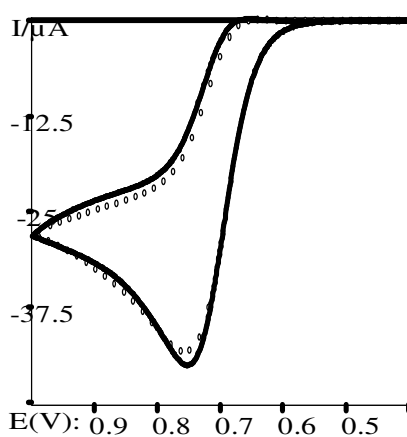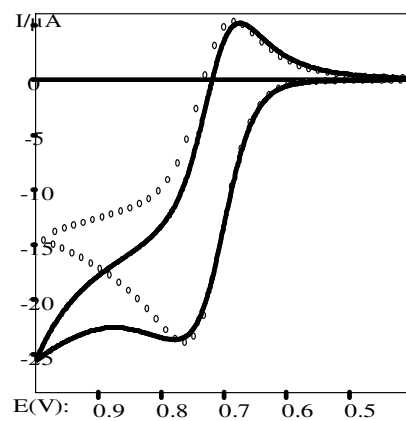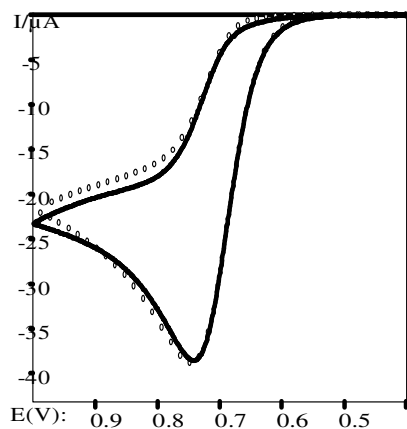
Simulated CV's for oxidation of GSH in 25 mM PB, pH 7.0. Scan rates: 100, 200, 300 mV/s. $k_3 = 4.78 \pm 0.6 \times 10^5$ $M^{-1}s^{-1}$; $k_{dep} = 1 \times 10^7$ $M^{-1}s^{-1}$; $K_{dep} = 0.035$; $K_{eq3} = 1 \times 10^6$; $E^o = 0.72$ V; $k_h = 0.1$ cm/s; $\alpha = 0.5$.

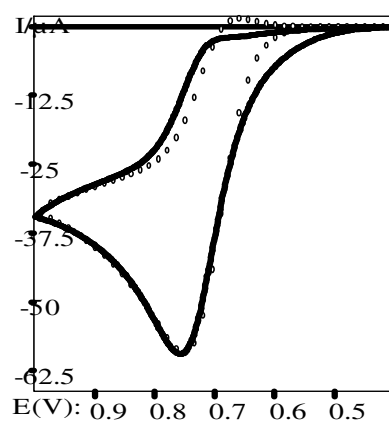Simulated CV's for oxidation of GSH in 5 mM PB, pH 7.0. Scan rates: 50, 100, 200 mV/s. $k_3 = 4.91 \times 10^4$ $M^{-1}s^{-1}$; $k_{dep} = 1 \times 10^7$ $M^{-1}s^{-1}$; $K_{dep} = 0.035$; $K_{eq3} = 1 \times 10^4$; $E^o = 0.72$ V; $k_h = 0.1$ cm/s; $\alpha = 0.5$.
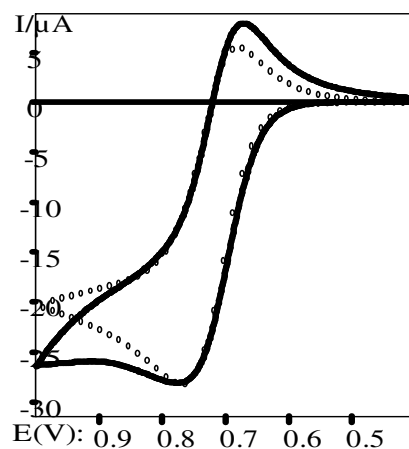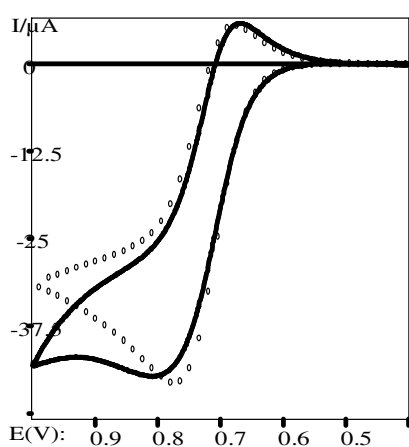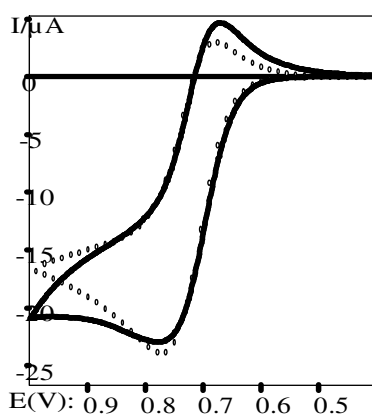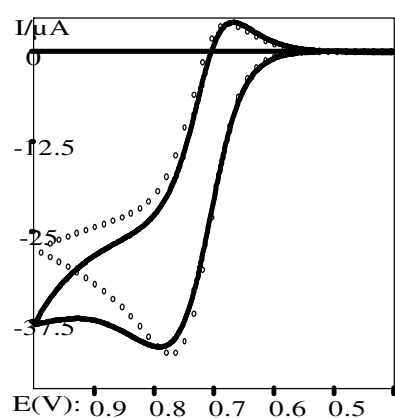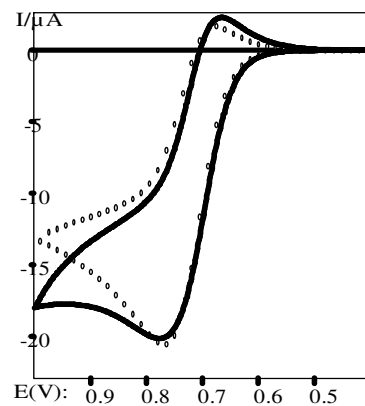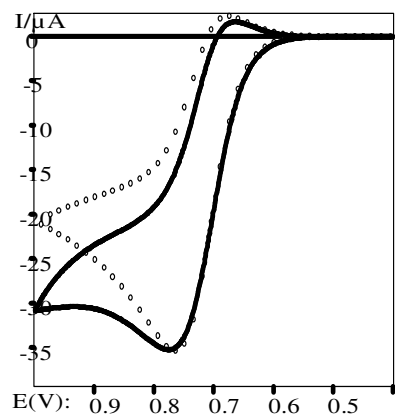
Simulated CV's for oxidation of GSH in 10 mM PB, pH 7.0. Scan rates: 50, 100, 200 mV/s. $k_3 = 2.44 \pm 2.1 \times 10^5$ $M^{-1}s^{-1}$; $k_{dep} = 1 \times 10^7$ $M^{-1}s^{-1}$; $K_{dep} = 0.035$; $K_{eq3} = 1 \times 10^6$; $E^o = 0.72$ V; $k_h = 0.1$ cm/s; $\alpha = 0.5$.

Simulated CV's for oxidation of GSH in 10 mM PB, pD 7.0. Scan rates: 50, 100, 200 mV/s. $k_3 = 7.71 \pm 1.0 \times 10^4$ $M^{-1}s^{-1}$; $k_{dep} = 1 \times 10^7$ $M^{-1}s^{-1}$; $K_{dep} = 0.035$; $K_{eq3} = 1 \times 10^6$; $E^o = 0.72$ V; $k_h = 0.1$ cm/s; $\alpha = 0.5$.
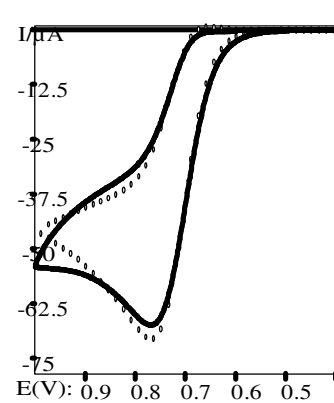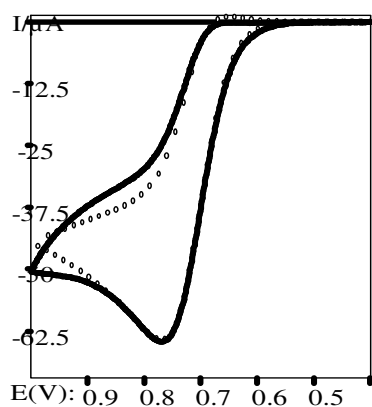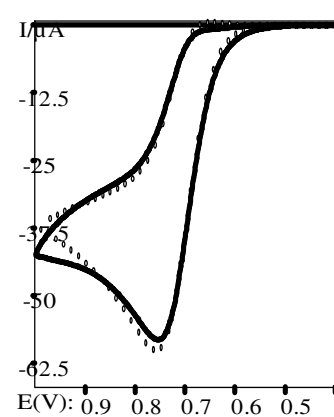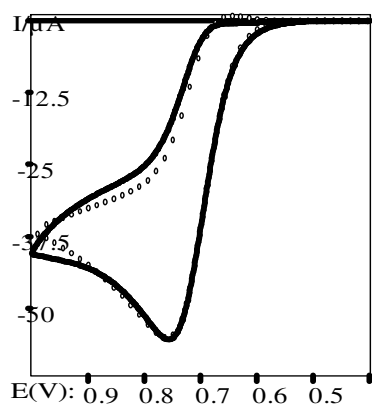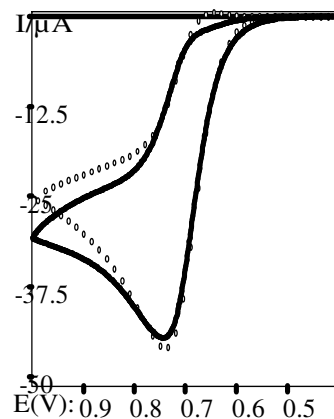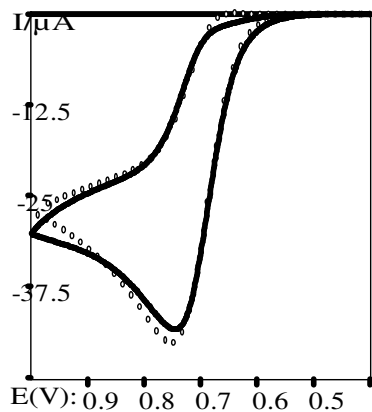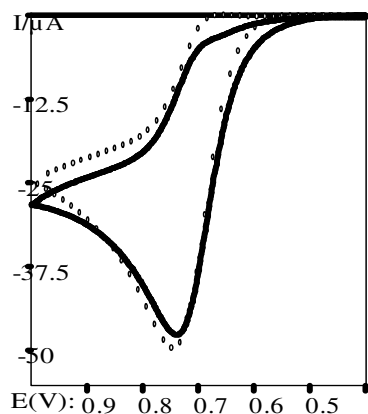
Simulated CV's for oxidation of GSH in 35 mM PB, pH 8.0. Scan rates: 50, 100, 200 mV/s. $k_3 = 1.32 \pm 0.2 \times 10^5$ M^{-1}s^{-1}; $k_{dep} = 1 \times 10^7$ M^{-1}s^{-1}; $K_{dep} = 0.035$; $K_{eq3} = 1 \times 10^6$; $E^o = 0.72$ V; $k_h = 0.1$ cm/s; $\alpha = 0.5$.

Simulated CV's for oxidation of GSH in 35 mM PB, pH 9.0. Scan rates: 100, 200, 300 mV/s. $k_3 = 5.27 \pm 0.8 \times 10^4$ M^{-1}s^{-1}; $k_{dep} = 1 \times 10^7$ M^{-1}s^{-1}; $K_{dep} = 0.035$; $K_{eq3} = 1 \times 10^5$; $E^o = 0.72$ V; $k_h = 0.1$ cm/s; $\alpha = 0.5$.
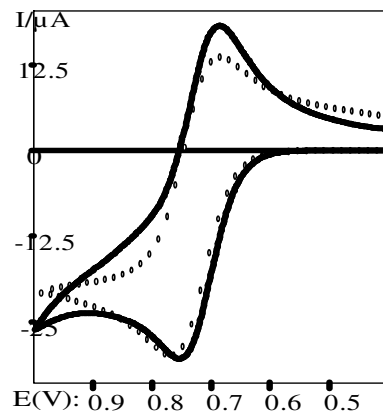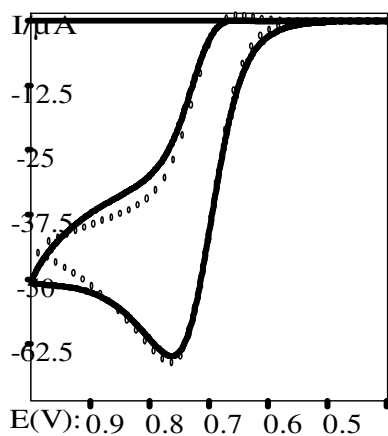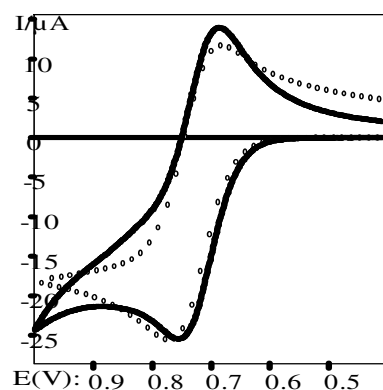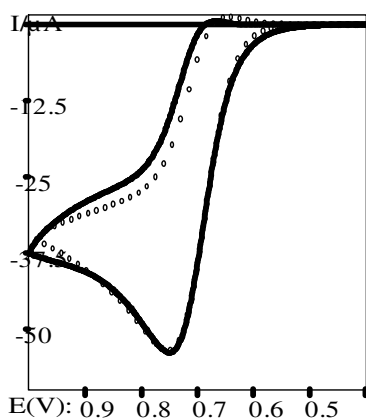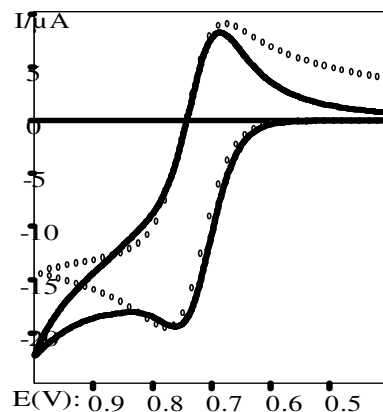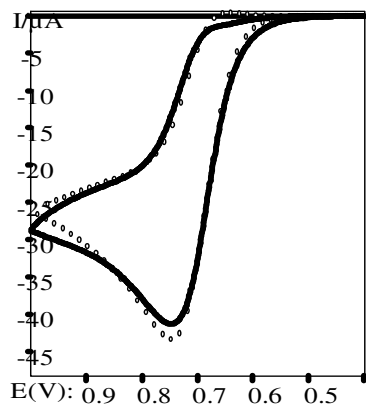
Simulated CV's for oxidation of GSH in 35 mM PB, pH 10. Scan rates: 100, 200, 300 mV/s. $k_3 = 2.49 \pm 0.6 \times 10^4$ $M^{-1}s^{-1}$; $k_{dep} = 1 \times 10^7$ $M^{-1}s^{-1}$; $K_{dep} = 0.035$; $K_{eq3} = 5 \times 10^4$; $E^o = 0.72$ V; $k_h = 0.1$ cm/s; $\alpha = 0.5$.

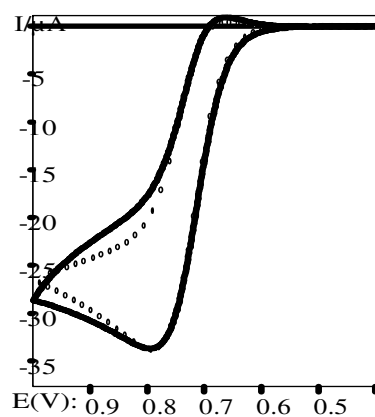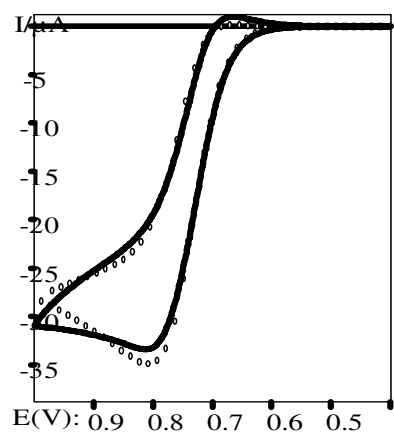Simulated CV's for oxidation of GSH in 0.1 M NaCl, pH 10. Scan rates: 100, 200, 300 mV/s. $k_2 = 8.95 \pm 1.2 \times 10^2$ $M^{-1}s^{-1}$; $K_{eq2} = 0.9$; $E^o = 0.72$ V; $k_h = 0.1$ cm/s; $\alpha = 0.5$. Representative simulated CV's for pH 5.0-11.
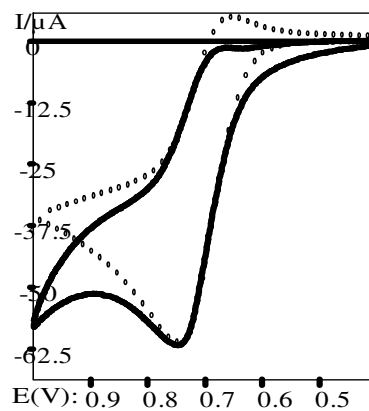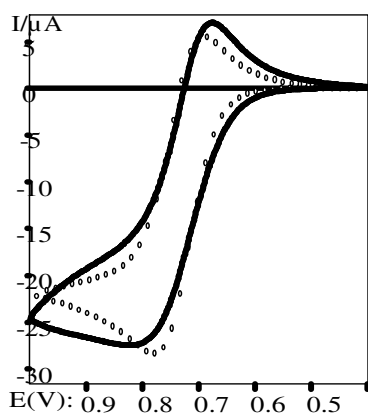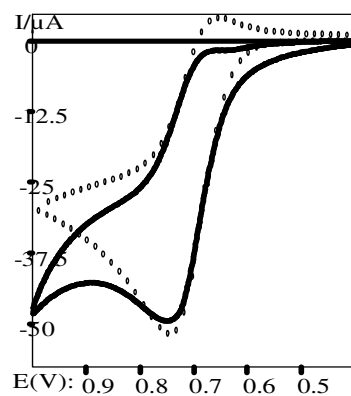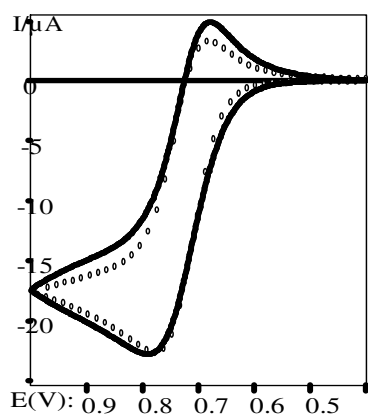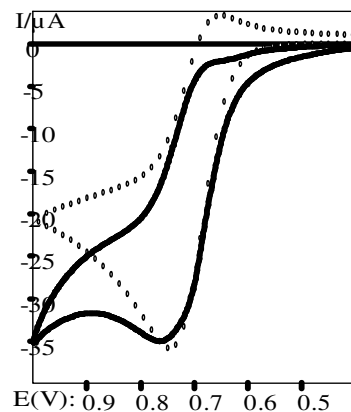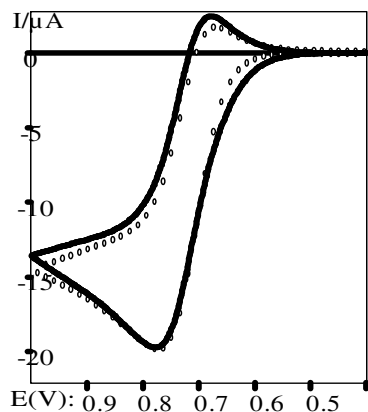
Simulated CV's for oxidation of GSH in 0.1 M NaCl, pH 11.5. Scan rates: 50, 100, 200 mV/s. $k_3 = 1.75 \pm 0.3 \times 10^3$ $M^{-1}s^{-1}$; $k_{dep} = 1 \times 10^7$ $M^{-1}s^{-1}$; $K_{dep} = 0.11$; $K_{eq3} = 2.6 \times 10^2$; $E^o = 0.72$ V; $k_h = 0.1$ cm/s; $\alpha = 0.5$.

Simulated CV's for oxidation of GSH in 0.1 M NaCl, pH 12. Scan rates: 100, 200, 300 mV/s. $k_3 = 2.65 \pm 1.2 \times 10^4$ $M^{-1}s^{-1}$; $k_{dep} = 1 \times 10^7$ $M^{-1}s^{-1}$; $K_{dep} = 0.12$; $K_{eq3} = 2.6 \times 10^2$; $E^o = 0.72$ V; $k_h = 0.1$ cm/s; $\alpha = 0.5$.
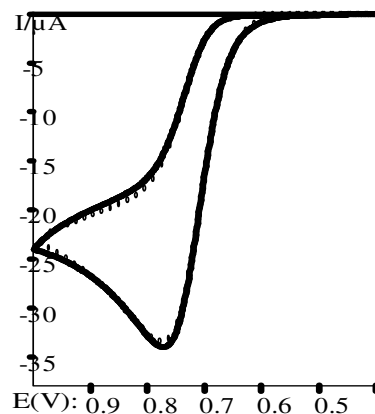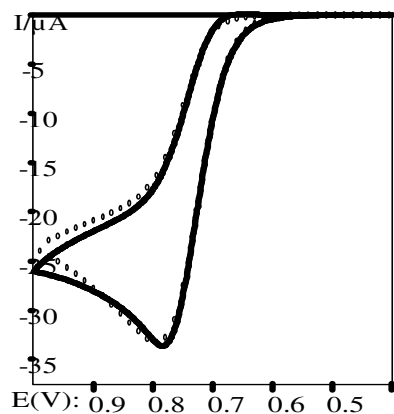
3. OXIDATION OF HCSH BY IrCl$_6^{2-}$
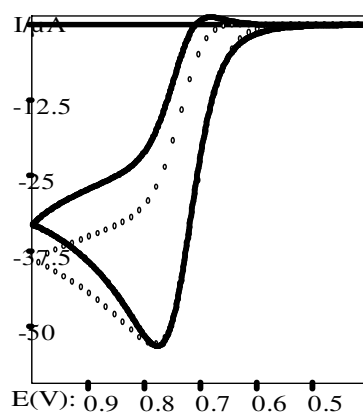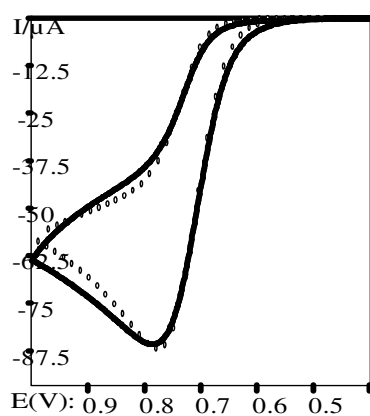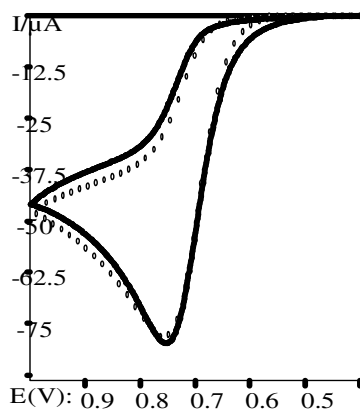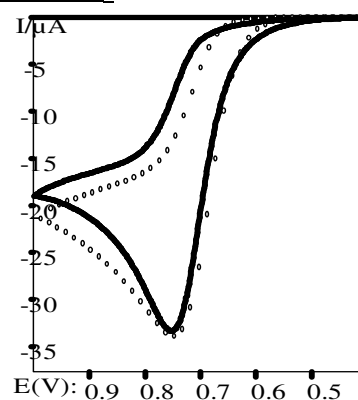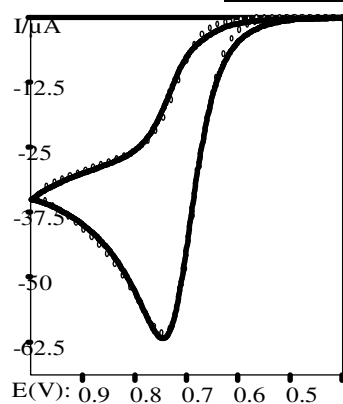
Simulated CV's for oxidation of HCSH in 35 mM PB, pH 7.0. Scan rates: 100, 200, 300 mV/s. $k_3 = 2.13 \pm 0.3 \times 10^6$ M^{-1}s^{-1}; $k_{dep} = 1 \times 10^7$ M^{-1}s^{-1}; $K_{dep} = 0.02$; $K_{eq3} = 1 \times 10^6$; $E^o = 0.72$ V; $k_h = 0.1$ cm/s; $\alpha = 0.5$.

Simulated CV's for oxidation of HCSH in 35 mM PB, pD 7.0. Scan rates: 50, 100, 200 mV/s. $k_3 = 6.29 \pm 1.8 \times 10^5$ M^{-1}s^{-1}; $k_{dep} = 1 \times 10^7$ M^{-1}s^{-1}; $K_{dep} = 0.02$; $K_{eq3} = 1 \times 10^6$; $E^o = 0.72$ V; $k_h = 0.1$ cm/s; $\alpha = 0.5$.
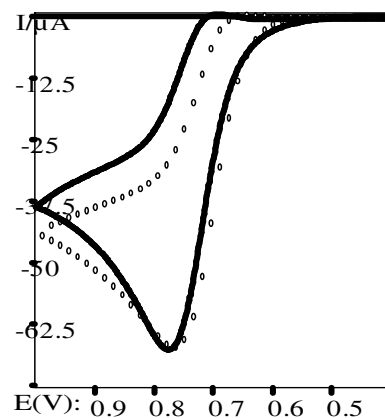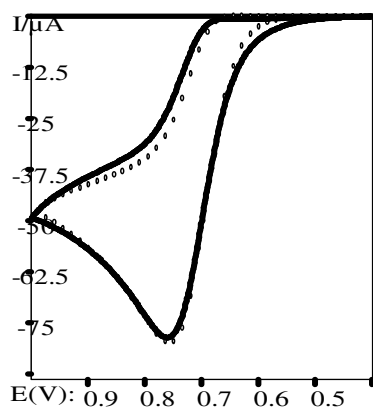
Simulated CV's for oxidation of HCSH in 35 mM PB, pH 8.0. Scan rates: 100, 200, 300 mV/s. $k_3 = 4.41 \pm 1.3 \times 10^5$ $M^{-1}s^{-1}$; $k_{dep} = 1 \times 10^7$ $M^{-1}s^{-1}$; $K_{dep} = 0.02$; $K_{eq3} = 1 \times 10^6$; $E^o = 0.72$ V; $k_h = 0.1$ cm/s; $\alpha = 0.5$.

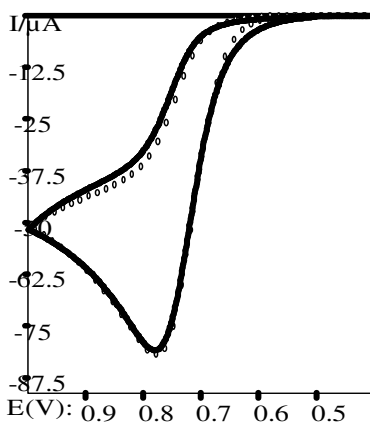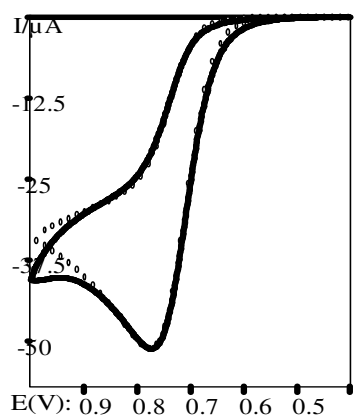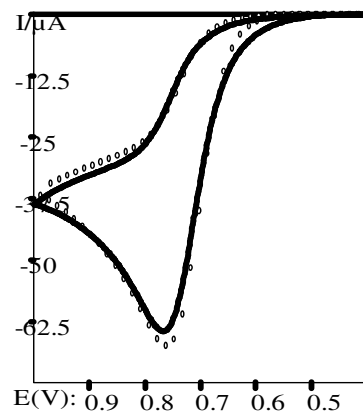Simulated CV's for oxidation of HCSH in 35 mM PB, pD 8.0. Scan rates: 100, 200, 300 mV/s. $k_3 = 2.20 \pm 0.6 \times 10^5$ $M^{-1}s^{-1}$; $k_{dep} = 1 \times 10^7$ $M^{-1}s^{-1}$; $K_{dep} = 0.02$; $K_{eq3} = 1 \times 10^6$; $E^o = 0.72$ V; $k_h = 0.1$ cm/s; $\alpha = 0.5$.
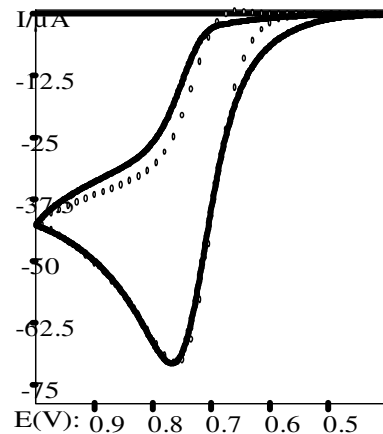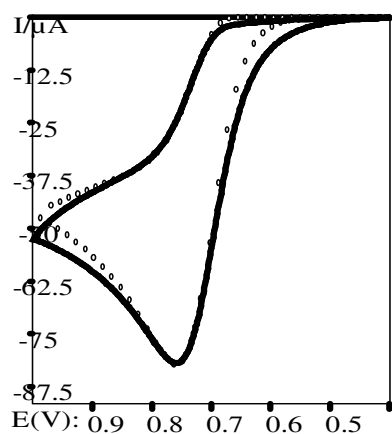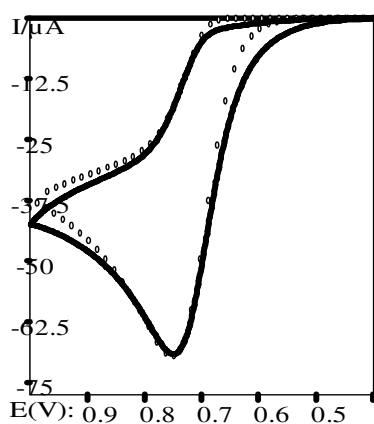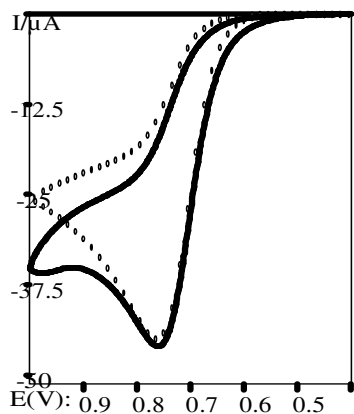
Simulated CV's for oxidation of HCSH in 35 mM PB, pH 9.0. Scan rates: 100, 200, 300 mV/s. $k_3 = 2.24 \pm 0.4 \times 10^5$ $M^{-1}s^{-1}$; $k_{dep} = 1 \times 10^7$ $M^{-1}s^{-1}$; $K_{dep} = 0.02$; $K_{eq3} = 3 \times 10^5$; $E^o = 0.72$ V; $k_h = 0.1$ cm/s; $\alpha = 0.5$.

Simulated CV's for oxidation of HCSH in 35 mM PB, pD 9.0. Scan rates: 100, 200, 300 mV/s. $k_3 = 1.44 \pm 0.4 \times 10^5$ $M^{-1}s^{-1}$; $k_{dep} = 1 \times 10^7$ $M^{-1}s^{-1}$; $K_{dep} = 0.02$; $K_{eq3} = 3 \times 10^5$; $E^o = 0.72$ V; $k_h = 0.1$ cm/s; $\alpha = 0.5$.
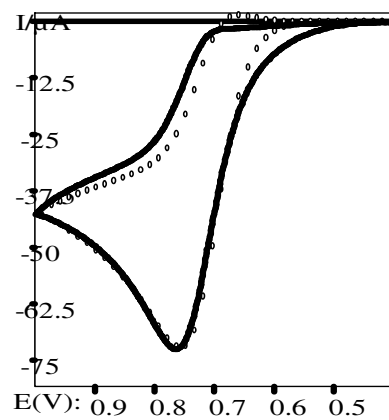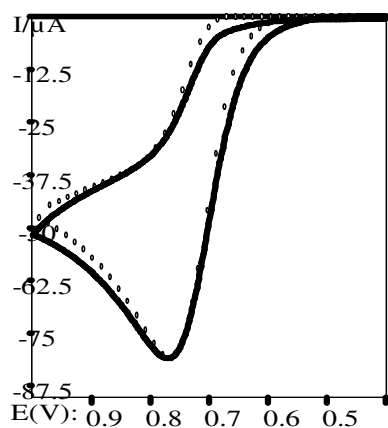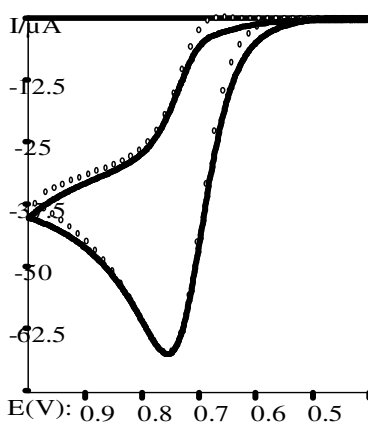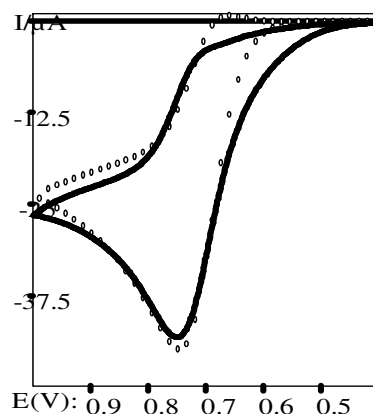
Simulated CV's for oxidation of HCSH in 35 mM PB, pH 10. Scan rates: 100, 200, 300 mV/s. $k_3 = 1.66 \pm 0.3 \times 10^5$ $M^{-1}s^{-1}$; $k_{dep} = 1 \times 10^7$ $M^{-1}s^{-1}$; $K_{dep} = 0.02$; $K_{eq3} = 3 \times 10^5$; $E^o = 0.72$ V; $k_h = 0.1$ cm/s; $\alpha = 0.5$.

Simulated CV's for oxidation of HCSH in 35 mM PB, pD 10. Scan rates: 100, 200, 300 mV/s. $k_3 = 1.22 \pm 0.4 \times 10^5$ $M^{-1}s^{-1}$; $k_{dep} = 1 \times 10^7$ $M^{-1}s^{-1}$; $K_{dep} = 0.02$; $K_{eq3} = 3 \times 10^5$; $E^o = 0.72$ V; $k_h = 0.1$ cm/s; $\alpha = 0.5$.
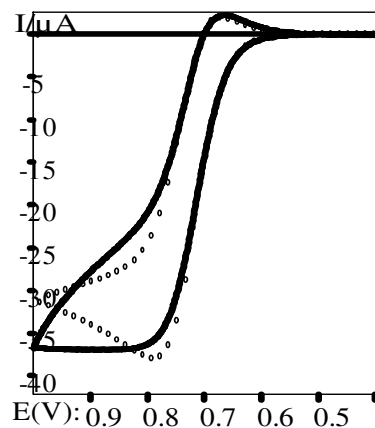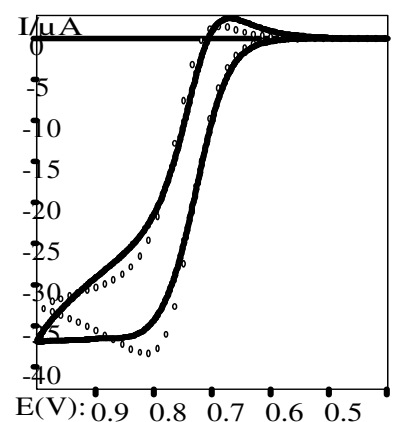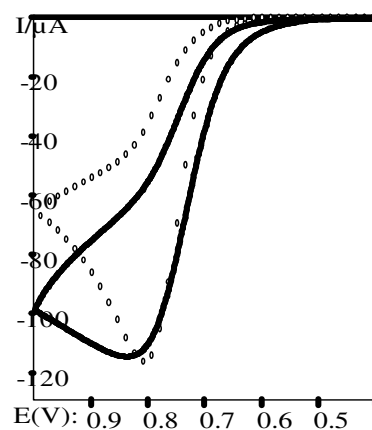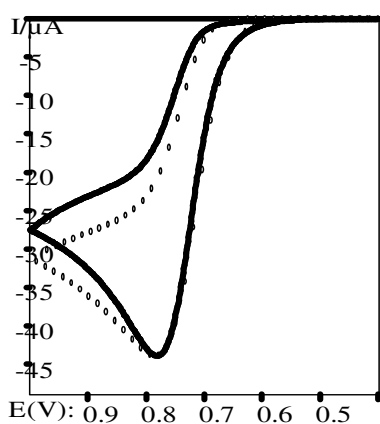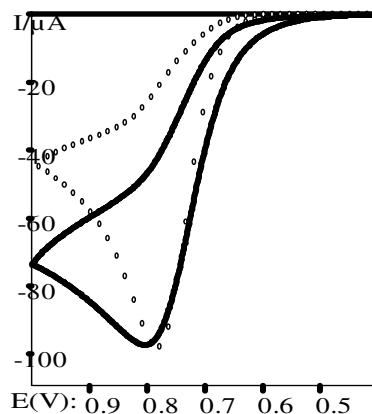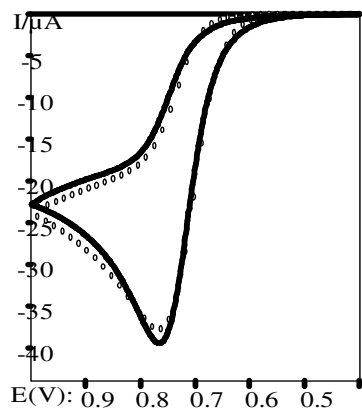
Simulated CV's for oxidation of HCSH in 35 mM PA, pH 4.9. Scan rates: 50, 100, 200 mV/s. $k_3 = 5.71 \pm 0.9 \times 10^4$ $M^{-1}s^{-1}$; $k_{ass} = 1 \times 10^7$ $M^{-1}s^{-1}$; $K_{ass} = 2.8$; $K_{eq3} = 1 \times 10^6$; $E^o = 0.72$ V; $k_h = 0.1$ cm/s; $\alpha = 0.5$.

Simulated CV's for oxidation of HCSH in 35 mM MA, pH 6.2. Scan rates: 100, 200, 300 mV/s. $k_3 = 5.54 \pm 1.5 \times 10^5$ $M^{-1}s^{-1}$; $k_{dep} = 1 \times 10^7$ $M^{-1}s^{-1}$; $K_{dep} = 0.004$; $K_{eq3} = 1 \times 10^6$; $E^o = 0.72$ V; $k_h = 0.1$ cm/s; $\alpha = 0.5$.
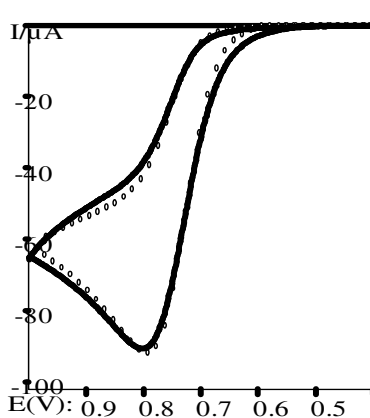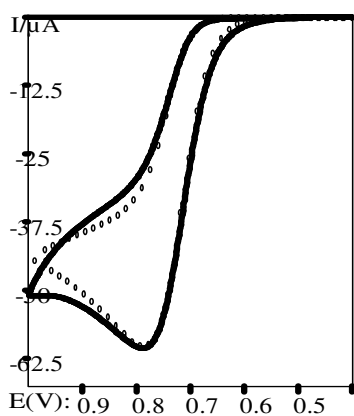
Simulated CV's for oxidation of GSH in 35 mM PB, pH 6.8. Scan rates: 100, 200, 300 mV/s. $k_3 = 9.87 \pm 1.2 \times 10^5$ M^{-1}s^{-1}; $k_{dep} = 1 \times 10^7$ M^{-1}s^{-1}; $K_{dep} = 0.008$; $K_{eq3} = 1 \times 10^6$; $E^o = 0.72$ V; $k_h = 0.1$ cm/s; $\alpha = 0.5$.

Simulated CV's for oxidation of GSH in 35 mM PB, pH 7.2. Scan rates: 100, 200, 300 mV/s. $k_3 = 1.76 \times 10^6$ M^{-1}s^{-1}; $k_{dep} = 1 \times 10^7$ M^{-1}s^{-1}; $K_{dep} = 0.02$; $K_{eq3} = 1 \times 10^6$; $E^o = 0.72$ V; $k_h = 0.1$ cm/s; $\alpha = 0.5$.
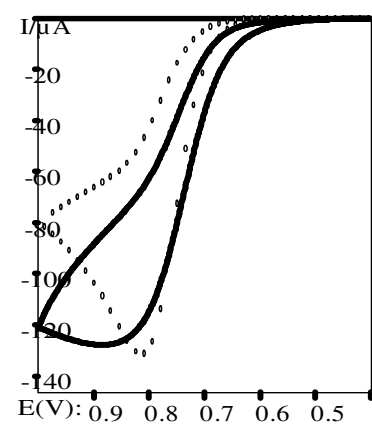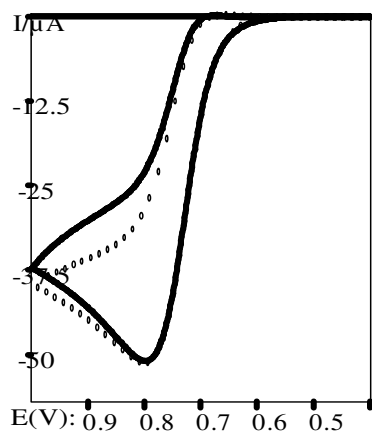
Simulated CV's for oxidation of GSH in 35 mM PB, pH 7.0 (10 ^{o}C). Scan rates: 50, 100, 200 mV/s. $k_3 = 4.28 \pm 0.4 \times 10^5$ $M^{-1}s^{-1}$; $k_{dep} = 1 \times 10^7$ $M^{-1}s^{-1}$; $K_{dep} = 0.02$; $K_{eq3} = 1 \times 10^6$; $E^o = 0.72$ V; $k_h = 0.1$ cm/s; $\alpha = 0.5$.

Simulated CV's for oxidation of GSH in 35 mM PB, pH 7.0 (30 ^{o}C). Scan rates: 100, 200, 300 mV/s. $k_3 = 1.15 \pm 0.2 \times 10^7$ $M^{-1}s^{-1}$; $k_{dep} = 1 \times 10^7$ $M^{-1}s^{-1}$; $K_{dep} = 0.02$; $K_{eq3} = 1 \times 10^6$; $E^o = 0.72$ V; $k_h = 0.1$ cm/s; $\alpha = 0.5$.

VITA

Olufemi Olanrewaju Oyesanya, a Nigerian citizen, was born on September 14, 1975 in Lagos, Nigeria. He received his Ordinary National Diploma (OND) in Science Laboratory Technology from the then Ogun State Polytechnic, Abeokuta, and his Bachelor of Science in Chemical Sciences from University of Agriculture, Abeokuta, both of which are located in Ogun State, Nigeria. Olufemi was first admitted into Graduate Studies in Chemistry in the U.S. by South Dakota State University, Brookings, after which he decided to continue his Graduate Studies in the Department of Chemistry, Virginia Commonwealth University, Richmond, Virginia. He has authored/co-authored a paper, and has presented his research work at several conferences.

Pu, Q.; **Oyesanya, O**.; Thompson, B.; Liu, S.; Alvarez, J., "On-chip micropatterning of plastic (cyclic olefin copolymer, COC) microfluidic channels for the fabrication of biomolecule microarrays using photografting methods." *Langmuir* **2007**, *23*(*3*), 1577-83.